INVESTIGATIONS ON THE RADIATION CHARACTERISTICS OF FLANGED SECTORAL HORN ANTENNAS AND CORNER REFLECTOR SYSTEMS

A THESIS SUBMITTED BY

K. VASUDEVAN

IN PARTIAL FULFILMENT OF
THE REQUIREMENTS
FOR THE DEGREE OF
DOCTOR OF PHILOSOPHY
TO
THE UNIVERSITY OF COCHIN

MICROWAVE LABORATORY, DEPARTMENT OF PHYSICS
UNIVERSITY OF COCHIN, COCHIN - 682 022
INDIA

1982

CERTIFICATE

This is to certify that this thesis is a report of the original work carried out by Mr.K. Vasudevan, under my supervision and guidance in the Microwave Laboratory, Department of Physics, University of Cochin, Cochin 682022 and that no part thereof has been presented for any other degree.

Mr.K. Vasudevan has passed the M.Sc. Degree Examination of the University of Calicut in First Class with First Rank, taking Electronics as special subject in 1976. He has also passed the Ph.D. Qualifying Examination of the University of Cochin in April 1979.
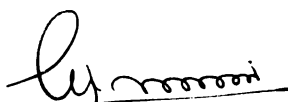
Dr.K.G. Nair
(Supervising Teacher)
Professor and Head of the
Department of Electronics and
Communication Systems
University of Cochin.

Cochin 682022,
19th April 1982.

DECLARATION

Certified that the work presented in this thesis is based on the original work done by me under the supervision of Dr.K.G. Nair in the Department of Physics, Cochin University and that no part thereof has been presented for any other degree.

Cochin 682022,
19th April 1982.

K. Vasudevan.

CONTENTS

Page

LIST OF SYMBOLS USED

B   — Flange/reflector width

   — Twice the path difference between primary and secondary source (Sec.5.1(i))

B_p — Distance between p^{th} element and primary radiator (horn or dipole)

D   — Larger dimension of the aperture

d   — Slot width

E   — Electric field at any point with bearing angle θ (Sec.5.1(ii))

E_o — Maximum electric field (Sec.5.1(ii))

E_θ — The resultant electric field at P due to the tips of corrugations

E'_θ — The resultant electric field at P due to the primary and the image sources

G   — Antenna gain

h   — Corrugation depth

I_{max} — Maximum value of intensity in the direction of maximum radiation (Sec.3.4)

I_{max} — Maximum value of crystal current at the antinode in a standing wave pattern

I_{min} — Minimum value of crystal current at the node in a standing wave pattern

I_θ — Field intensity at the point P

K,K'   — Amplitude of the resultant due to secondary radiators on flange/CR elements 1 and 2

v

k   — Amplitude of excitation of the secondary radiators

        — Wave number (Sec.5.1(ii))

N   — Number of corrugations per cm on the flange/
           reflector surface

N'   — Total number of corrugations on the inclined
           corrugated flange/reflector surface

N_1 — Total number of corrugations on the straight
           corrugated flange/reflector surface

O   — Primary source (horn or dipole)

O',O'' — Images of the horn aperture cast by flange
           elements 1 and 2

P   — A distant point whose bearing angle at the
           primary source (horn or dipole) is θ

P_{max} — Power at the antinode in a standing wave pattern

P_{min} — Power at the node in a standing wave pattern

P_o — Reference power (Appendix II)

P_r — The power reflected from the absorbing surface
           (Appendix II)

R(dB)   — Reflectivity of the absorbing surface

S   — Voltage Standing Wave Ratio (Sec.3.2)

        — Primary radiator (Sec.5.1(i))

S_1, S_2 — Secondary sources (Sec.5.1(i))

S_p — p^{th} element on the flange/reflector surface

V   — Magnitude of the secondary relative to the primary
           (Sec.5.1(i))

V_s — Resultant of the secondary sources at the horn aperture (Sec.5.1(i))

Z — Position of the primary feed (horn or dipole) from the apex of the system

β — Half the flange/CR angle

δ, δ' — The relative phase of O' and O''

δ_n, δ_n' — The relative phase of nth image due to reflector element 1 and 2

$\varepsilon, \varepsilon'$ — The relative phase of E_j and E_2'

ε_n — A constant depending upon the value of n (Sec.5.1(ii))

η_p — The phase difference between the pth element on flange/reflector element 1 and the primary source

η_p' — The phase difference between the pth element on flange/reflector element 2 and the primary source

Θ — The bearing angle of point P at the primary radiator

λ — The operating wavelength

φ, φ' — The phase of the resultant vectors K and K'

τ — Tilt angle of the polarization ellipse

LIST OF FIGURES

LIST OF TABLES

INVESTIGATIONS ON THE RADIATION CHARACTERISTICS

OF FLANGED SECTORAL HORN ANTENNAS AND

CORNER REFLECTOR SYSTEMS

CHAPTER I

INTRODUCTION

Antennas play an important role in determining the characteristics of any electronic system which depends on free space as the propagation medium. Basically, an antenna can be considered as the connecting link between free space and the transmitter or receiver. For radar and navigational purposes the directional properties of an antenna is its most basic requirement as it determines the distribution of radiated energy. Hence the study of directional properties of antennas has got special significance and several useful applications.

Scientific investigators have turned their attention to electromagnetic antennas ever since Hertz launched the decimeter radiation from a parabolic mirror antenna fed by a dipole in 1888. Since antennas are employed for a variety of applications, many different types of antennas had been developed, each suited to a particular type of application.

1.1 Types of Antennas

Antennas may be broadly categorised into dipole and aperture types. Simple one dimensional antennas like short and long wires, monopoles, dipoles and loops come

1

under the category of dipole antennas. Aperture antennas
concentrate, confine and guide the radiated energy so that
it appears as though passing through an aperture.

1.1(i) Dipole Antennas

One dimensional linear wire antenna is the
simplest form of an antenna. This type of short and long
wires which provide information for comparing other antennas,
have a uniform current distribution over its entire length.

One of the most commonly used antennas is the
centre-fed dipole which consists of a wire whose length is
an appreciable portion of a wavelength. This wire is fed
by a voltage generator at its centre. The current distri-
bution on these types of antennas is approximately sinusoidal
with zero currents at the ends of the antennas. For short
dipoles, the current distribution is approximately triangular,
instead of sinusoidal.

Another type of antenna that is widely used for
broadcast applications, is the monopole antenna. This is
a modification of the dipole in which a plane conducting
screen is placed at the centre of the antenna at right
angles to the antenna axis. Currents flowing in the condu-
cting screen simulate the missing half of dipole to create
an image in the same way as a mirror forms an optical

image. The monopole antenna is usually preferred to a
dipole for situations requiring an omnidirectional, verti-
cally polarized antenna because the monopole is cheaper to
construct and the earth can be easily used as the conduct-
ing ground plane.

Folded dipole is a modification of ordinary
dipole and it consists of two or more electric dipoles
joined at the ends. In this case the antenna terminals
are located at the centre of one of the conductors. Another
important antenna which finds extensive application in
direction finding is the loop antenna. It is made up of
one or more turns of highly conducting wire around a frame
that may have a circular, square or rectangular shape. A
small loop antenna is also used as a probe for measuring
magnetic fields.

Many other types of antennas have been developed
for special applications. Turnstile antenna, consisting
of two dipoles oriented at right angles to each other, is
widely used for producing elliptically and circularly
polarized beams. A few of the different types of dipole
antennas are shown in Fig.1.1(i)(a).

1.1(ii) Aperture Antennas

Dipole antennas have low gain and omnidirectional
radiation patterns. Hence antennas having larger effective

Ordinary dipole   Folded dipole   Biconical dipole
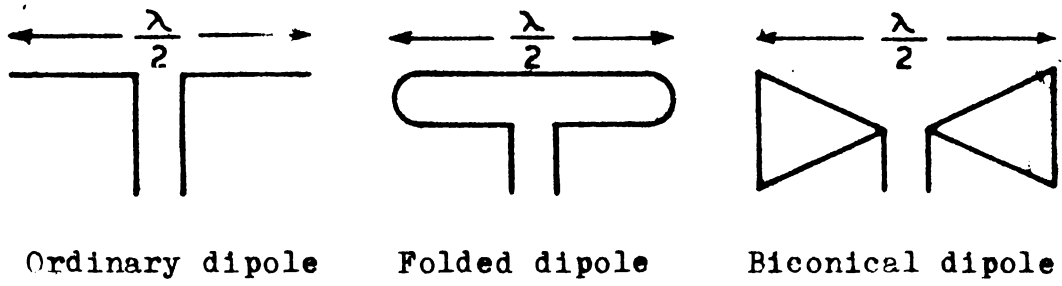
Fig.1.1(i)(a)   Sketch of different types of half-wave
dipole antennas.

S_a

Horn   Lens   Reflector
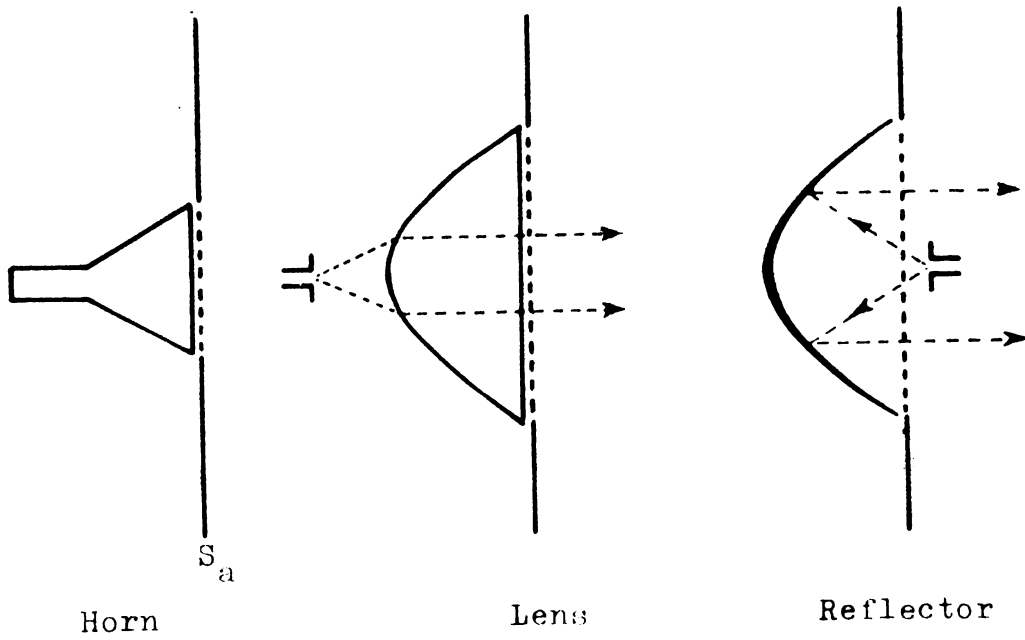
Fig.1.1(ii)(a)   Sketch of different aperture type
antennas. S_a is the aperture surface.

4

area, called aperture antennas, are employed for situations requiring higher gain and more directive radiation patterns.

There are many types of aperture antennas for which the electromagnetic radiation may be considered as passing through a physical aperture. The horn, lens and reflector antennas, shown in Fig.1.1(ii)(a), belong to these class of antennas.

Horn antennas have a variety of shapes in order to control the different antenna characteristics like gain, radiation pattern and impedance. An important advantage of horns is that it can eliminate feed-to-radiator transition losses[98]. A detailed discussion of these types of antennas will be presented in the next section.

Reflector antennas are used with radar and communication systems in which a large gain is required. These antennas consist of a relatively small feed and a large reflecting surface and produce pencil, fan or specially shaped radiation patterns. For paraboloidal reflector antennas, which is generally used for many applications, the reflector is conventionally a symmetrical, cylindrical or offset parabola. In order to avoid the aperture blocking due to the feed and losses encountered with a small driven element, a special type of reflector antennas, called

Cassegrain antennas, are employed. In this system, the energy is fed through the rear of the centre of the main parabolic surface.

Corner reflectors are another type of directive radiators which use a dipole as the primary radiator. Different characteristics of this type of antennas will be given later. There are several other reflectors like pill box, parabolic torus and hog horn designed for specific applications.

Microwave lens antennas employ dielectric material to focus the energy and to produce narrow pencil beam radiation. One of the advantages of the lens antennas over the reflector types is that it has considerably less rearward radiation.

Surface wave antennas, a type of aperture antennas, operate because of the discontinuity of guiding surface which causes the wave to give out power. Another type called slotted waveguide antenna radiates energy by virtue of the discontinuities introduced by insertion of longitudinal slots. By varying the length and position of the slots, the radiation from these antennas can be conveniently controlled.

Arrays of these aperture antennas are also widely used for obtaining higher directivity and gain.

1.2 Electromagnetic Horn Antennas

Electromagnetic horn antennas are the convenient form of directional antenna systems, capable of accommodating a broad band of frequencies. In the words of Southworth[1] " An electrical horn not only possesses considerable directivity but it may also provide a moderately good termination for the pipe to which it is connected. In so doing, its function is probably quite analogous to that of a true acoustic horn which provides an efficient radiating load for its sound motor".

Since the directivity is proportional to the aperture size, it may seem that higher directivity can be achieved by increasing the waveguide dimensions. But, if the dimensions of the waveguide are sufficiently large, higher order modes will be generated. Greater directivities without higher order modes can be achieved by a gradual transition produced by flaring the terminal section of waveguide to form an electromagnetic horn. Though higher order modes are generated at the throat, the horn acts as a filtering device allowing only a single mode to be propagated freely to the aperture. The horn will not support

free propagation of a particular mode until roughly the transverse dimensions of the horn exceed those of a waveguide which would support the given mode. Thus, unless the flare angle is too large, all but the dominant mode will be attenuated to a negligible amplitude in the throat region before free propagation in the horn space is possible.

Horn antennas are constructed in a wide variety of shapes to suit specific requirements. Pyramidal horns, sectoral horns and circular horns are the most frequently used types of horns. Fig.1.2(i) shows the different types of horns.

For a pyramidal horn, with flaring in both the principal planes, the gain can be calculated from its dimensions to a good degree of accuracy. Hence, these are commonly used as primary gain standard. Again, these are used to obtain certain specific radiation patterns independently in the two principal planes.

Sectoral horns are a special type of pyramidal horns where only one plane (E or H) is flared, with the other two opposite sides remaining parallel to each other. If the E-plane of a rectangular waveguide is flared, then it is called an E-plane sectoral horn and if the H-plane is flared it is called an H-plane sectoral horn. They are
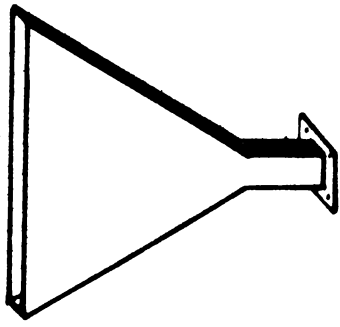
H-plane sectoral horn
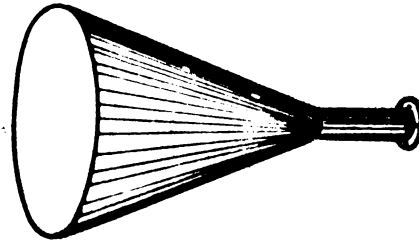
Conical horn
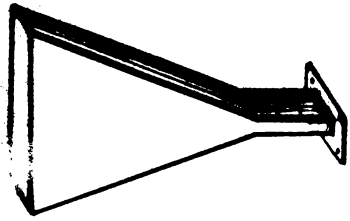
E-plane sectoral horn
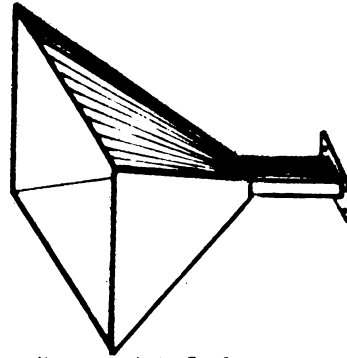
Pyramidal horn

Fig.1.2(i)   Sketch of the different types of horns
that are generally used.

9

generally used to obtain beams of specified sharpness in the plane containing the flare. The pattern in the unflared plane will be the same as that of an open-ended waveguide.

Conical horns are simple antenna structures, capable of handling any polarization due to its complete axial symmetry. These are also used as primary gain standard because the gain of conical horns can be accurately calculated.

Another type of horn antenna which gives rotationally symmetric radiation patterns and broad band performance was realized by Simmons and Kay[33] and is called 'scalar feed'. The 'scalar feed' is a conical horn antenna with grooves perpendicular to the wall of the horn.

The biconical horn finds use where an omni-directional horizontal radiation pattern is desired. This type of antenna finds extensive use in the VHF-UHF band for broadcasting purposes.

Besides, there are different types of horns like hog horn and asymmetric horn which are used as efficient feeds for parabolic antennas.

1.3 Beam Shaping of Sectoral Horns

Several methods have been developed[52-59] to
modify the radiation from sectoral horn antennas. Corrugat-
ing the walls of sectoral horns is one method to obtain
symmetric beam pattern and broadband performance.

Another method of improving the directivity of
sectoral horns is the use of metal plate lenses suggested by
Rust[8]. Dielectric pieces cut in specific shapes placed at
the mouth of sectoral horns also have been found to be
improving the radiation characteristics of sectoral horn
antennas. The use of such dielectric loaded horn antennas
can increase the directivity of the antenna in its flared
plane.

For many applications like illuminating a para-
boloidal reflector antenna, it is desirable that the
radiation pattern of the feed should be symmetrical about
their principal axes. Hence, in order to get a symmetrical
radiation pattern from a sectoral horn, the beam shape in
its unflared plane also should be modified. The flange
technique, suggested by Owen and Reynolds[57] and later
modified by several other workers[58-67], is an efficient
and simple method to control the pattern shape in the
unflared plane of sectoral horns. They have shown that,

by controlling the various flange parameters like flange
width, flange angle etc., the radiation pattern in the
unflared plane of H and E-plane sectoral horns can be con-
veniently adjusted.

1.4 Horn Antennas as Circularly Polarized Radiators

Circularly polarized radiators are often required
by communication satellite antenna because it can respond
to a linearly polarized wave of arbitrary orientation. A
horn antenna can be used to produce circularly polarized
radiation, if it is fed with waveguide capable of propagat-
ing vertically and horizontally polarized waves simultaneously.

When the horn is fed through a square waveguide
with equal amplitude vertically and horizontally polarized
modes arranged to be in quadrature, a circularly polarized
field will be obtained at the peak of the radiation. At
other points on the radiation pattern, the radiated field
will not be circularly polarized because the beamwidths of
the vertically and horizontally polarized radiation patterns
will be different in any particular plane.

A diagonal horn antenna, suggested by Love[85]
also can be used to produce circularly polarized waves. In
a diagonal horn antenna, the mode of propagation within the
horn is such that the electric vector is parallel to one of

the diagonals. By inserting a differential phase shifter in the waveguide, a phase quadrature between the two orthogonal modes in the diagonal horn can be obtained. A properly designed differential phase shift section can produce circular polarization over a wide range of frequencies.

1.5 Corner Reflector (CR) Antennas

This new type of antenna system was first suggested by Kraus[73]. The corner reflector antenna, which consists of two conducting planes that intersect at an angle and a driven radiator (usually a half-wave dipole), has been widely used as a compact high gain antenna because of the simplicity of its construction. The dipole radiator of the CR antenna can be either vertically oriented (parallel to the apex of the CR system) or horizontally oriented (perpendicular to apex), as shown in Figs.1.5(i) and (ii) respectively. Assuming the reflector elements to be perfectly conducting and infinite in extent and by using the method of images Kraus derived analytical expressions for the gain and directional radiation patterns of the antenna.

The distance of the primary feed (usually dipole) from the apex of the reflectors and the corner angle of the CR system are important parameters determining the shape of the radiation pattern of the antenna. According to Kraus[73],
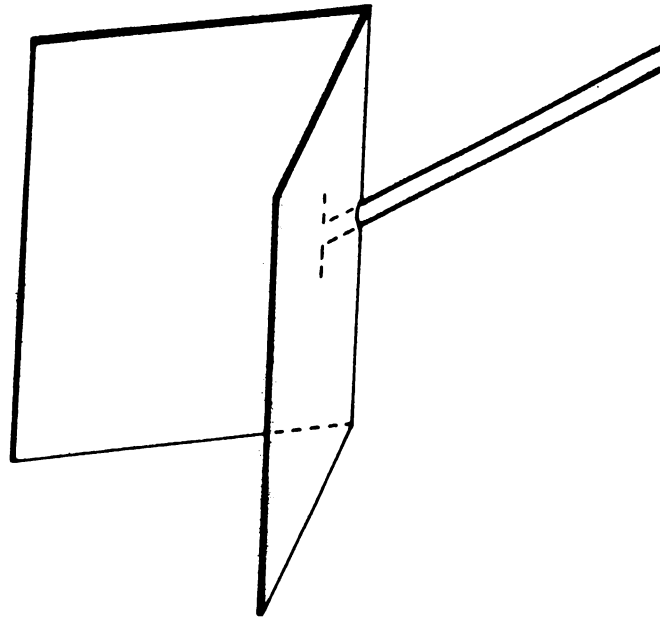
Fig.1.5(i)   Schematic representation of corner
             reflector antenna with vertically
             oriented dipole feed.
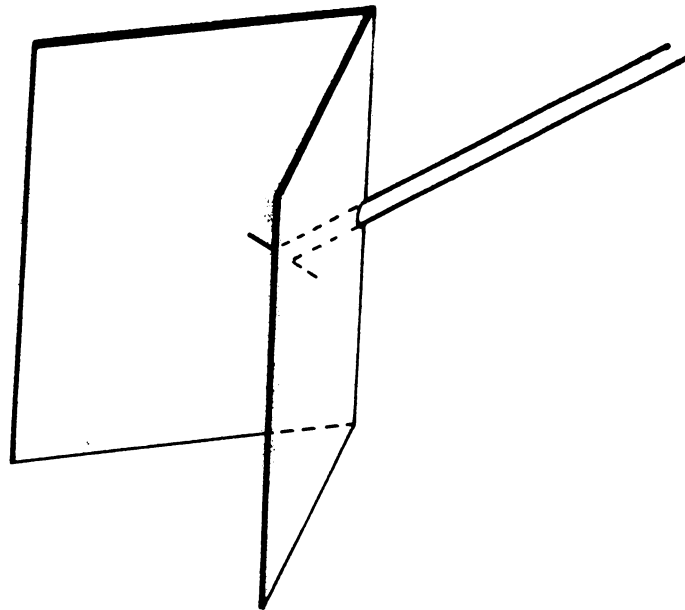
Fig.1.5(ii) Schematic representation of corner
             reflector antenna with horizontally
             oriented dipole feed.

14

when the reflector elements have large dimensions, the width and length of the elements have negligible effect on the radiation pattern. One of the important effect of corner reflectors is to concentrate the radiation in the direction of the bisector of the corner and to produce a focused beam in the axial direction.

When the corner angle is 90°, the reflecting sheets intersect at right angles, forming a "square corner reflector". An interesting property of the square corner reflector is that, when the driven dipole is displaced to one side of the plane bisecting the corner angle, the maximum of the directional pattern is displaced to the opposite side. Thus, by using two suitably displaced dipoles, two directional patterns are obtained having their maxima displaced to opposite sides of the bisecting plane. Such an arrangement finds very useful applications in a single-course radio range beacon or an airport runway localizer.

An important characteristic of the CR antenna is that it will return a signal in the same direction exactly in which it was received. Because of this characteristic, military vehicles and ships avoid, in their design, sharp corners which can form corner reflectors. Such structures make it easier to be detected by enemy radars. Again, a uniform directional pattern in the horizontal plane, often

required in radio broadcasting, can be easily achieved by employing a number of CR antennas, oriented in different directions. Since the reflector dimensions are not critical regarding the frequency, the CR systems are well suited for transmission and reception of broad frequency bands, such as used in television and wideband frequency modulation.

Corner reflector antennas also can be used for producing circularly polarised radiation by adjusting the various antenna parameters. For certain corner angles such that the horizontal and vertical components of radiation are in phase quadrature, the orientation of the dipole can be adjusted so that they have equal magnitude, and the resultant radiation is then circularly polarized. For corner reflectors whose apex angles are submultiples of 90°, circular polarization is found to be possible for every dipole-to-apex spacing except those for which the horizontal or vertical component of radiation becomes zero. Thus, by properly adjusting the distance of the primary feed dipole and its orientation, the simple CR antenna can be easily converted to a circularly polarized radiator.

1.6   Brief Sketch of the Present Work

Improving the performance of sectoral horns and corner reflector antennas have been a subject of interest

for many years, because of their suitability in communication
and radar applications. The use of corrugated surfaces have
already been proved to be effective in improving the radiation
characteristics of sectoral horn antennas[33-35]. In the
present study, the possibility of controlling the different
antenna characteristics like radiation patterns and matching
conditions of sectoral horns and CR systems have been investi-
gated in detail.

Investigations were carried out on the various
antenna characteristics of plane flanged sectoral horns and
plane CR systems. The important aspects taken for this
study include the variations in beamshape, gain and impedance
conditions with various parameters like frequency and
included angle of flanges or reflectors. A comparative
analysis between the results obtained with both systems have
indicated an analogy between the behaviour of flanged horns
and CR systems. Hence, intense study on both systems using
corrugated flanges and corrugated reflectors were performed
to investigate the validity of this analogy between the two
systems and to improve the performance of these antennas.
A method has also been developed to obtain elliptically and
circularly polarized radiation from both flanged horns and
CR systems using surfaces with inclined corrugations.

A theoretical analysis of the radiation from flanged sectoral horns is attempted on the basis of the Line Source Theory. For explaining the results obtained using CR system, the method of images have been employed. Radiation patterns were computed on the basis of these theories and they show fairly good agreement with the experimental results.

A brief outline of the work presented in this thesis is as follows: Chapter 2 presents a comprehensive study of the past work done in the field of electromagnetic horns and CR systems. In this chapter, various papers dealing with theoretical and experimental investigations on horns and corner reflectors are reviewed. Different methods to modify the radiation characteristics of these antennas are studied. The purpose of this chapter is to provide an insight into the different types of techniques employed for beam shaping of sectoral horns and corner reflectors.

Chapter 3 is exclusively devoted for describing the various experimental techniques employed in the present investigation. The important equipment and antenna components used in this study are also described in this chapter.

In chapter 4, the experimental results obtained using flanged sectoral horns and CR systems are presented. The results obtained using inclined corrugated flanges and reflectors for producing elliptically and circularly polarized radiation are also given in this chapter.

Theoretical aspects of flanged sectoral horns and CR systems are discussed in chapter 5. Radiation patterns, plotted using the theoretical expressions derived, have been compared with the experimental results. In analysing the radiation from the CR systems, the primary feed dipole has been approximated as an infinitesimal one.

In chapter 6, the final conclusions drawn from the study on flanged sectoral horns and CR systems are presented. The advantages obtained by the use of corrugated surfaces and the similarity in behaviour between the two systems are pointed out in this chapter. The scope for further work in this field is also indicated.

While taking antenna measurements inside an anechoic chamber, an antenna positioner (turn-table) has been used. The positioner is fully automatic and is operated from outside where recording instruments are arranged. This remote control system was designed and fabricated as an ancilliary work and a description of this is presented in Appendix I.

A major part of the work presented in this thesis was performed inside a microwave anechoic chamber, the design and fabrication of which is recently completed. The performance evaluation of this chamber was a part of the activity of the author. This evaluation procedure and the results therefrom are discussed in Appendix II.

CHAPTER II

REVIEW OF THE PAST WORK IN THE FIELD

Radiation characteristics of electromagnetic horn antennas and corner reflector systems were studied theoretically and experimentally by several investigators. A bulk of such investigations have been reported in literature. This chapter provides a brief review of the work published in the field of electromagnetic horns and corner reflector antennas.

2.1 Electromagnetic Horn Antennas in General

Though, Barrow[2] suggested the concept of electromagnetic horn in 1936, the actual experimental investigations on horn antennas were started only in 1939 by Barrow and Lewis[3]. They conducted elaborate experimental investigations on sectoral horns. Their studies revealed that electromagnetic horn antennas possessed broad bandwidth, high directivity and low side lobe level.

In a companion paper, Barrow and Chu[4] gave theoretical analysis of the operation of the electromagnetic horns, based on Maxwell's equations. Though the analysis applies specifically to sectoral horns, it provides a clear physical picture of the operation of electromagnetic horns of any shape.

21

Using Huygens' principle, they calculated the shape of the radiation field at a large distance from the mouth of the horn, by assuming the distribution across the mouth to be same as if the sides of the horn were extended to infinity. The radiation patterns calculated on the basis of this analysis were found to be in satisfactory agreement with the experimental results reported by Barrow and Lewis[3].

Southworth and King[5] conducted experiments to determine the directive properties of circular waveguides and conical horns. Their investigations showed that conical horns can provide power improvements of some hundred times that of an ordinary simple half-wave antenna. They also studied the effect of horn dimensions on the directivity of the antenna and showed that there is an optimum angle of flare giving maximum directivity.

Some important principles for the design of sectoral and pyramidal horns were given by Chu and Barrow[6]. According to them, for sufficiently great horn lengths, the beamwidth of the radiation pattern is almost equal in magnitude to the flare angle.

In another paper, Chu[7] gave a theoretical analysis for the radiation properties of hollow pipes and horns. Using vector Kirchhoff formula, he derived expressions for the

radiation fields from the transverse electric wave in hollow pipes of circular and rectangular cross section. The formulae for the radiation fields of TE_{01} and TE_{10} waves in a sectoral horn are also given in this paper.

A 'microwave lens' technique for phase correction of horn radiators was put forward by Rust[8] in 1946. He used metal partitions acting as sections of waveguides to obtain the correction. The partitions were arranged radially and the correction is effected by adjusting their length.

Extensive experimental investigations on the radiation patterns of electromagnetic horn antennas were carried out by Rhodes[9]. He measured the radiation patterns of a number of horns with lengths ranging from zero to fifty wavelengths. His results showed that, as the aperture of the horn becomes very large, the E-plane pattern has large number of side lobes of considerable magnitude.

Bennett[10] analysed the sectoral horn antenna by considering it as one component of an over-all microwave transmission system. Equivalent network functions were derived on the assumption of the sectoral horn as a non-uniform transmission line. The physical significance of the derived normalised functions is also discussed in this paper.

A method for computing the radiation patterns of rectangular and circular horns for some common modes of vibration is developed by Horton[11]. He argued that the radiation patterns derived for an open waveguide may be applied directly to an electromagnetic horn, as long as the flare angle is not too large. He also presented a few experimental observations to illustrate the fairly good agreement between theory and experiment.

King[12] reported the experimental results observed with conical horn antennas employing waveguide excitation. Conical horns giving maximum gain for a given axial length were considered by him as optimum horns. He gave the dimensional data in terms of wavelength for the design of optimum horns.

In the same year, Schorr and Beck[13] published a paper in which they calculated the radiation from conical horn in integral form. The calculated radiation patterns showed fairly good agreement with experimental results, for horns of small flare angle and moderate length.

Jakes[14] performed experimental investigations to calculate the gain of pyramidal horns. By measuring the power transmitted between two identical horns, he estimated the error experimentally in the theoretical value of the gain and found it to be less than 0.2 db.

Braun[15] gave further experimental verification
for the variations in the measured gain with aperture separa-
tion of horns. He also developed a theory which was found to
be in good agreement with experimental data. He presented a
set of curves from which the error in gain can be directly
determined.

In a subsequent paper, Braun[16] presented a table
from which the gain of sectoral horns can be readily deter-
mined by knowing their aperture dimensions. He gave a simple
procedure for the design of optimum horns having specified
characteristics.

Epis[17] employed several aperture modifications to
conical and square-pyramidal horns, for obtaining an axially
symmetric radiation pattern. The important advantage of
these types of horns, called compensated horns, is that the
equalisation of E- and H-plane patterns is present for all
polarizations.

Walton and Sundberg[18] suggested a method to
increase the bandwidth of operation of ridged horns. The
large phase error occurring at the mouth of the horn is the
basic reason for the low bandwidth of these types of horns.
According to their design, a dielectric lens can be easily
used to reduce the phase error to a minimum.

A method for calculating the E-plane pattern of horn antennas using diffraction theory was put forward by Russo et al[19] in 1965. When the diffraction theory is applied to horns, the radiation from the horn is considered to be due to the diffraction by the E-plane edges and by direct radiation from apex of the horn. Theoretical and experimental patterns were found to be in excellent agreement. In another paper, Yu et al[20] used the same edge diffraction techniques to analyse the radiation from typical horn antennas. In their paper, the higher order diffraction at the edge and the reflection inside the antenna had also been taken into consideration.

Using near field power transmission formula, Chu and Semplak[21] calculated correction ratios for the far zone gain of pyramidal horns. They applied these calculated corrections in the absolute gain measurement of a standard horn. Using these corrections they achieved an accuracy well below 0.1 db in the gain measurement of pyramidal horns.

Jull[22] gave some revised corrections to determine the gain measurements more accurately. He also estimated the accuracy of Schelkunoff's[23] gain-expression. In another paper, Jull[24] incorporated the finite-range effects in the Fresnel zone into Schelkunoff's gain-formula for pyramidal horns. Thus he obtained a more accurate expression for the

gain of pyramidal horn antennas. The gain of E- and H-plane sectoral horns could be easily found by omitting certain terms from this expression. Jull[25] also used the geometrical theory of diffraction to account for the small oscillations observed in the gain versus wavelength curve of horns.

Hamid[26] applied the geometrical theory of diffraction by Keller, to investigate the gain and radiation pattern of conical horns. In his analysis the edge rays excited at the aperture plane of the horn were also taken into account. The predicted results for the gain and radiation pattern of conical horns of various dimensions showed excellent agreement with the experimental results of King[12].

Muehldorf[27] calculated the phase centres of different antennas, based on a vector approach. He also gave graphs to show the dependence of the phase centres on the horn dimensions.

Kerr[28] reported the design of short axial length broadband horns which find extensive use for electromagnetic compatability measurements.

Using geometrical theory of diffraction, Jull[29] derived the complex reflection coefficient of a long E-plane sectoral horn which agrees well with experiment.

Jull[30], in another paper, developed a new gain
formula in accordance with one of his earlier proposals[31].
This new formula was found to agree much more with experiment.

Mentzer[32] used slope diffraction function to
evaluate the H-plane pattern of a horn antenna. The computed
patterns showed excellent agreement with experimental results.

2.2 Corrugated Horns

Investigations by Simmons and Kay[33], in the United
States, indicated that grooved walls in a horn can produce a
tapered aperture field distribution in all planes. The chara-
cteristic of such a grooved wide flare angle horn, called
'scalar feed', is that the radiated energy is confined to the
angular sector determined by the horn's flare angle. Besides,
the beamwidth of the horn is a constant over a wide frequency
band. His studies also showed that the gain of the 'scalar
feed' is 0.6 to 0.8 db higher than that of a standard feed.

Lawrie and Peters[34] have demonstrated that the use
of a corrugated structure in the walls of a horn can reduce
the back lobe level of the antenna. Such a horn was found to
produce an equal E- and H-plane pattern.

Clarricoats and Saha[35] analysed the propagation
behaviour of corrugated cylinder and presented results which

help to the design of horns with narrow-flare-angles and of circular cross sections. A procedure for obtaining a balanced hybrid condition in the horn aperture was also discussed by him.

The effect of frequency on the symmetry properties of the balanced-hybrid-mode fields propagating in corrugated conical horns were studied by MacA. Thomas[36].

Narasimhan and Rao[37,38] derived expressions for the radiation pattern and gain of corrugated conical horns. Their theoretical results were in close agreement with the experimental results of Jeuken[39,40].

Clarricoats and Saha[41,42] in a long two-part paper, reported an exhaustive theoretical and experimental investigation of the propagation and radiation behaviour of corrugated feeds. The first part of these papers deals with the analysis of corrugated waveguides. In the second part, the radiation patterns of corrugated conical horns obtained by a Kirchhoff-Huygen aperture integration method and a new method, called modal expansion, are presented.

Clarricoats et al[43], in another paper, analysed the near-field radiation characteristics of corrugated horns by a spherical-mode-expansion method. Typical results

obtained for horns with flare semiangles of 12° and 70° are also presented in this paper.

Considering the radiation from the finite aperture of a corrugated horn, Baldwin and McInnes[44] checked experimentally an expression derived by Anderson[45] for the radiation pattern of a surface wave antenna.

Mentzer and Peters[46] studied the influence of corrugation parameters on the power loss, surface current and the scattering from a groundplane-corrugated surface junction. The same authors, in another paper[47], analysed the radiation patterns of corrugated horns using aperture integration and diffraction theory. Their method could predict the E-plane side lobe and back lobe levels of corrugated horns.

Baldwin and McInnes[48] studied the propagation and radiation characteristics of moderate-flare-angle rectangular horns which have transverse corrugations on two walls. In the same year, these authors published another paper[49] which described the design of a corrugated horn to produce an elliptical beam for either of two orthogonally polarized signals.

Bielli et al[50] developed a new method for computing the phase centre of corrugated horns. The same authors[51]

also analysed the characteristics of corrugated conical horns radiating in a balanced hybrid mode.

2.3 Beam Shaping and Polarization Characteristics of Horn Antennas

Pao[52] from his elaborate study on horn antennas, observed that small pins and other obstacles placed at the mouth of H-plane sectoral horns are useful in narrowing the primary H-plane patterns of the antenna. The impedance matching was also found to be improved by the presence of the pins.

Hariharan and Nair[53-54] conducted a series of experiments on sectoral horn antennas fitted with grills. Their investigations indicated that the grill system modifies the E-plane radiation patterns of E-plane sectoral horns with considerable improvement in impedance conditions. Nair et al[55-56] analysed the effect of grills on the radiation patterns of sectoral horns. Their theoretical results were in good agreement with experimental observations.

Owen and Reynolds[57] were the first to study the effect of flanges on the E-plane patterns of H-plane sectoral horns. Later Butson and Thompson[58] conducted an exhaustive study on flange mounted sectoral horns and waveguides. They

derived an expression for the far field radiation patterns from these antennas, assuming the aperture of sectoral horn as a linear source.

Nair and Srivastava[59] observed that the position of flanges from the aperture of horn affects tremendously the shape of the radiation pattern. A bulk of experimental and theoretical investigations were reported by Nair et al[59-67] to establish the effect of flanges on the radiation characteristics of sectoral horns. They also found[68] that the H-plane pattern of E-plane sectoral horns could be controlled with metallic flanges.

Ching and Wickert[69] developed a multimode rectangular horn antenna generating a circularly polarized beam. Polarization properties of this antenna reveal that it has a very low off-axis polarization axial ratio.

Using circular waveguide loaded with reactive irises, Gruner[70] designed a circularly polarized feed horn. He obtained axial ratio below 1.65 db, over a wide frequency band. Ebisui et al[71] also used flare-iris type dual-mode horn antenna to obtain a perfect circularly polarized radiation.

Ebisui[72], in another paper, described the theory
of a circularly polarized flare-iris type dual-mode horn
antenna and measured the radiation and polarization chara-
cteristics by a model antenna. They obtained an axial ratio
below 0.3 db in the frequency band 3.9 to 4.2 GHz.

2.4 Corner Reflector Antennas

Kraus[73] found that a highly effective directional
system results from the use of two flat, conducting sheets
arranged to intersect at an angle forming a corner. The
performance of such a beam antenna called corner reflector,
was theoretically and experimentally studied by him. He used
the method of images to calculate the radiation from corner
reflector. The computed and measured directional patterns
were in good agreement.

Moullin[74] gave more theoretical background and
design data of corner reflector antennas. He proved that the
directional pattern of a corner reflector system can be
expressed in the form of a series of Bessel functions. Wait[75]
showed that Moullin's theory can be extended to any angle by
simply admitting multi-valued solutions of the wave equations
in cylindrical coordinates.

Harris[76] reported a detailed experimental investigation on the radiation patterns of corner reflector antennas. He studied in a systematic manner the variation in radiation patterns with different parameters of the corner reflector. He also investigated the beam tilting of the radiation pattern, when the driven dipole is kept off-axis.

Cottony and Wilson[77-78] also conducted exhaustive experimental investigations on the gain and radiation patterns of finite-size corner reflectors. They made a detailed and systematic study of the effects of length and width of reflecting surfaces on the gain of the antenna. In their second paper, they summarised the effect of widths and lengths of the surfaces on the widths of the main lobe in a series of curves. Their results also revealed that quite low levels of secondary radiation may be obtained by the use of corner reflector antennas of moderate dimensions.

Using geometrical method of diffraction, Ohba[79] calculated the gain and radiation patterns of corner reflect antennas finite in width. The results were compared with th experimental results of Cottony and Wilson[77-78]. In the rear direction, it was necessary to take into account the effects of the waves diffracted by the upper and lower edge of the reflector. His method can be used to compute the backscattering from an antenna having conducting plates finite in extent.

Proctor[80] presented a series of computer derived
design charts for maximising the radiated field from a corner
reflector. He has also given the optimum feed positions for
various corner reflector angles. According to him, the
length of the reflector should not exceed around three times
the spacing between the driven element and apex.

Aoki and Tsukiji[81] reported an analytic method
using field theory, for finding the radiation field of finite-
size corner reflector antenna. The method is useful to
analyse corner reflectors having arbitrary aperture angle
and unsymmetrical structure.

Ja[82] determined phase centres in the principal
H-plane of corner reflector antennas from computed and
measured phase patterns using numerical methods. Experiment-
al and theoretical results compare favourably with each
other. It is found that the distance between the phase centre
and the apex increases when the aperture angle decreases from
180° to 60°.

Woodward suggested[83] that circularly polarized
radiation can be obtained from corner reflectors by tilting
the orientation of the primary feed dipole. He used the
method of images to develop the basic theory of the antenna
producing circularly polarized radiation. Experimental

investigations have been carried out on the radiation characteristics as a function of the geometric parameters of the antenna. From this data, a circularly polarized corner reflector has been designed.

Klopfenstein[84] developed a theory for the corner reflector antenna excited by an infinitesimal dipole source which is tangent to a circular cylinder having the corner reflector as its axis. The results are applicable to reflectors of arbitrary apex angle. The various characteristics like electromagnetic field, directive gain etc. have been found in terms of an infinite series of Bessel functions. It has been shown that, for corner reflectors whose apex angles are sub-multiples of 90°, circular polarization is possible for every dipole-to-apex spacing except those for which horizontal or vertical gain becomes zero.

The importance of the study of radiation characteristics of sectoral horns and corner reflector systems can be understood from this review of the past work. It can be seen that no attempt has so far been made to conduct a detailed and systematic investigation on plane and corrugated corner reflector systems, and to present an exhaustive comparative study of the CR system with plane and corrugated flanged horns. The close similarity between the two systems is also not well established earlier. The work presented in this thesis is oriented towards these problems.

CHAPTER   III

EXPERIMENTAL ARRANGEMENTS AND MEASUREMENT TECHNIQUES

This chapter gives a brief description of the different equipment used and the techniques employed for the study of the various antenna characteristics presented in this thesis.

3.1   General Description of the Equipment

The microwave source, different waveguide components, sectoral horns, metallic flanges and corner reflectors are the major equipment used in this investigation.   Measurements have been mainly carried out at the X-band frequencies of 8.67 GHz, 9.3 GHz, 10.18 GHz and 10.76 GHz.   Just to verify the results obtained in the X-band, a few observations were made in the S-band frequency of 4.2 GHz also.   A description of the various equipment used in this study are given below.

3.1(i) Microwave Source and Waveguide Components

Reflex Klystron oscillator was used as the microwave source at 9.3 GHz.   A Gunn diode, with its power supply, was employed for obtaining power at other frequencies in the

X-band. At the S-band, a compact variable frequency unit consisting of a stabilized power supply and a Klystron, was used.

The reflex Klystron, mounted on a Klystron mount, couples microwave power through a probe to the waveguide system. A stabilized power supply is used for supplying necessary voltages to the Klystron. There is also provision for modulating the signal from the microwave source. Frequency of oscillation of the Klystron can be slightly varied by tuning its external cavity by means of small plugs which, when screwed into or out of the cavity, changes its size and resonant frequency.

The Gunn oscillator consists of a diode mounted in a high Q waveguide cavity tuned by a micrometer controlled moving short. The oscillator can be tuned over a broad range of frequencies in the X-band. A power supply having a voltage regulating circuit supplies necessary D.C. voltage to the Gunn oscillator. Amplitude modulation of the continuous wave output of the oscillator can be achieved by employing a PIN modulator. The same power supply used for the oscillator, also provides the necessary square wave voltage to the PIN modulator. In order to protect the oscillator from the R.F. power reflected by the PIN diode, an isolator or attenuator is usually used in between the oscillator and diode.

The S-band microwave source consists of the reflex Klystron mounted in an external co-axial resonator. The frequency of oscillations can be varied from 1.8 GHz to 4.2 GHz using a movable plunger which varies the resonant frequency of the cavity. The output power can be either continuous, amplitude or frequency modulated.

Attenuator, frequency meter, slotted line section, circulator and crystal detector are the important waveguide components used in this study. The attenuator controls the power output from the microwave source. For measuring the exact frequency of oscillation of the microwave power, a direct-reading frequency meter is employed. A slotted section with movable probe carriage is used to measure the voltage standing wave ratio. Three port circulator with one end terminating in a matched load is used as an isolator to protect the Klystron from any power reflected back from the antenna connected at the other end of the waveguide system. The crystal detector is mounted on a waveguide, having a variable short circuiting plunger.

3.1(ii)   Sectoral Horns

One of the major components in the equipment used for this investigation is the sectoral horn. For most of the experimental observations reported in this thesis,

H-plane sectoral horns are used. In order to compare the
action of vertically oriented corner reflectors with flanged
horns, a few observations are taken with E-plane sectoral
horns also. The sectoral horns are locally made with
moderately thin copper or brass sheets. The inner surfaces
are well polished to provide good conductivity. The horns
are constructed very carefully, in order to ensure symmetri-
cal patterns about the axis. A schematic diagram of the
E- and H-plane sectoral horns is shown in Fig.1(2)(i).

3.1(iii) Flanges

Metallic plane and corrugated flanges constitute
the most important part of the experimental set up for this
study. A flange is simply a metallic plane or corrugated
sheet with provisions for attaching to the horn. The flanges
are attached to a frame which can move smoothly over the
horn by means of a rack and pinion arrangement. Since the
flanges are attached to the frame by hinges, the flange
angle can be easily varied. A calibrated scale on the
parallel walls of the horn through the central line enables
measurement of distance of flange from aperture of horn.

In addition to the plane flanges, two types of
corrugated flanges have been used in the experimental study.
In one type of flanges, the corrugations are straight so

that, when the flange is mounted on the horn, the corruga-
tions will be perpendicular to the E-vector. In the other
type, called the inclined corrugated flanges, the corruga-
tions will be inclined at 45° to the electric vector.
Fig.3.1(iii)(a) gives a photograph of the different types
of corrugated flanges used in this study. Tables 3.1(I)
and 3.1(II) present the various parameters of the straight
and inclined corrugated flanges respectively. Fig.3.1(iii)(b)
is a photograph of the sectoral horn fitted with flanges.

3.1(iv) Corner Reflector

A corner reflector antenna consists of a driven
dipole radiator kept along the bisector of two metallic
reflectors which are joined along a line. A schematic view
of the corner reflector systems is shown in Fig.1.5(i) and
(ii). The driven dipole radiator used in this study is a
half wave dipole. As shown in Fig.1.5(i) and (ii), the
corner reflector can be fed either by horizontally oriented
dipole or by vertically oriented dipole. Most of the experi-
mental studies have been carried out using horizontally
oriented dipole fed corner reflector. The waveguide is
coupled to a co-axial cable, the other end of which feeds
the dipole. The cable passes through a small hole cut at
the centre of the wedge of the corner reflector. A cali-
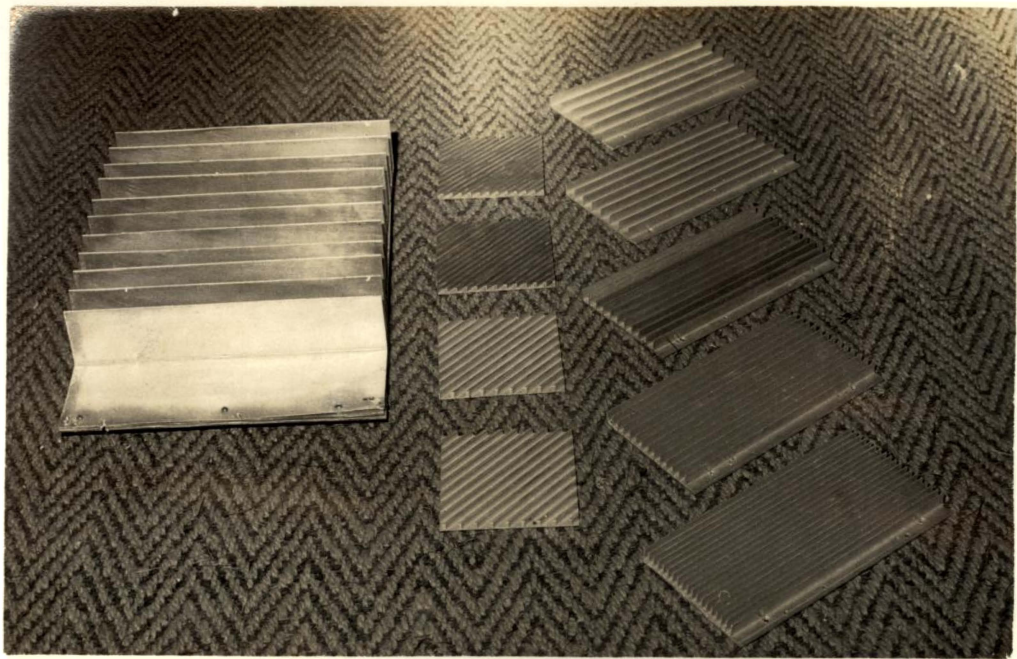brated scale on the cable is used to measure the distance

Fig.3.1(iii)(a) The various **corrugated flange/CR** **elements used in this study**

Fig.3.1(iii)(b) View of the flange mounted sectoral horn

Table 3.1(I)

Parameters of the different straight corrugated flange/
reflector elements used in this study

Flange/ reflector No.	Flange/ reflector width B (mm)	Corrugation depth h (mm)	Slot width d (mm)	Number of corrugations/ cm (N)
1	100	10	16	0.6
2	100	10	12	0.8
3	100	10	8	1.1
4	100	10	6	1.4
5	100	10	4	1.9
6	265	50	23	0.4

Table 3.1(II)

Parameters of the different inclined corrugated flange/
reflector elements used in this study

Flange/ reflector No.	Flange/ reflector width B (mm)	Corrugation depth h (mm)	Slot width d (mm)	Total No. of corrugations on the flange/ reflector element (N')
1	100	4.5	14.5	6
2	100	4.5	7	13
3	100	4.5	6	17
4	100	4.5	4.5	24

of the dipole from apex of corner reflector. For a comparative study between the behaviour of flanged horns and corner reflectors, identical systems had to be used in both cases. Hence, the dimensions and different parameters of the corrugated reflectors used are the same as those of the corrugated flanges. Fig.3.1(iv)(a) is a photograph of the corner reflector antenna used as a transmitter.

3.1(v)   Anechoic Chamber and Antenna Positioner

Though a major part of the work has been performed inside an anechoic chamber, the earlier part was done inside the laboratory using ordinary facilities. During the early stages of the work, a wooden turn-table capable of rotation about a vertical axis was used for mounting the test antenna. The turn-table was manually rotated in steps, and in each case the received power was noted using a high-sensitive spot galvanometer.

For making precise antenna measurements, a microwave anechoic chamber with remote control automatic pattern recording facilities was used. The anechoic chamber is an artificially simulated free-space environment in which antenna measurements can be performed without any interaction from external objects. The chamber is a large room, the interior surfaces of which are completely covered with
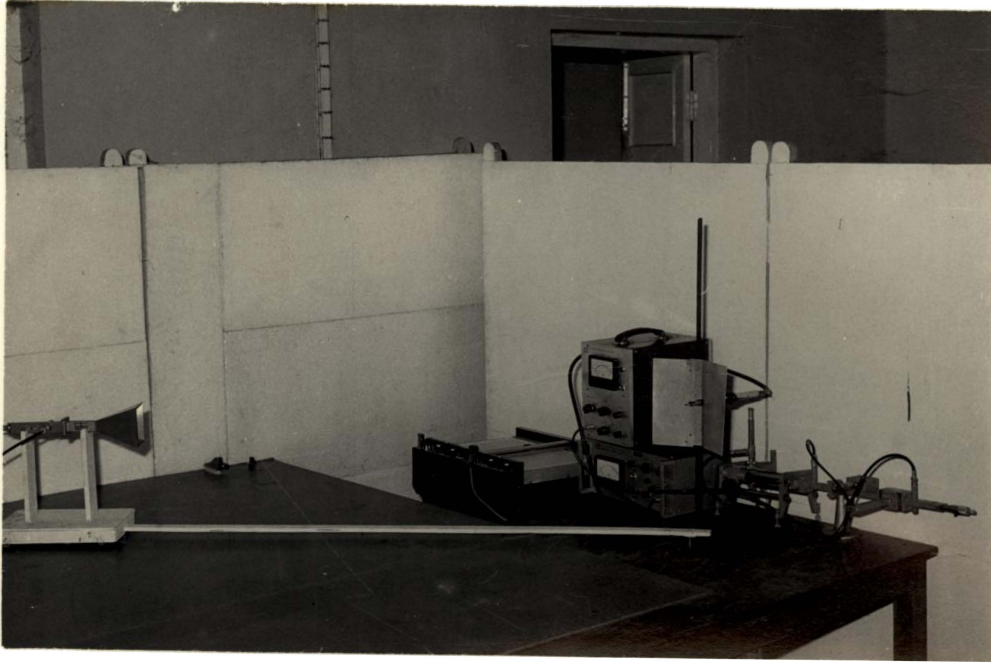
45

Fig.3.1(iv)(a)   Experimental set up for plotting radiation
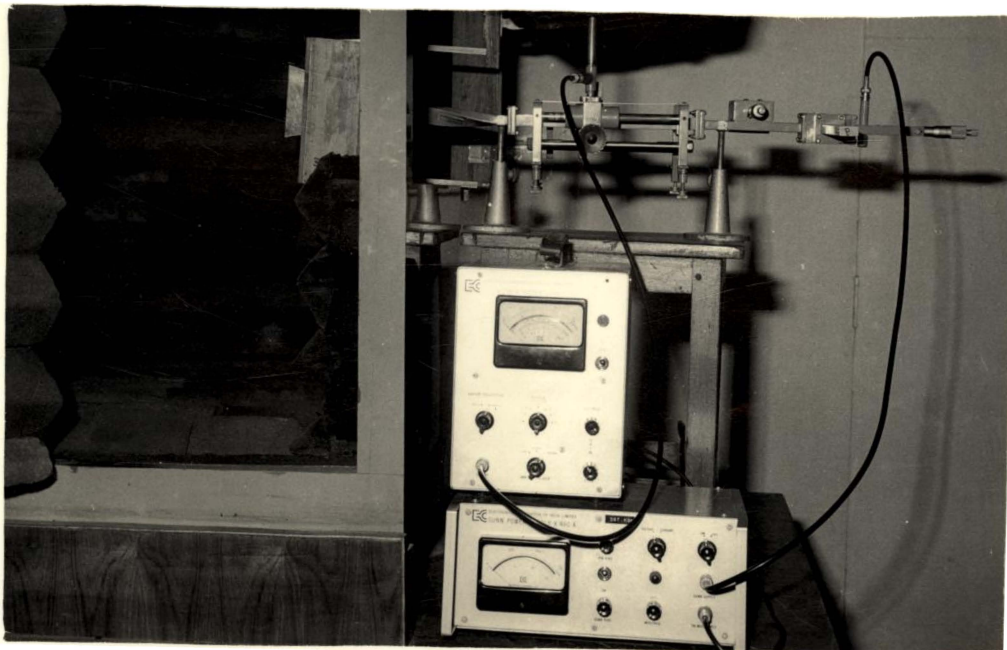patterns of corner reflector

Fig.3.2(i)   Experimental set up for measuring the VSWR
of flanged sectoral horn

microwave absorbing materials in the form of wedges and pyramids. In order to avoid external electromagnetic inter-ferences, a metallic shielding is given to this chamber. A description of the design, fabrication and evaluation of this anechoic chamber is given in Appendix II. The trans-mitter is set exactly at the apex of the tapered portion of the chamber.

An antenna positioner (turn-table) with full remote control facilities is employed for plotting the radiation pattern of the antenna under test. The turn-table is capable of rotation about a vertical axis at a uniform speed of 1 rpm. There is also provision for reversing the direction of rotation. After a certain angle of rotation, the turn-table will be stopped automatically with the help of limit switches. A wire wound potentio-meter, the shaft of which rotates in synchronisation with the turn-table platform, is employed for obtaining the angular position at any instant of the rotating platform. The voltage at the wiper terminals of the potentiometer is directly proportional to the angle through which the plat-form has rotated, and it is fed to the X-input of the X-Y recorder. The received microwave signal from the antenna, after rectification by the crystal diode, is fed to the Y-axis of the recorder. The turn-table control

system, the recorder and other measuring instruments are
kept in a control room adjacent to the anechoic chamber.
A detailed description of the design and fabrication of
the antenna positioner is given in Appendix I.

3.2   Measurement of On-axis Power Density and VSWR

On-axis power is the power of the electromagnetic
energy radiated along the axis of the antenna system. It
is an important characteristic because it is generally an
index to the sharpness of the radiation pattern of the
antenna.

In order to measure the on-axis power, a small
pyramidal horn receiver was placed at a point along the
axis of the test antenna. The distance of the pyramidal
horn from the test antenna is adjusted to be greater than
$\frac{2D^2}{\lambda}$, so that the point under consideration will be in the
far field of the test antenna, where D is the larger dimen-
sion of the antenna and λ is the free-space wavelength.
The axis of the pyramidal horn receiver mounted on an
adjustable stand is arranged to be collinear with the axis
of the transmitting test antenna. The output of the
crystal detector is fed to a sensitive spot galvanometer,
whose deflections are directly proportional to the
crystal current and hence to the power of the radiated

energy at the point where the crystal is kept. The galvano-
meter deflections can thus be taken as a measure of the on-
axis power density at the point. The readings are taken
manually for different types of flanged horns and corner
reflectors.

Impedance of an antenna system is of considerable
importance because it directly affects the efficiency of
energy transfer to or from the antenna. When the antenna
is not perfectly matched to the free space, the impedance
mismatch at the antenna aperture creates a reflected wave
forming a standing wave pattern in the waveguide. Using the
standing wave detector, the VSWR of the system can be
measured.

Since the VSWR of both flanged horns and corner
reflector systems are mostly measured at the 'Optimum' and
'Minimum' positions[59], the measurements of VSWR and on-
axis power density were conducted simultaneously. The
presence of the receiving horn will not affect the VSWR
of the transmitting flanged horn (or corner reflector) due
to the large distance between the two antennas. In order
to avoid any possible interaction from external objects,
the measurements are performed inside the anechoic chamber.

The conventional slotted line techniques is
employed for measuring the VSWR. A photograph of the
experimental set up for measuring the VSWR is shown in
Fig.3.2(i). The movable probe in the standing wave dete-
ctor, connected just before the test antenna, is adjusted
to have minimum probe penetration. The VSWR was measured
using a direct-reading VSWR meter. The amplitude modula-
tion of the microwave signal, required for this VSWR meter,
was obtained using a PIN modulator. The VSWR can also be
obtained by measuring the crystal current from the detect-
ing probe with a high sensitivity spot galvanometer or D.C.
micro-ammeter. By moving the probe through the slotted
section, the maximum (I_{max}) and minimum (I_{min}) values of
the crystal currents are noted. Since the output current
from the crystal is proportional to power, the VSWR S of
the system is given by

$$S = \frac{\sqrt{P_{max}}}{\sqrt{P_{min}}} = \frac{\sqrt{I_{max}}}{\sqrt{I_{min}}}$$

The values of VSWR were calculated for various parameters of
the flanged horns and corner reflector systems.

3.3 Radiation Pattern

The radiation pattern of an antenna is its most
important characteristic since it determines the spatial

distribution of the radiated energy. It is a graphical representation of the radiated energy as a function of direction. For plotting the radiation pattern of an antenna, different methods can be used. One method is to use the antenna under test as the transmitter of electro-magnetic waves. In the other method, the test antenna is used as the receiver of microwave signal transmitted by a standard pyramidal horn. According to the theorem of reciprocity, the antenna characteristic will be the same in both these cases. Most of the patterns presented in this thesis have been plotted using the second method. The first method is also employed in certain cases, especially for taking some observations on corner reflector antennas.

In order to plot the radiation pattern using the first technique, the antenna under test is used as the transmitter of CW signal from a Klystron or Gunn source. A small pyramidal horn receiver, mounted on a stand, is capable of rotation about an axis passing through the centre of the aperture of the test antenna. Thus the receiving antenna can be moved along the circumference of a circle of radius $R > \frac{2D^2}{\lambda}$, with the transmitter at its centre. As pointed out in the earlier section, the limit of the distance criteria is adopted for taking the observations only in the far-field region of the antenna. The power

received by the pyramidal horn, after rectification by a microwave diode (usually type IN21, IN23 or IN415B), is fed to the Y-input of a X-Y recorder. A potentiometer at the centre of the circle is capable of rotating with the movement of the receiving antenna. The wiper voltage of the potentiometer, giving the angular position of the receiver, is fed to the X-input of the recorder.

In the second method of plotting radiation patterns, the test antenna, used as the receiver, is mounted on a turn-table. In the earlier part of the work the radiation patterns were taken manually using a wooden turn-table with a circular scale attached to it, and a sensitive galvanometer. In the latter part of the work, an automatic turn-table and an X-Y recorder have been used for recording the patterns. The measurements were taken inside an anechoic chamber, with the turn-table placed at the centre of the quiet-zone. The transmitting pyramidal horn was placed at the apex of the anechoic chamber as shown in Fig.3.3(i). The rectified signal output from the receiver and the wiper voltage from the potentiometer of turn-table are fed to the two axes of the X-Y recorder. For plotting the patterns, a highly sensitive HP model 7047A X-Y recorder is used. Figs.3.3(ii) and (iii) give the photographs of the transmitter set-up used in the X- and S-bands respectively.
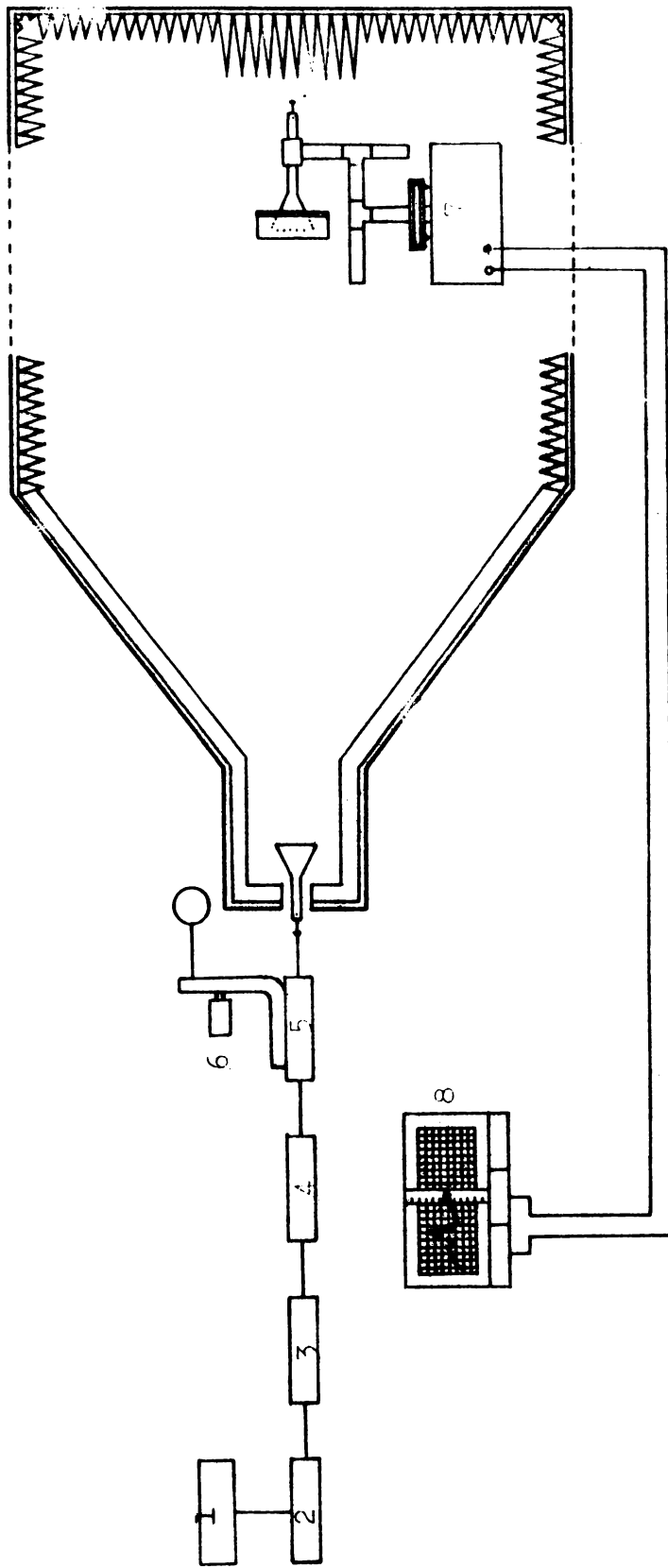
Fig.3.3(i) Schematic representation of the experimental set up used to plot radiation patterns of flanged sectoral horns. 1. Gunn power suppl., 2. Gunn oscillator, 3. Isolator, 4. Attenuator, 5. Directional coupler, 6. Frequency meter, 7. Turn-table, 8. X-Y Recorder.
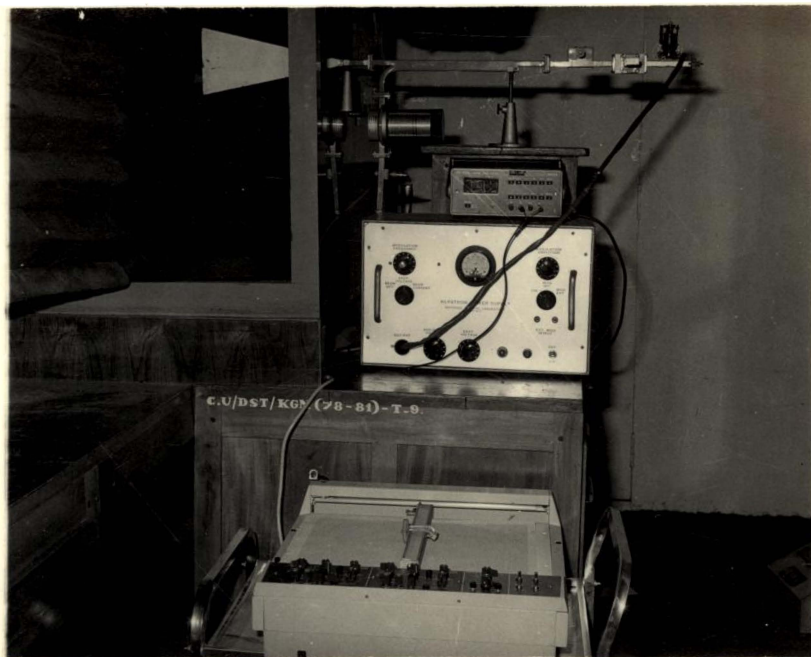
Fig.3.3(ii) Transmitter set up for plotting radiation
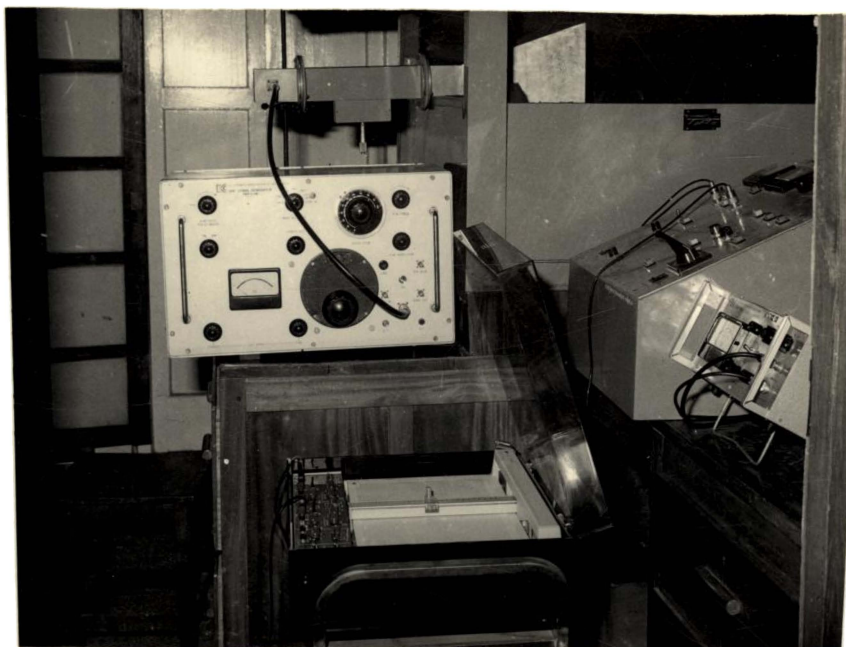   patterns in the X-band

Fig.3.3(iii) Transmitter set up for plotting radiation
             patterns in the S-band

3.4 Half Power Beam Width (HPBW) and Gain

The antenna beam width is the angular width of
the antenna radiation pattern between points where the power
level has decreased to a specified amount below the maximum
value. Half Power Beam Width (3dB), 10dB width and 20dB
width are the generally used beam widths. In this thesis,
only the Half Power Beam Width have been considered. For
determining the HPBW from the normalised power pattern, the
points corresponding to half of the maximum value (0.5 in
this case) are marked on the pattern. The angle between
the lines joining these points to the origin of the circu-
lar co-ordinate graph gives the HPBW. For certain purposes,
the radiation patterns have to be plotted as intensity
patterns. For these patterns, the HPBW will be the angle
between the points corresponding to 0.707 of the maximum
value. Fig.3.4(i) gives the typical normalised power and
intensity patterns.

Directive gain of an antenna in the plane where
the radiation pattern is plotted, can be determined by the
numerical integration method[92] of the intensity pattern
in rectangular co-ordinates.

$$\text{Gain } G = \frac{2\pi\ I_{max}}{\int_{0}^{2\pi} I_{\theta}\ d\theta}$$

Power pattern

Intensity pattern
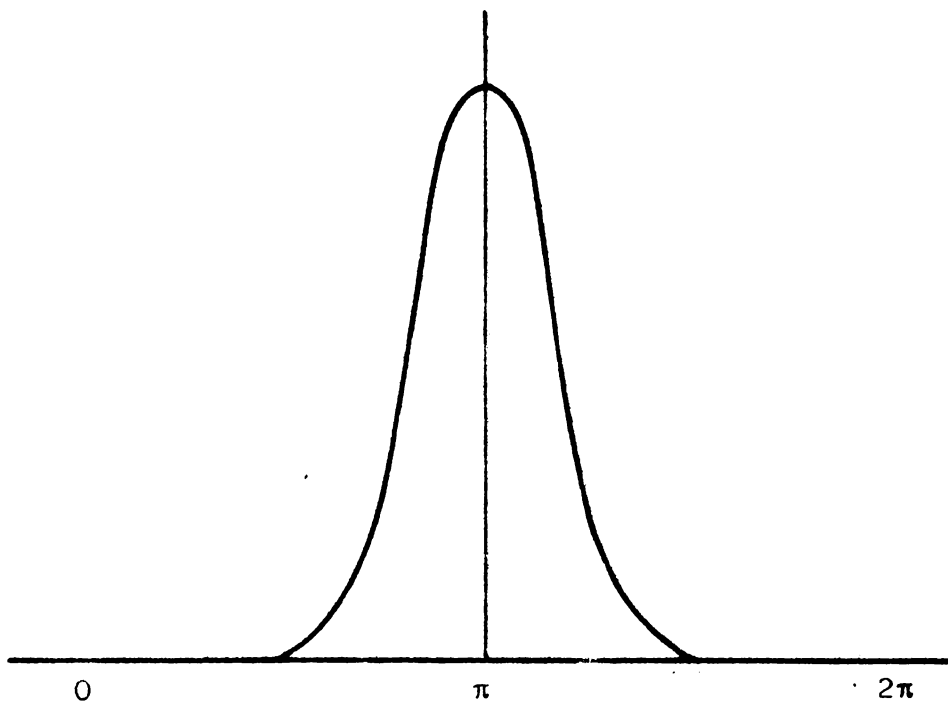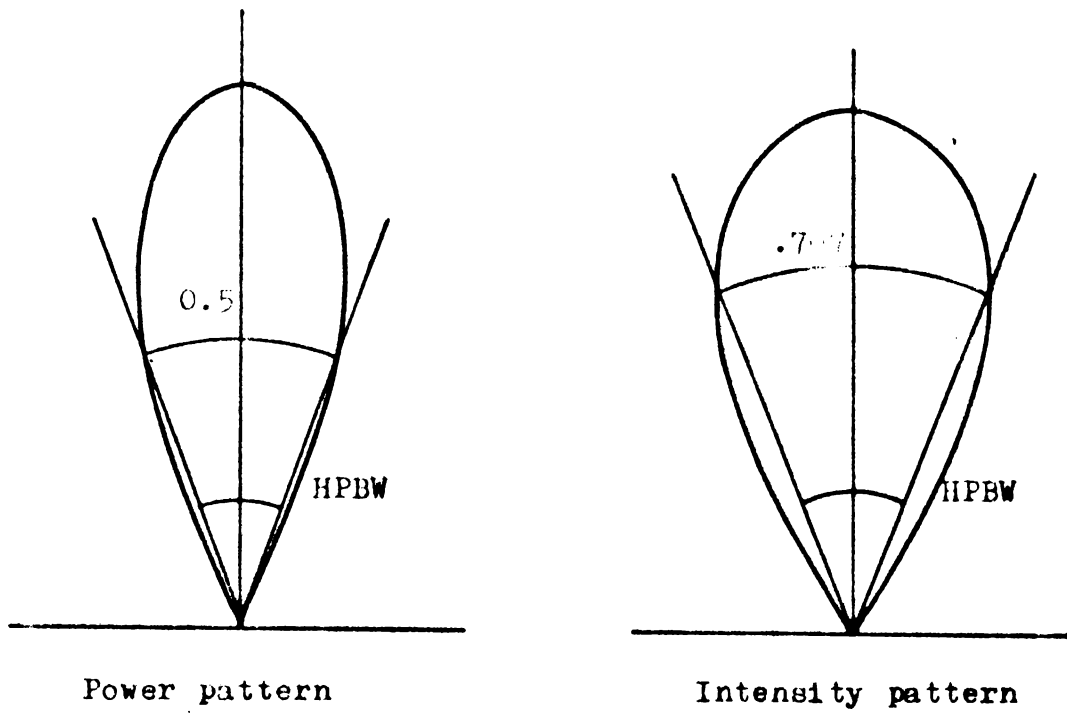
Intensity pattern in rectangular co-ordinates

Fig.3.4(i)   Typical power and intensity patterns.

where I_{max} is the maximum value of intensity in the direction
of maximum radiation and I_{θ} is the intensity corresponding
to any bearing angle θ . The gain in only one plane can be
determined using this method. $\int_{0}^{2\pi} I_{\theta} \, d\theta$ is numerically given
by the area enclosed between the intensity curve and the
θ-axis within the limits $\theta = 0$ to 2π.

In decibels gain is given by

$$G_{dB} = 20 \log_{10} \frac{2\pi \, I_{max}}{\int_{0}^{2\pi} I_{\theta} \, d\theta}$$

3.5 Polarization Measurements

The major polarization measurements carried out
are the measurement of the axial ratio and tilt angle of
the major axis of the polarization ellipse. The experimental
set up for these measurements consist of a linearly polarized
pyramidal horn which receives signal from the elliptically
polarized antenna. The stand of the receiver horn is capa-
ble of rotation about a horizontal axis and the angle of
rotation can be measured using a calibrated dial on the
stand.

3.5(i) Axial Ratio

Axial ratio is the ratio of the major axis to the minor axis of the polarization ellipse taken on the axis of the radiated beam. In order to determine the axial ratio of the elliptically polarized beam, the small pyramidal horn receiver is placed at a point in the far field along the axis of the test antenna. As the receiver is rotated about a horizontal axis, the received relative field-intensity traces out a polarization ellipse as shown in Fig.3.5(i)(a). From the polarization ellipse, the axial ratio can be readily calculated by measuring the major and minor axes of the ellipse.

3.5(ii) Tilt Angle

The polarization ellipse, described in the earlier section, is usually tilted in space with respect to the co-ordinate axes. The angle of tilt of the major axis of the polarization ellipse with the horizontal coordinate is referred as tilt angle of the elliptically radiated beam. For measuring the tilt angle, the polarization ellipse of the elliptically polarized beam is traced by the method given in the earlier section. The tilt angle of the
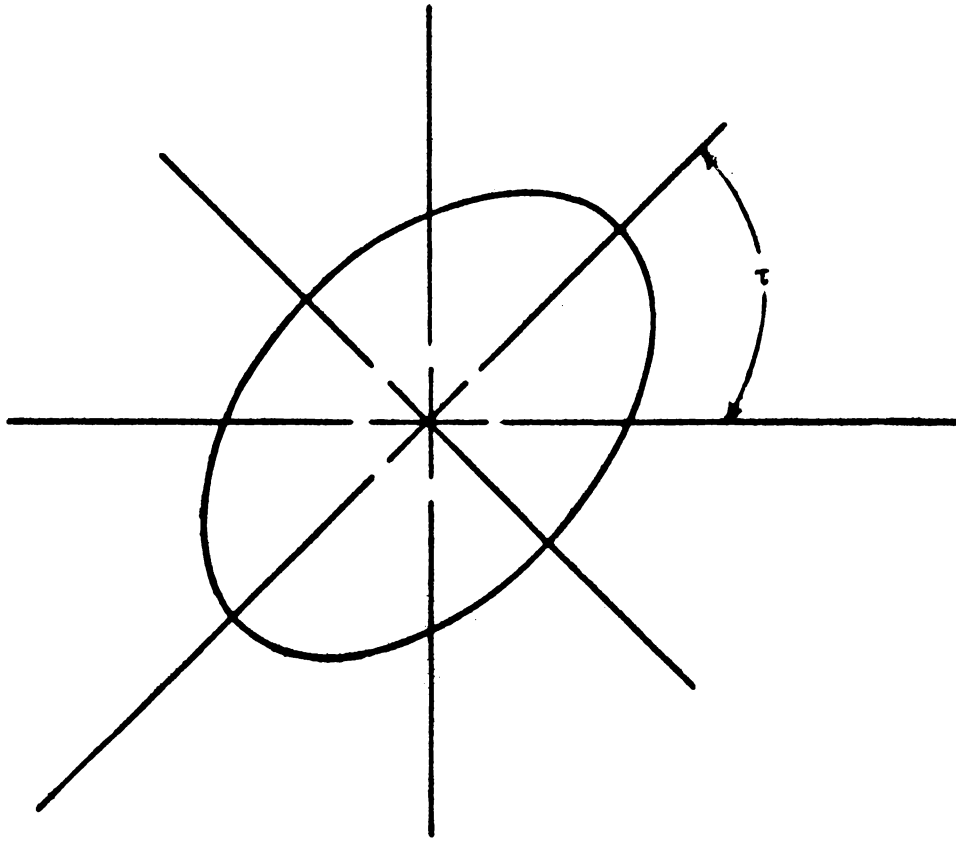
Fig.3.5(i)(a) A typical tilted polarization
ellipse. τ is the tilt angle.

58

polarization ellipse can then be obtained by measuring the
angle between the major axis of the ellipse and the hori-
zontal coordinate. In Fig.3.5(i)(a), angle τ gives the
tilt angle of the polarization ellipse.

CHAPTER IV

RESULTS OF THE EXPERIMENTAL INVESTIGATIONS

This chapter presents the various experimental
results obtained from a detailed investigation carried out
on flanged sectoral horn antennas and corner reflector
systems. For comparing the behaviour of flanges on sector-
al horns with that of corner reflectors, the experimental
results have been divided into three parts. In the first
part, the experimental investigations performed on plane
flanged sectoral horns and plane corner reflectors are
described. Results obtained using corrugated flange mounted
sectoral horns and corrugated corner reflectors will be
discussed in the second part. The third part presents the
results of an attempt to produce elliptically and circularly
polarised radiation using inclined corrugated flanges and
reflectors. The important aspects taken for investigation
on plane and corrugated systems are:

  i) Variation in the on-axis power density due to
     changes in flange or corner reflector
     parameters.

 ii) Changes in the VSWR of the system.

60

iii) Radiation patterns corresponding to positions
of the primary feed giving maximum and minimum
on-axis power density.

iv) Half Power Beam Width.

v) Gain of the antenna systems.

vi) Effect of asymmetry imposed on flange or
reflector parameters.

In the case of inclined corrugated systems, the
polarization property and matching conditions of the antennas
have been studied. The effect of different flange/reflector
parameters and frequency of operation on these antenna chara-
cteristics have been studied for both flanged horn antennas
and corner reflectors and a comparative analysis of the
behaviour of these two systems has been presented. Measure-
ments were taken at different frequencies in the X- and
S-bands using various horns, flanges and corner reflector
elements. In these measurements, the flange or corner
reflector angle was set at different values in the range 0°
to 180°. Theoretical aspects of both these systems and a
detailed analysis of the corrugated CR system are given in
the next chapter.

Part I   Investigations on Plane Flanged Sectoral Horns and
          Plane Corner Reflector Systems

4.1   On-axis Power Density

On-axis power density is the power radiated along
the axis of the system. It is an important characteristic
of the antenna system to be investigated in detail, because
of its major role in determining the shape of the radiation
pattern of the antenna. The on-axis power density is found
to be varying with different parameters like distance of the
primary feed (Z) from the apex of the flange or corner
reflector, flange angle (or corner angle in the case of
corner reflector), frequency of operation etc. Its depend-
ence on the position of the primary feed from the apex of the
system will be dealt with in this section.

4.1(i)   Variation of On-axis Power Density with Position of
          Primary Feed

In order to study the changes in the on-axis power
with position of the flange system, the sectoral horn mounted
with flanges is used as the transmitter. A small pyramidal
horn kept at a point in the far field, along the axis of the
system, receives the power radiated along the axis. In the
case of corner reflectors also, a similar arrangement is
employed. The details of these experimental set up are
described in the previous chapter.

In both these systems, when the distance of the primary feed from apex of flanges/reflectors is changed, the on-axis power was found to be fluctuating. Figs.4.1(i)(a) and (b) show the variation in the on-axis power density with distance of the flange from the aperture of horn, for different flange angles. The flange position[59] giving, maximum on-axis power is called 'O-position' (Optimum position) and the position corresponding to minimum on-axis power is termed as 'M-position' (Minimum position). Such maximum and minimum on-axis power positions exist in the case of CR systems also, as can be seen from Figs.4.1(i)(c) and (d).

Comparing Figs.4.1(i)(a) and (b) with (c) and (d), it can be seen that, under identical conditions both flanged horns and CR systems behave almost in the same manner. When the position of the flange system is varied, the phase difference of the electric fields at a point in the far field, due to the two edges of the flanges and the primary horn radiator[61] changes. This causes a change in the on-axis power density of the system. For the corner reflectors, it is the variation in the phase differences of electric fields due to the images[73] and the primary dipole radiator that causes the on-axis power variations. Table 4.1(i)(I) presents the distances of the primary feed from apex of the flange (or CR system, as the case may be), giving maximum
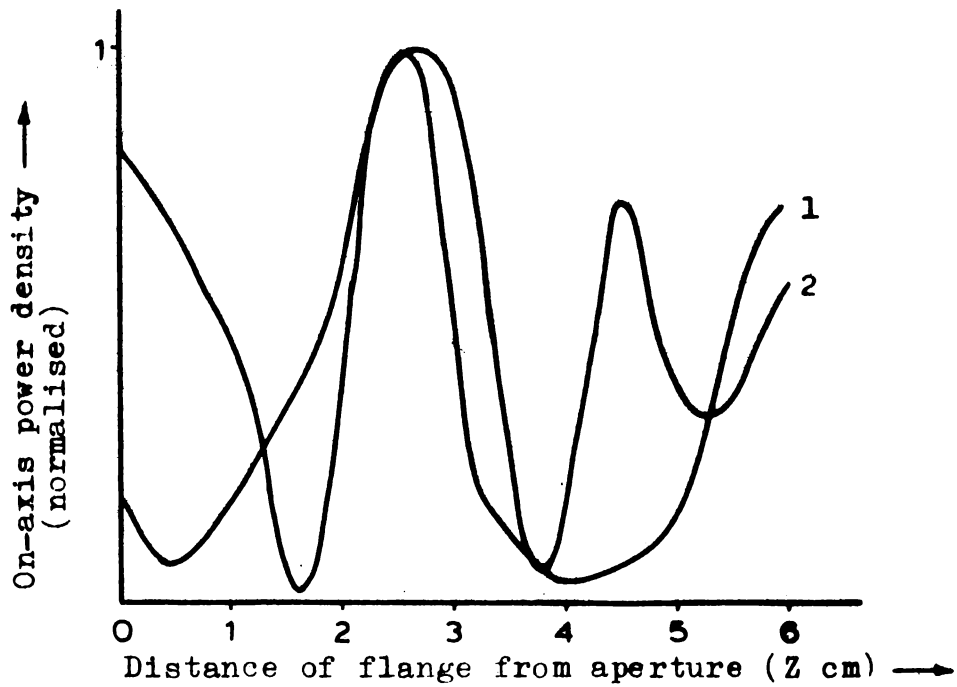
Fig.4.1(i)(a)   Variation of on-axis power density with
flange position for different flange
angles. 1 - 2β = 90°, 2 - 2β = 120°,
Frequency = 9.3 GHz.

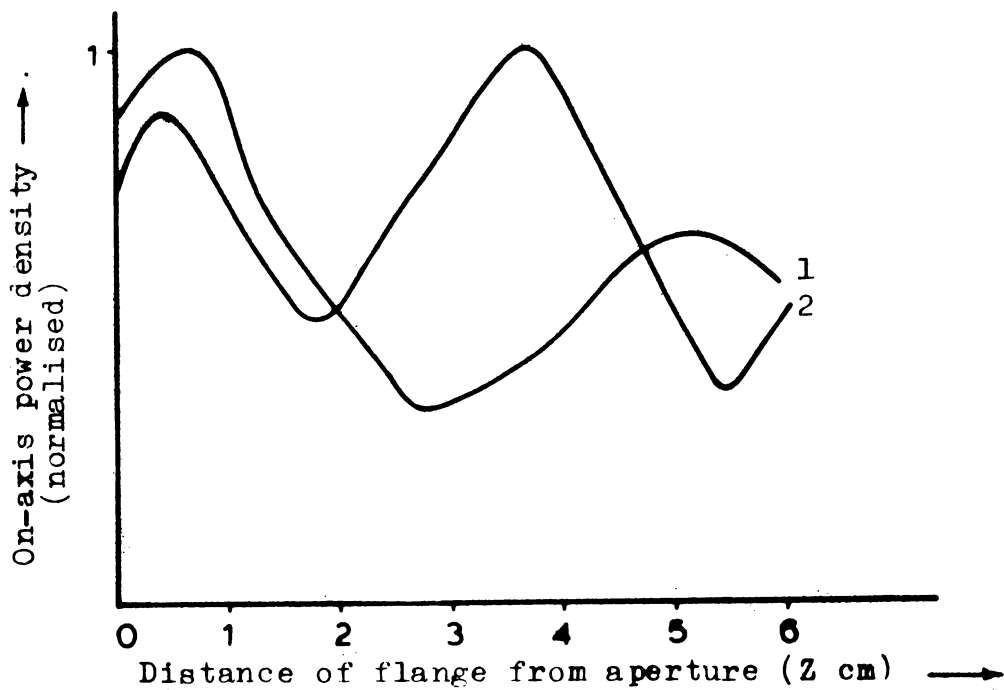
Fig.4.1(i)(b)   Variation of on-axis power density with
flange position for different flange
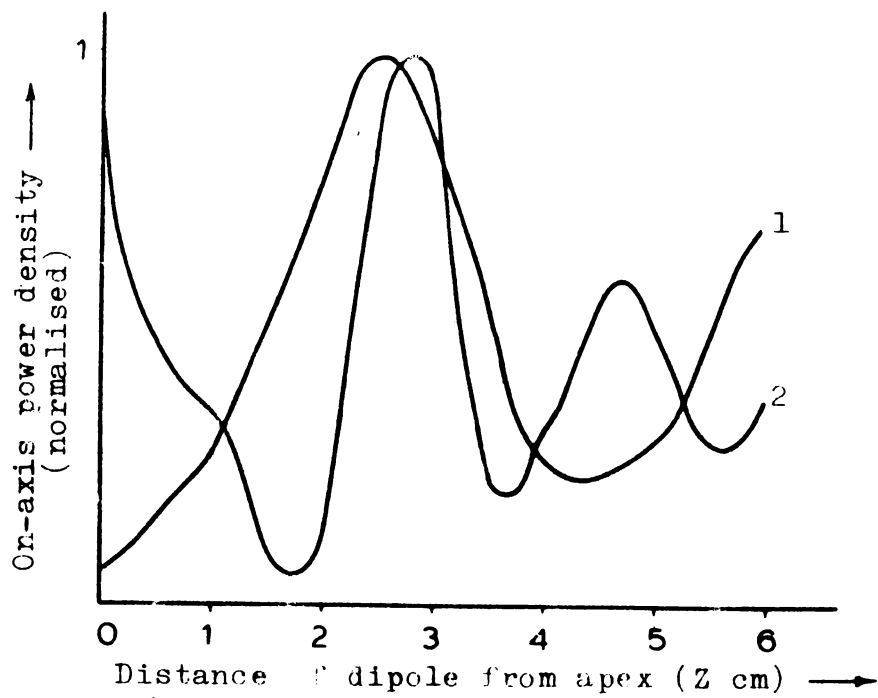angles. 1 - 2β = 60°, 2 - 2β = 45°,
Frequency = 9.3 GHz.

Fig.4.1(i)(c) Variation of on-axis power density with
position of dipole of the corner reflector.
1 - 2β = 90°,   - 2β = 120°, Frequency = 9.3 GHz
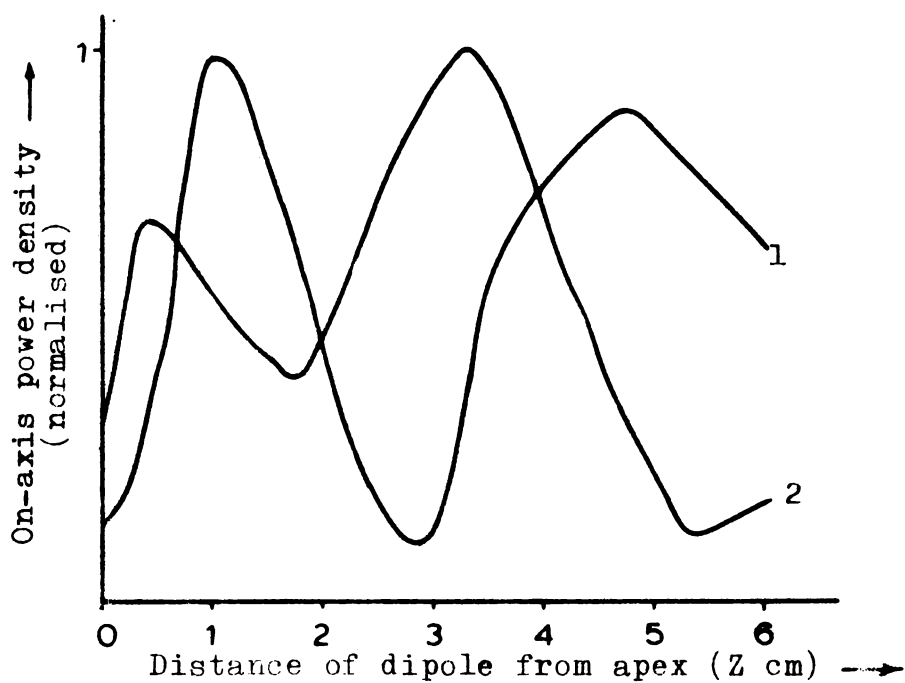

Fig.4.1(i)(d) Variation of on-axis power density with
position of dipole of the corner reflector.
1 - 2β = 60°, 2 - 2β = 45°, Frequency = 9.3 GHz.

65

Table 4.1(i)(I)

Positions giving maximum and minimum on-axis power
density for plane flanged horns and plane CR systems

Flange/ Corner angle 2β	Distance of primary feed from apex, giving maximum on-axis power (Z_o cms)		Distance of primary feed from apex, giving minimum on-axis power (Z_m cms)	
	Flange	Corner reflector	Flange	Corner reflector
45°	3.7	3.45	5.45	5.3
60°	0.75	1	2.7	2.83
90°	2.6	2.5	4	4.35
120°	2.8	2.7	1.6	1.7

on-axis power (Z_O) and minimum on-axis power (Z_m) for both systems. It may be noted that, for both flanged horns and CR systems, the values of Z_O and Z_m are approximately equal which shows the similarity between the behaviour of the two systems.

4.2 Voltage Standing Wave Ratio (VSWR)

Many changes occur to the matching conditions of the antenna systems, as the flange/reflector parameters are varied. These changes in the impedance of the systems are studied by measuring the VSWR using the usual slotted line method.

4.2(i) Effect of Flange/CR Angle on VSWR

For both systems, the VSWR was noted at two positions, namely 'Optimum position' and 'Minimum position'. At these positions the included angle of the flanges was varied and the VSWR was measured. The results show that the matching conditions of the antennas are strongly influenced by flange angle variations.

The dependence of the VSWR of the flanged horn on flange angle is presented in Figs.4.2(i)(a) and (b). Both at O- and M-positions, the VSWR is found to be varying
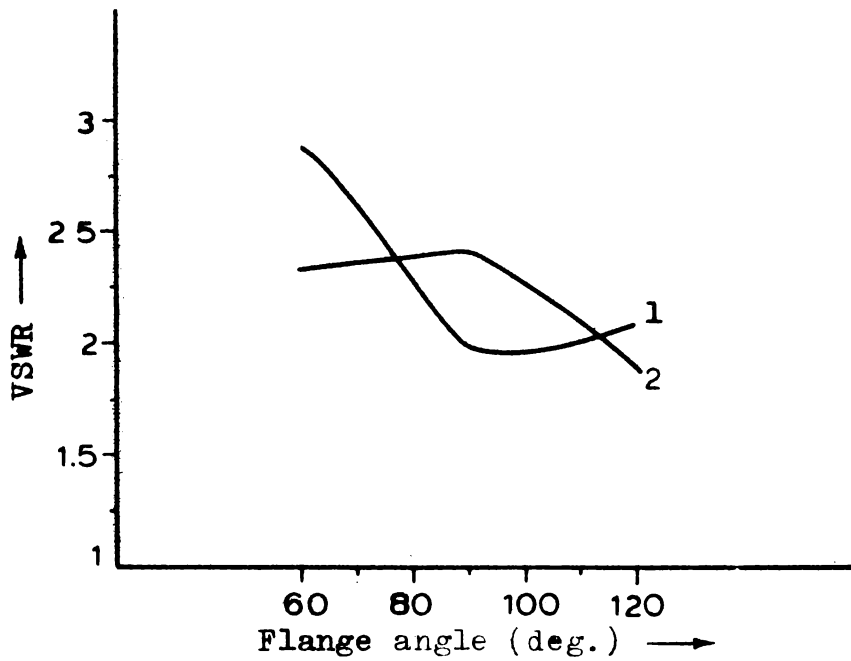
Fig.4.2(i)(a) Variation of VSWR with flange angle when
the flanges are kept at the O-position.
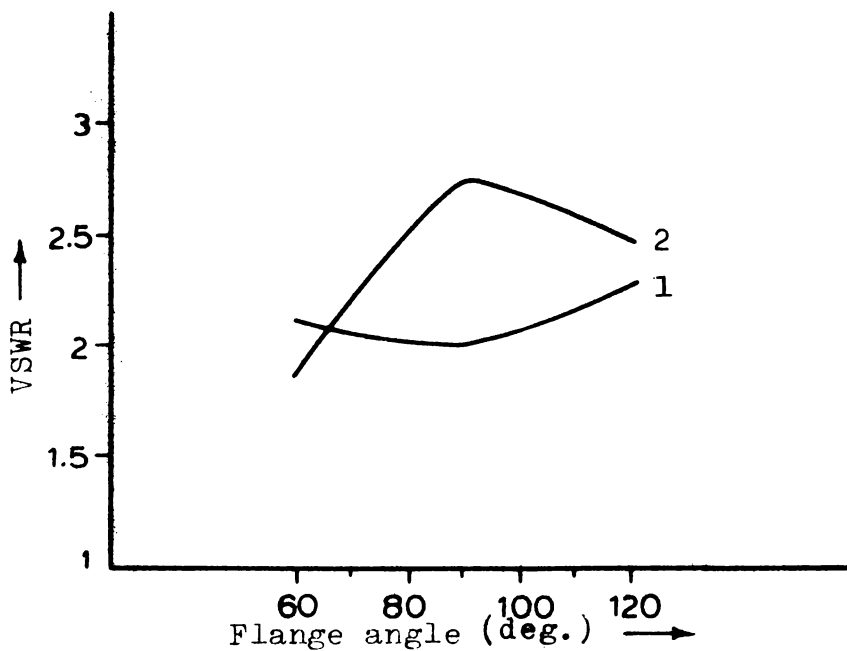1 - 9.3 GHz, 2 - 8.67 GHz.

Fig.4.2(i)(b) Variation of VSWR with flange angle when
the flanges are kept at the M-position.
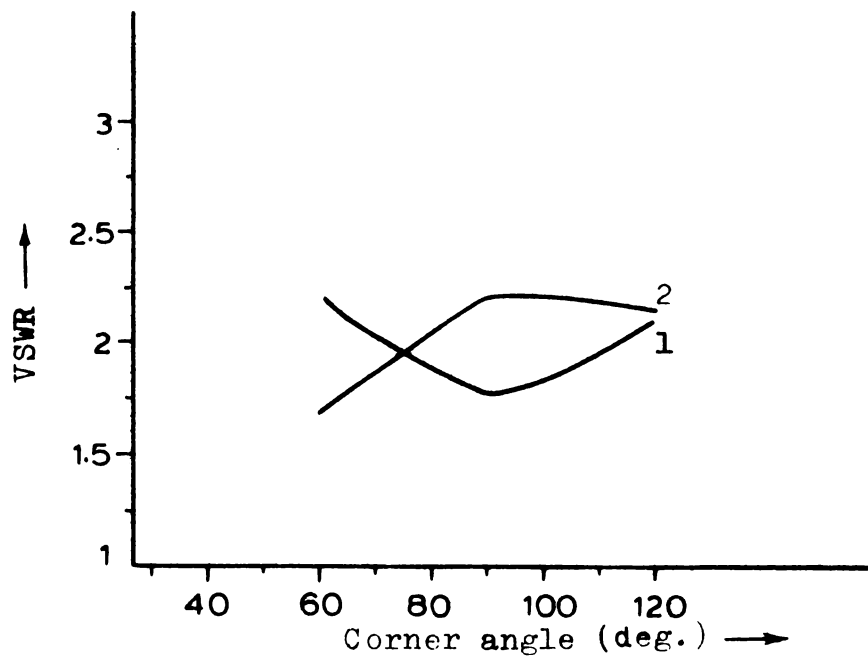1 - 9.3 GHz, 2 - 8.67 GHz.

Fig.4.2(i)(c)   Variation of VSWR with corner angle when the
                dipole is kept at the O-position. 1 - 9.3 GHz,
                2 - 8.67 GHz.
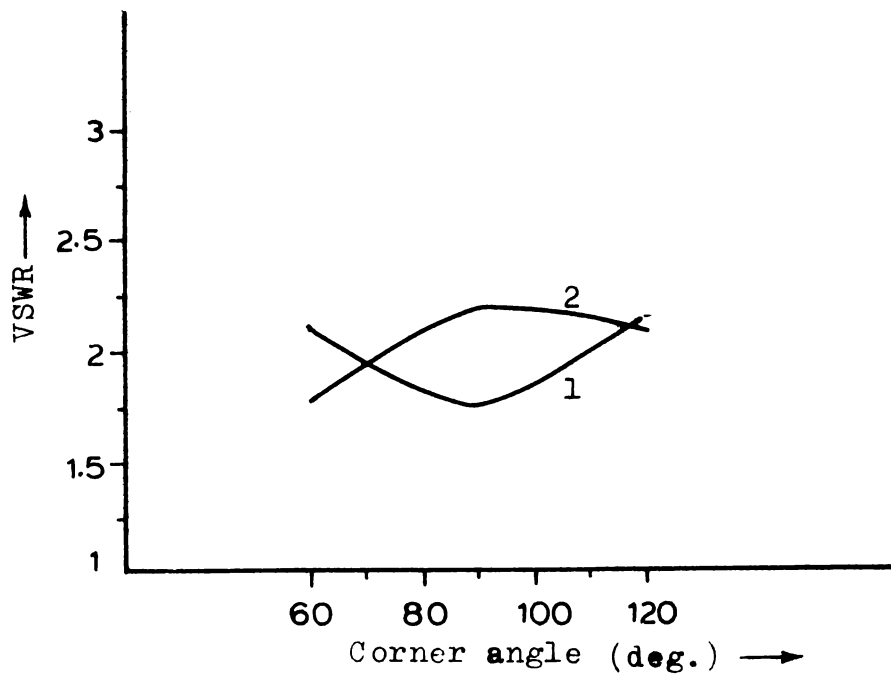

Fig.4.2(i)(d)   Variation of VSWR with corner angle when the
                dipole is kept at the M-position. 1 - 9.3 GHz,
                2 - 8.67 GHz.

with flange angle. Figs.4.2(i)(c) and (d), give the results obtained in the case of corner reflectors. The graphs presented for different frequencies show the similarity in the variation of VSWR with flange/corner angle, for both the systems. For flanged sectoral horns, edge diffraction at the horn aperture produces some mismatch and this causes a slightly higher VSWR observed in this case.

4.2(ii)   Change in VSWR with Frequency of Operation

The impedance conditions of the antennas are much depending up on the frequency of operation. This variation for both the systems are presented in Figs.4.2(ii)(a) and (b). The phase difference of the secondary wavelets from the edges of the flanges (images in the case of CR system) reaching the aperture of the horn (dipole for corner reflectors) depends upon the wavelength and this causes the changes observed in the VSWR. For both flanged horns and CR systems, the VSWR is found to be less at the Minimum position than at the Optimum position.

4.2(iii)   Variation of VSWR with Position of Primary Feed

Investigations on the matching conditions of flanged horns and corner reflectors reveal that the VSWR of the system are much affected by the position of the
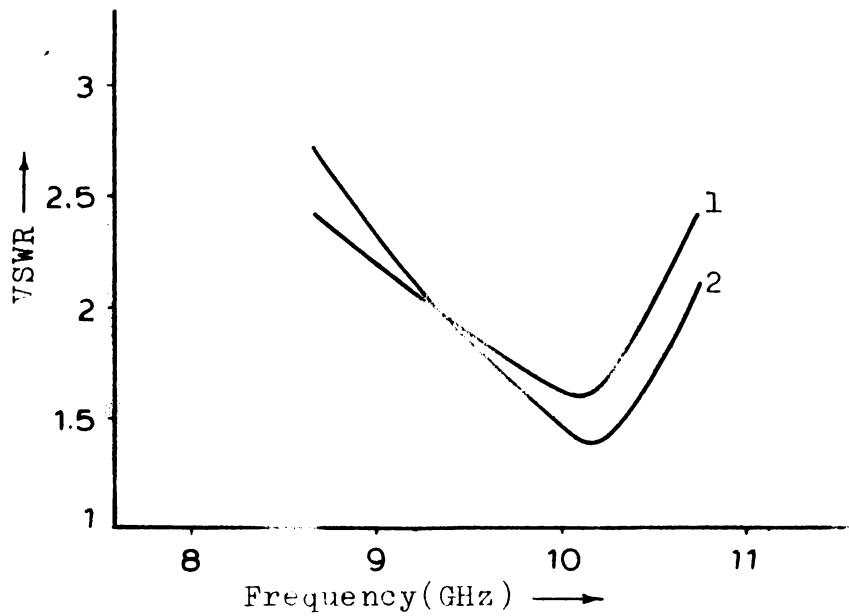
Fig.4.2(ii)(a)   Variation of VSWR with frequency when the
flanges are kept at the O- and M-positions.
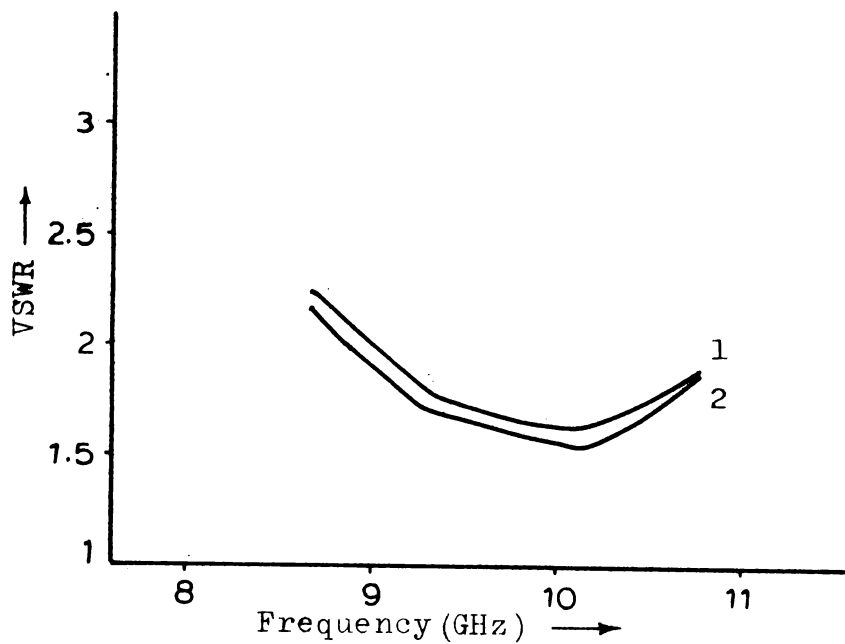1 - O-position, 2 - M-position, $2\beta = 90°$.

Fig.4.2(ii)(b)   Variation of VSWR with frequency when the
dipole feed of the CR system is kept at the
O- and M-positions. 1 - O-position,
2 - M-position, $2\beta = 90°$.

primary feed. These fluctuations in the VSWR are almost
similar in both systems under identical conditions, as
shown in Figs.4.2(iii)(a) and (b). The values of VSWR
obtained with flanged horns are higher than that for corner
reflectors. The explanation given in Section 4.2(i) is
applicable in this case also.

4.3 Radiation Pattern

The radiation pattern of sectoral horns and
dipoles can be conveniently shaped by proper adjustments
of the flange/reflector parameters. These changes produced
in the beam shape by varying the different flange/reflector
parameters are discussed in this section.

4.3(i) Change in Radiation Pattern with Position of Primary Feed

It has already been shown in Section 4.1(i) that
the on-axis power density fluctuates giving maxima and minima,
as flange/reflector position is varied. At these O- and
M-positions, the radiation patterns are plotted for both
systems. Both give focusing of the beam at O-position and
splitting at M-position. In between these two positions, it
gives a broadened or slightly split beam. The patterns plotted
for flange mounted H- and E-plane sectoral horns are given
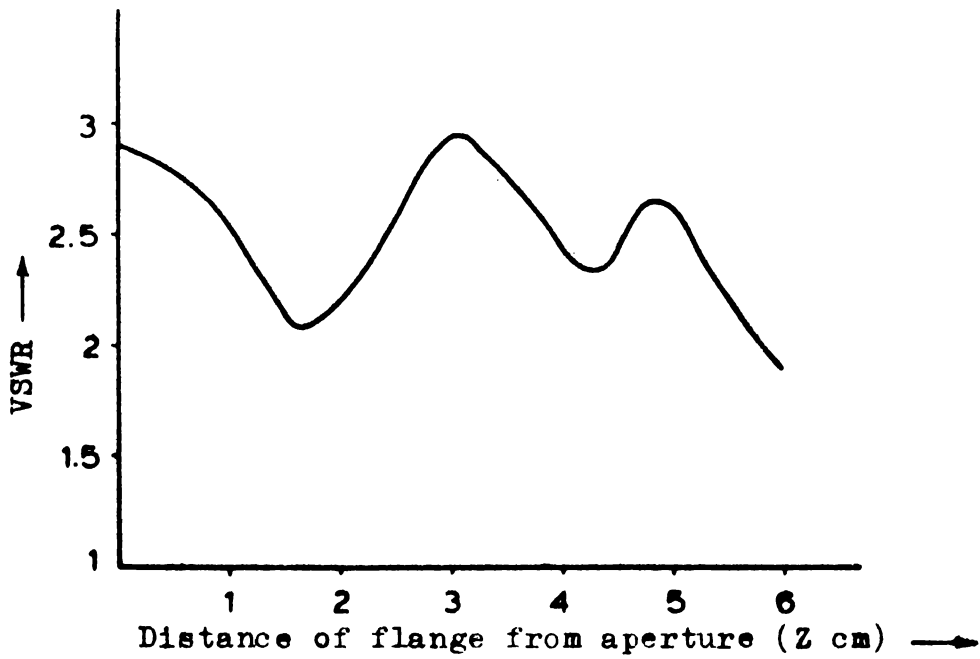
Fig.4.2(iii)(a) Variation of VSWR with flange position.
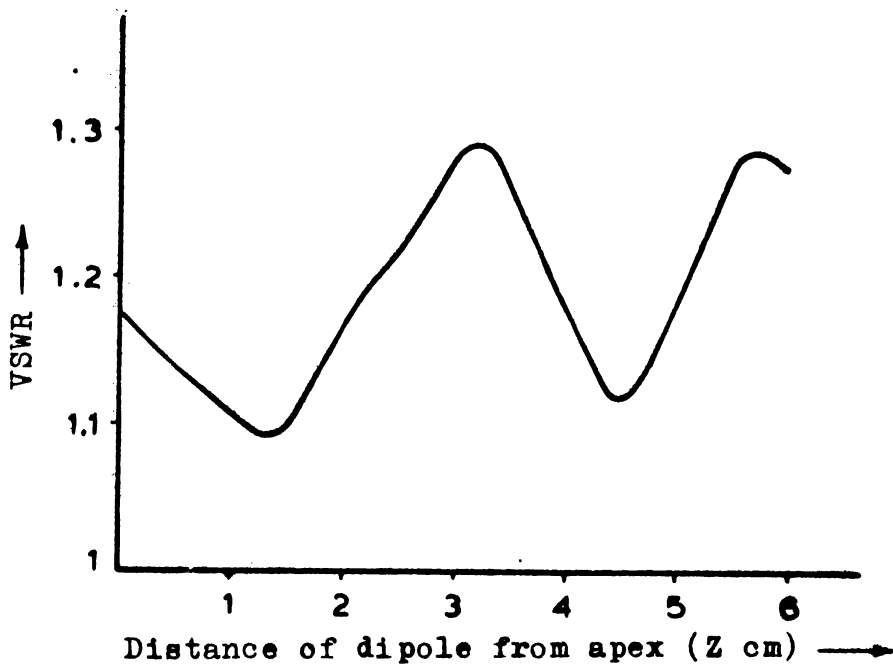$2\beta = 90^{\circ}$, Frequency = 9.3 GHz.

Fig.4.2(iii)(b) Variation of VSWR with position of dipole
of the corner reflector. $2\beta = 90^{\circ}$,
Frequency = 9.3 GHz.

in Fig.4.3(i)(a). The corresponding patterns for identical
corner reflectors operating at the same frequency are shown
in Fig.4.3(i)(b).

The figures show that, for both systems, the
changes observed in the beam shape due to variations in
flange/reflector position are almost similar. The actual
beam shapes of flanged horn and CR system are slightly
different at each O- and M-positions. The individual
radiation pattern of sectoral horn and dipole are different.
This causes the slight differences in actual beam shape
at O- and M-positions of each system.

4.4 Half Power Beam Width (HPBW)

In the preceding section, it was shown that
several changes occur to the beam shape of antenna by the
adjustments of different parameters. Half Power Beam
Width (HPBW) is a measure of the directivity of the beam.
The variation in beam shape produces changes in HPBW also.
These changes in HPBW due to variations in flange/reflector
parameters are investigated in detail and these are
presented in the following section.

4.4(i) Variation of HPBW with Flange/Corner Reflector Angle

Figs.4.4(i)(a) and (b) show the changes in HPBW
with flange/corner reflector angle, for flanged horns and

Flange system

CR system

(ii) M-posn.

(ii) O-posn.

(i) M-posn.

(i) O-posn.

(a)

(b)
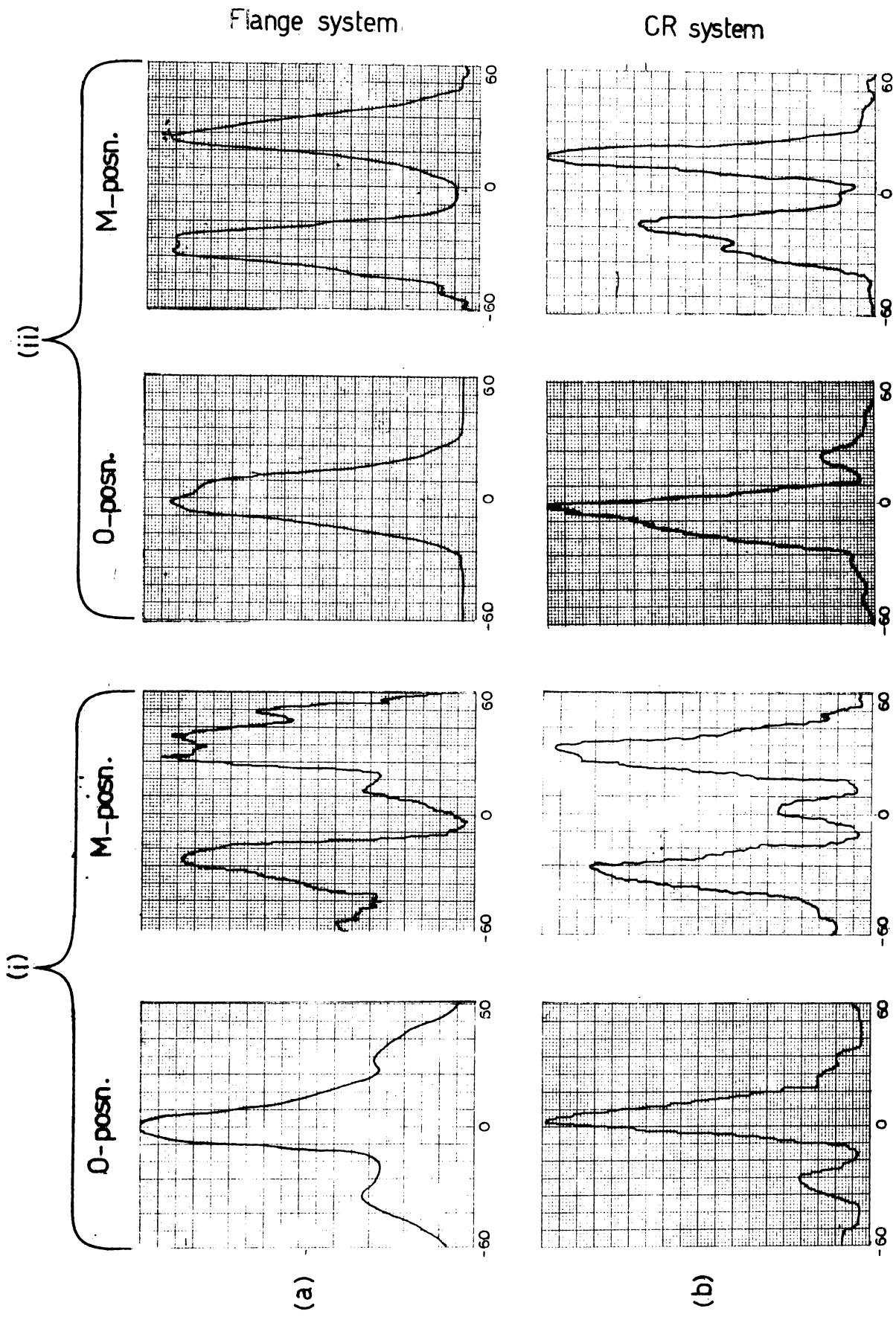
Fig. 4.3(i) Patterns of plane flanged horns and plane CR systems –

(i) with H-plane sectoral horns and horizontally oriented dipole

(ii) with E-plane sectoral horns and vertically oriented dipole. $2\beta=90$, Freq. = 8.67 GHz.

75

Fig.4.4(i)(a)   Variation of HPBW with flange angle when the
                 flanges are kept at the O- and M-positions.
                 1 - O-position, 2 - M-position, Frequency = 9.3 GHz.

Fig.4.4(i)(b)   Variation of HPBW with corner angle when the
                 dipole is kept at the O- and M-positions.
                 1 - O-position, 2 - M-position, Frequency = 9.3 GHz.

corner reflectors. Both at the O- and M-positions, the variations in HPBW with flange angle are similar for the two systems. For example, the lower value for HPBW in both the systems occur at $2\beta = 90^{\circ}$ and the higher val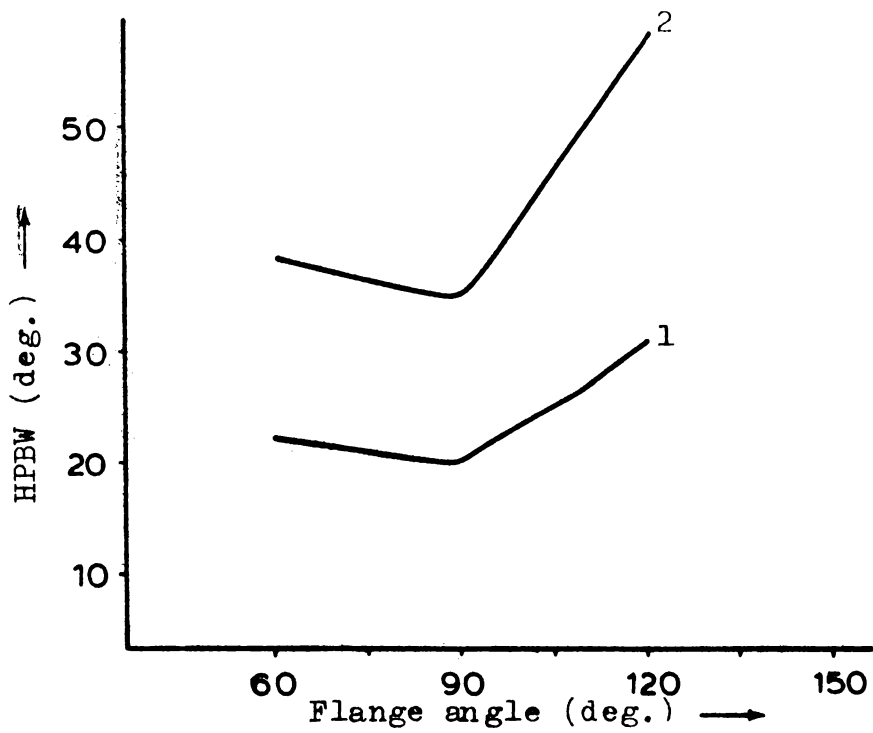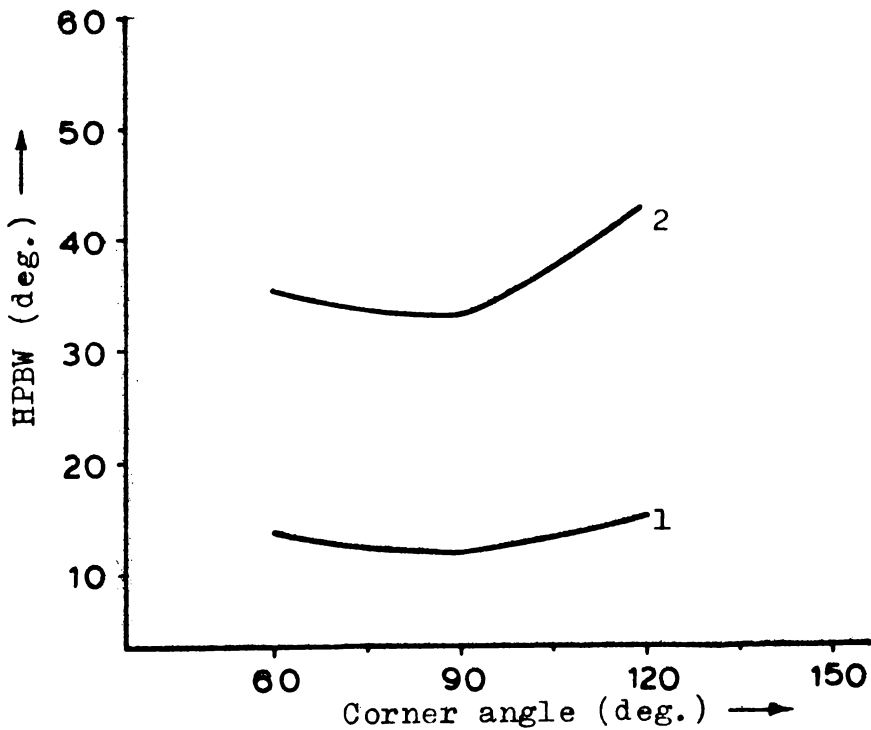ue at $2\beta = 120^{\circ}$. The values of HPBW obtained for CR system are slightly less than those obtained with flanged horns. The explanation given in the previous section holds good in this case also.

4.5 Gain of the Antenna Systems

Another important antenna characteristic taken for investigation is its gain. Since the variations in the flange parameters of H-plane sectoral horns do not affect its H-plane pattern, the gain in the magnetic plane of the system is found to be independent of different flange parameters. Hence, eventhough the overall gain of the antenna system depends on the gain in both planes, the gain in the electric plane alone is considered here.

4.5(i) Dependence of E-plane Gain on Flange/Corner Reflector Angle

As the flange angle is changed, the gain of both systems in the E-plane undergoes some variations. As seen from Figs.4.5(i)(a) and (b), these changes produced in the
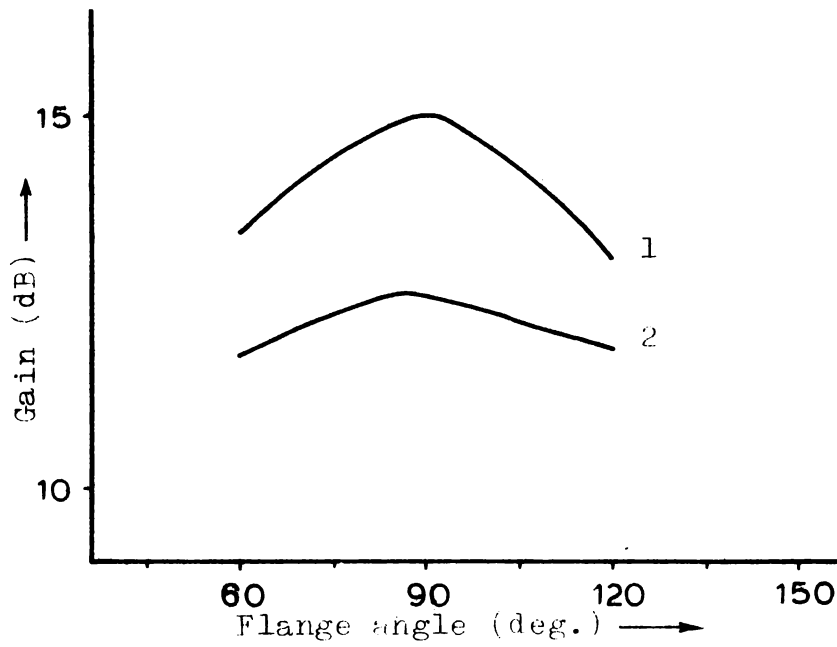
Fig.4.5(i)(a) Variation of gain with flange angle.

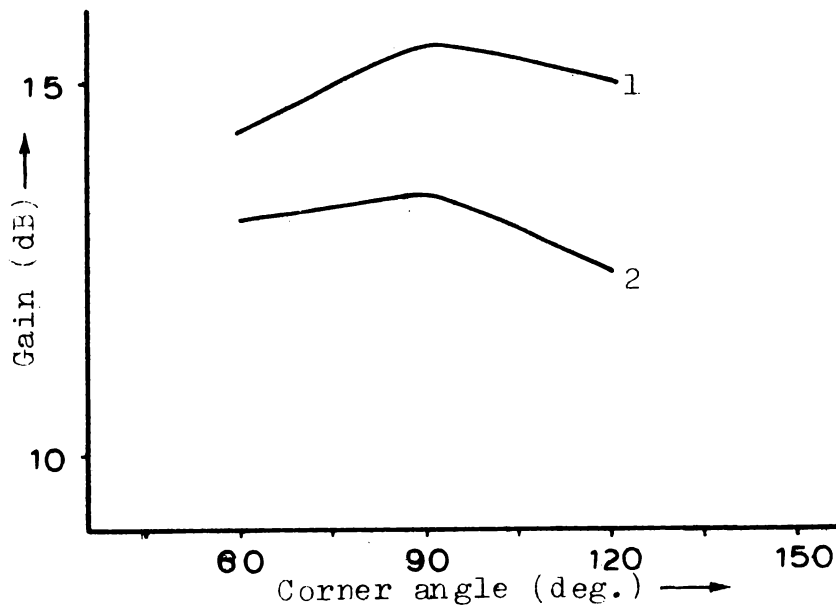1 - O-position, 2 - M-position, Frequency = 9.3 GHz.

Fig.4.5(i)(b) Variation of gain with corner angle.

1 - O-position, 2 - M-position, Frequency = 9.3 GHz.

gains of the systems also show some similarity in behaviour
of flanges and corner reflectors. The results obtained at
O- and M-positions establish this resemblance between the two
systems. These variations in gain are similar to the varia-
tions obtained in the case of HPBW which show that reduction
in HPBW results in a gain enhancement of the system.

4.6   Asymmetry Imposed on Flange/Reflector Elements

In all the previous sections, only symmetrical
flanged horns and corner reflector systems have been discussed.
This section deals with the asymmetry imposed on the different
parameters and its effect on the beam shape of the antenna
systems. The various asymmetries imposed on the systems
under consideration are:

    i) Off-axis primary feed, ie., axis asymmetry

   ii) Width asymmetry, and

  iii) Asymmetric reflector elements.

The position of primary feed is so adjusted to get
a focused beam of the antenna. Then, the primary feed is
displaced slightly to off axis. The resulting beam is found
to be tilted from its initial position. Such tilting of
beam is also obtained when the width of flange elements are

different (width asymmetry). In this case, the beam is
tilted towards the side of the flange element having larger
width. When a flange/corner reflector system with asymmetric
constitution (for eg. one element dielectric and the other
one metallic) is used, the beam is found to be tilted towards
the side of metallic element. Thus the asymmetries imposed
on both flanged horns and corner reflectors produce beam
tilting. Results obtained by imposing asymmetries on both
systems under identical conditions are presented in
Figs.4.6(i)(a) and (b).

Part II   Results Obtained with Corrugated Flange-Mounted
          Sectoral Horns and Corrugated CR Systems

4.7   On-axis Power Density

On-axis power density, as pointed out in Section
4.1, being one of the important characteristics of the
antenna system, its dependence upon the various flange/CR
parameters are discussed in detail in this section. In
the case of corrugated systems, in addition to the flange
position and flange angle, a third parameter called corru-
gation parameter has an important role in controlling the
different antenna characteristics. The changes produced in
any of these parameters are found to be strongly affecting
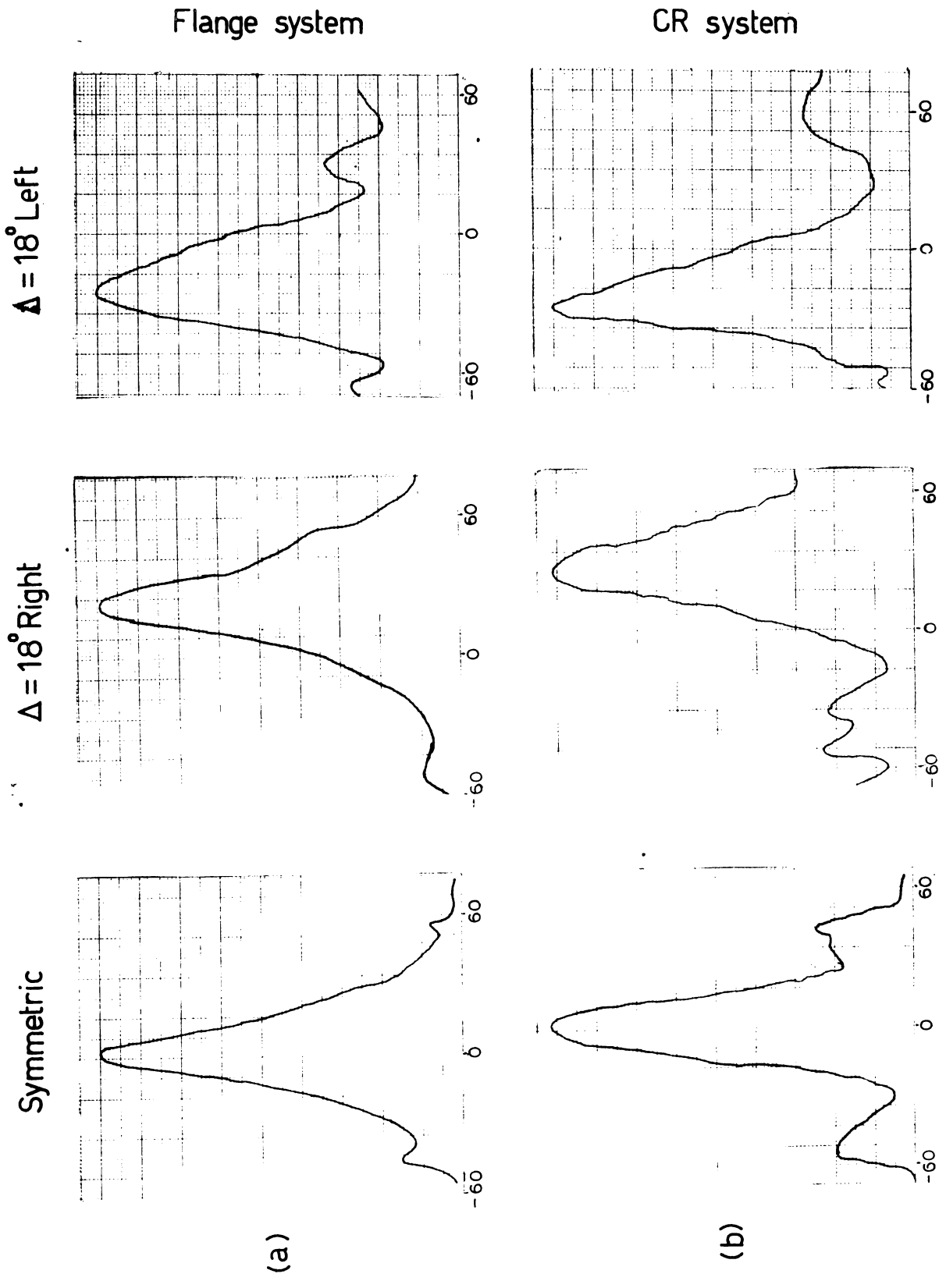the on-axis power density of the system.

Flange system

CR system

$\Delta = 18^\circ$ Left

$\Delta = 18^\circ$ Right

Symmetric

(a)

(b)

Fig. 4.6(i) Beam tilting due to axis asymmetry. $2\beta = 60^\circ$, Frequency = 10·76 GHz.

81

4.7(i)   Variation in On-axis Power Density with Changes in
         the Position of the Primary Feed

As in the case of plane flanges and CR systems,
the on-axis power, received by a pyramidal horn kept at a
point in the far field along the axis of the system, was
found to be fluctuating, as the position of the primary
feed (horn or dipole as the case may be) was changed. In
this case also, the position giving maximum on-axis power
density is termed as 'Optimum position' (O-position) and
minimum on-axis power density as 'Minimum position'
(M-position).

Fig.4.7(i)(a) presents the variation of on-axis
power density with distance of flange from aperture of the
horn, for different corrugated flanges. Fig.4.7(i)(b) is
the corresponding graph obtained in the case of corrugated
CR system. The figures show that for corner reflectors or
flanges having the same corrugation parameters the variation
in on-axis power density under identical conditions is
almost similar. In Table 4.7(i)(I), the distance of the
primary feed giving maximum and minimum on-axis power
density for different corrugated flanges or corner reflectors
having different flange/corner reflector angles are
tabulated. This table also illustrates that the positions
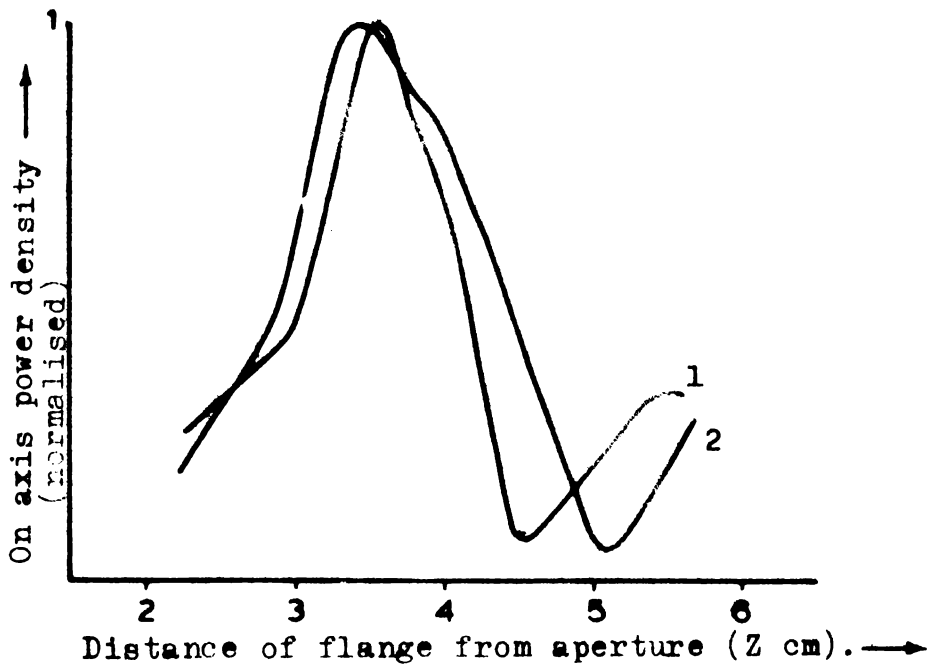corresponding to maximum and minimum on-axis power density
in both systems are almost same.

Fig.4.7(i)(a)   Variation of on-axis power density with position
of flanges. 1 - N = 1.9, 2 - N = 1.4, 2β = 90°,
Frequency = 9.3 GHz.
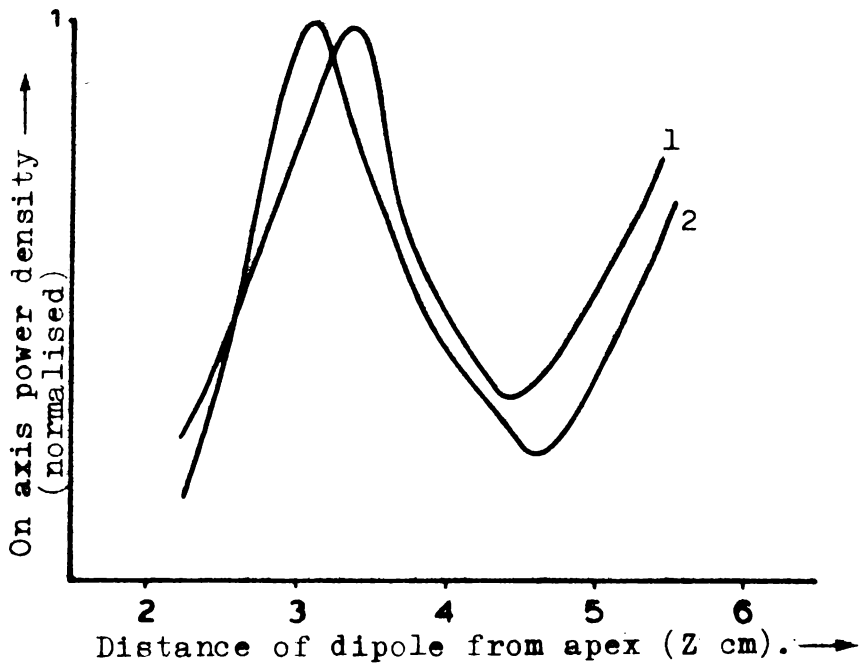
Fig.4.7(i)(b)   Variation of on-axis power density with position
of dipole of the corner reflector. 1 - N = 1.9,
2 - N = 1.4, 2β = 90°, Frequency = 9. GHz.

83

Table 4.7(i)(I)

Positions giving maximum and minimum on-axis power
density for corrugated flanged horns and corrugated
CR systems

Flange/ corner angle 2β	Number of corru- gations per cm N	Distance of primary feed giving maximum on-axis power (Z_o cm)		Distance of primary feed giving minimum on-axis power(Z_m cm)	
		Flanged horn	CR system	Flanged horn	CR System
90°	0.8	3.8	3.5	4.6	4.5
90°	1.1	3.6	3.4	4.5	4.4
90°	1.4	3.4	3.1	5.05	4.8
90°	1.9	3.75	3.6	4.6	4.5
120°	0.6	5	5.1	1.6	1.6
120°	0.8	5.3	5 6	1.6	1.8
60°	0.6	2.7	2.5	4.75	4.9

4.7(ii)   Variation in On-axis Power Density with Corrugation
          Parameter N

In the case of corrugated systems, the corrugation
parameter N (number of corrugations/cm) also affects the
different antenna characteristics. It is observed that the
on-axis power density at the optimum position is changing
with variations in the corrugation parameter. This is found
to be true for both flanged horns and CR systems.

Figs.4.7(ii)(a) and (b) show the variations in
on-axis power density at optimum position with the corruga-
tion parameter for flanged horns and CR systems respectively.
In the case of flanged horns, the maximum on-axis power is
obtained for a corrugated flange of N = 1.1, at a frequency
9.3 GHz. For the corrugated CR system also, the maximum
on-axis power is obtained for a reflector element of N = 1.1.
This similarity in behaviour of the two systems regarding
the variation in on-axis power density is also evident from
the graphs drawn for a frequency of 10.76 GHz. The tips of
corrugations act as secondary radiators in both these
systems. The on-axis power density at a point in the far
field depends on the phase difference between the primary
(i.e. horn or dipole) and the secondary radiators. When the
frequency of operation varies, this phase difference and
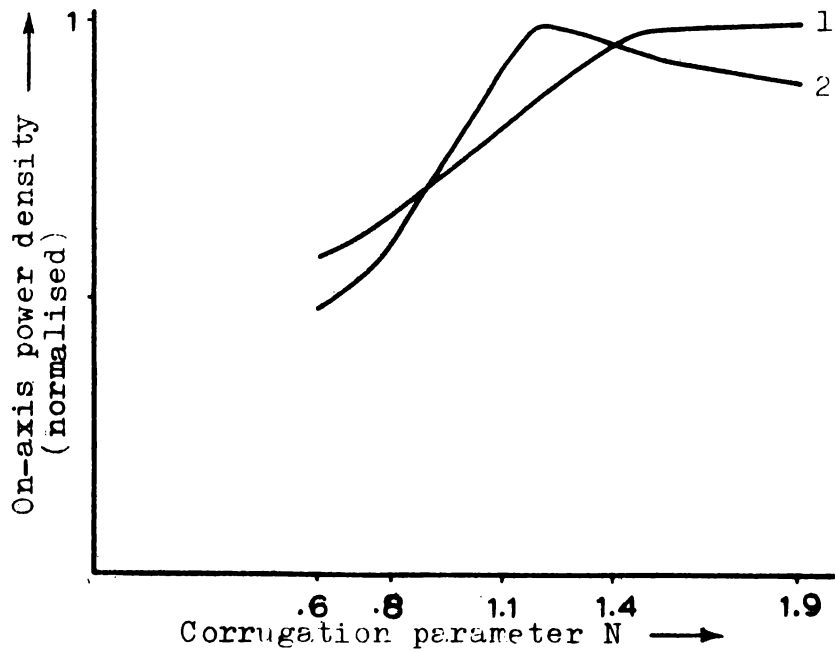hence the on-axis power density in the far field will change.

Fig.4.7(ii)(a)   Variation of on-axis power density with
corrugation parameter N when the flanges
are kept at the O-position.   1 - 10.76 GHz,
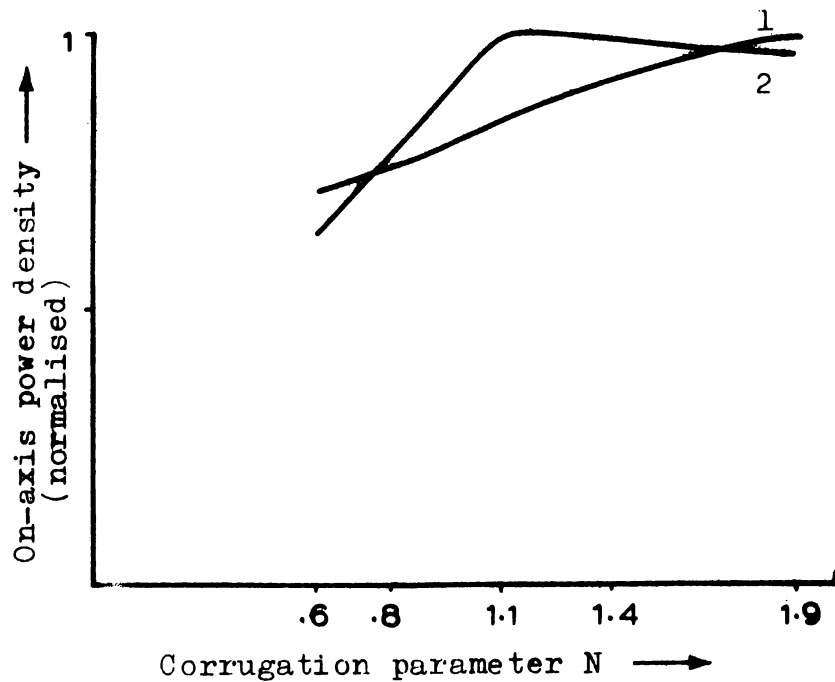2 - 9.3 GHz, $2\beta = 90^{\circ}$.

Fig.4.7(ii)(b)   Variation of on-axis power density with
corrugation parameter N when the dipole
is kept at the O-position, 1 - 10.76 GHz,
2 - 9.3 GHz, $2\beta = 90^{\circ}$.

Thus the value of corrugation parameter N giving maximum on-axis power density will be different for different frequencies, as is evident from the Figs.4.7(ii)(a) and (b).

4.7(iii)   Variation of On-axis Power Density with Flange/ Corner Angle

On-axis power density is found to be fluctuating with variations in the flange or corner reflector angle. For studying this effect, the values of on-axis power density obtained at the optimum position for different flange/corner reflector angles are noted.

For a flange of corrugation parameter N = 0.6, at 8.67 GHz, the maximum on-axis power at optimum position is obtained at a flange angle of 90°, as can be seen from Fig.4.7(iii)(a). The corresponding graphs for the CR system, shown in Fig.4.7(iii)(b), indicate that the maximum on-axis power density at optimum position occurs for CR system also at a corner angle of 90°. Thus, both systems show analogous behaviour with respect to variations in on-axis power density with flange/corner angles. The explanation given in the earlier section for getting different values of on-axis power at different frequencies can be applied here also to explain the different curves obtained for different values of corrugation parameter N.
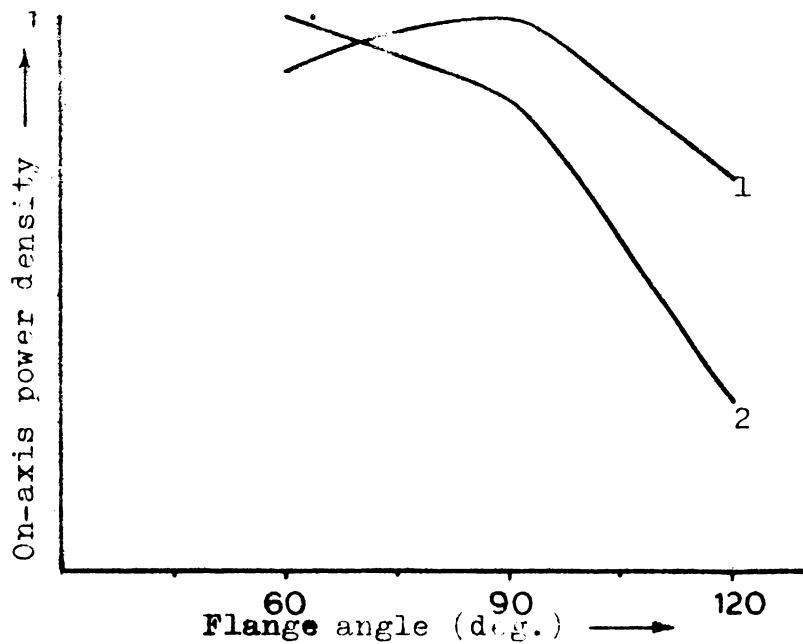
Fig.4.7(iii)(a) Variation of on-axis power density with flange angle when the flange is kept at the O-position.
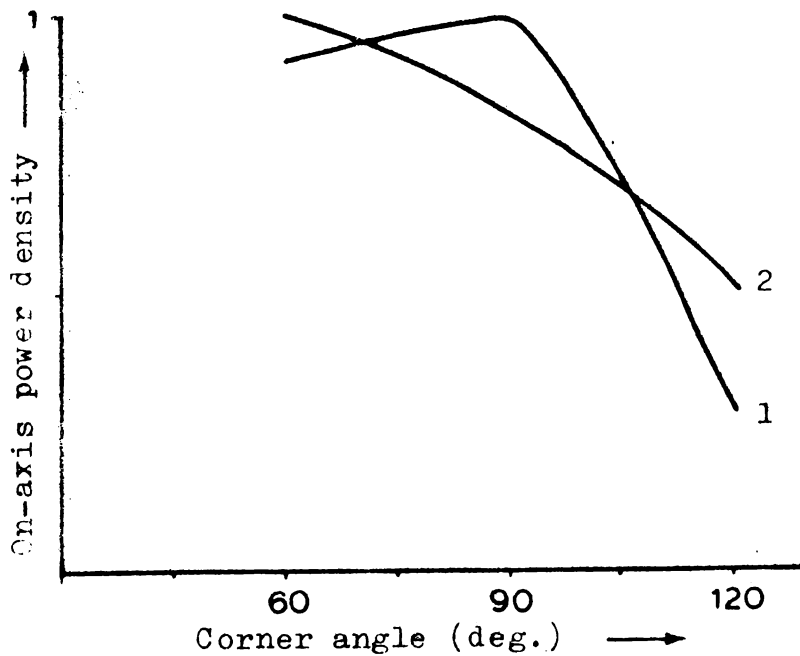1 - N = 0.6, 2 - N = 0.8, Frequency = 8.67 GHz.

Fig.4.7(iii)(b) Variation of on-axis power density with corner angle when the dipole is kept at the O-position.
1 = 0.6, 2 - N = 0.8, Frequency = 8. 7 GHz.

4.8 Voltage Standing Wave Ratio (VSWR)

Another important parameter taken for investigation is the changes produced in the matching conditions of both systems due to the variations in the different flange/reflector parameters. The impedance of these systems are investigated by measuring the VSWR and its dependence on the various parameters for both flanged horns and CR systems are studied.

4.8(i) Variation in VSWR with Flange/CR Angle

It is observed that VSWR of both systems are strongly dependent on the included angle of the flange/CR elements. VSWR at both 'Optimum position' and 'Minimum position' were noted for different flange/CR angles and the graphs are presented.

The variations of VSWR with flange angle at O-position and M-position for a corrugated flange of N = 0.8, at two different frequencies are shown in Figs.4.8(i)(a) and (b). The corresponding graphs obtained with corrugated CR system are shown in Figs. (c) and (d). Now, comparing Figs.4.8(i)(a) and (b) with (c) and (d) respectively, it can be seen that graphs obtained using flanged horns and CR systems show a general resemblance in its shape. For example, at frequency 10.76 GHz, both

Fig.4.8(i)(a)   Variaticn of VSWR with flange angle when the
flanges are kept at the 0- and M-positions.
1 - 0-position, 2 - M-position, N = 0.8,
Frequency = 10.76 GHz.

Fig.4.8(i)(b)   Variation of VSWR with flange angle when the
flanges are kept at the 0- and M-positions.
1 - 0-position, 2 - M-position, N = 0.8,
Frequency = 8.67 GHz.

90

Fig.4.8(i)(c)   Variation of VSWR with corner angle when the
                dipole is kept at the O- and M-positions.
                1 - O-position, 2 - M-position, N = 0.8,
                Frequency = 10.76 GHz.
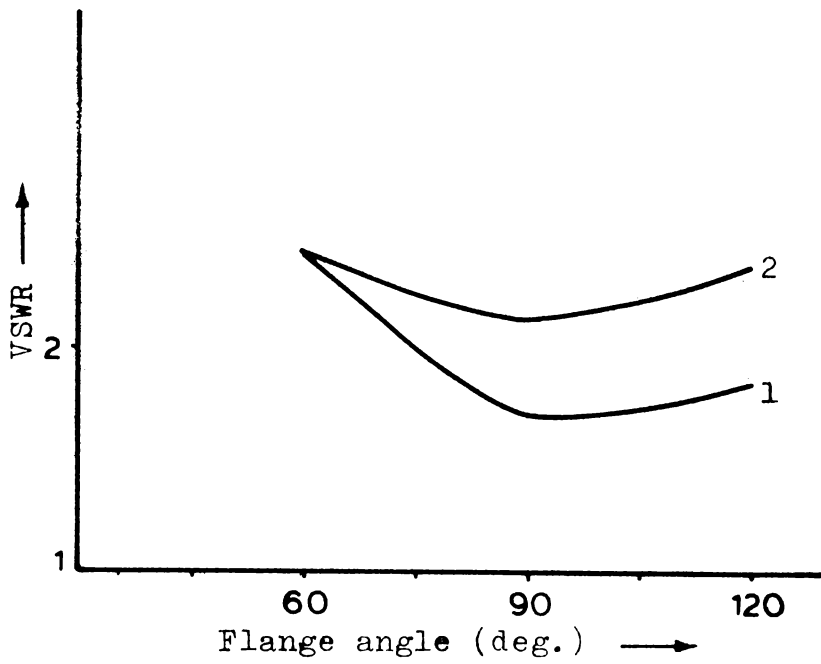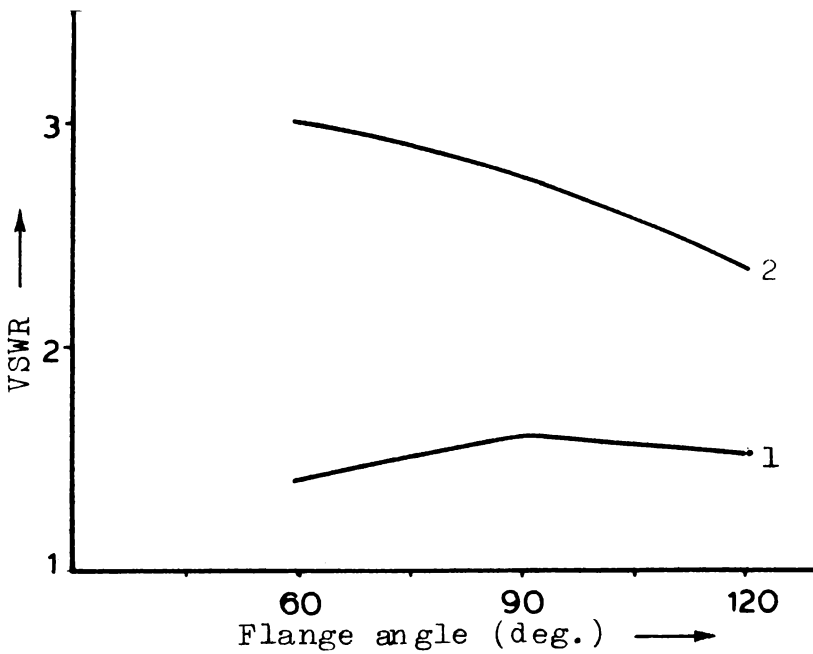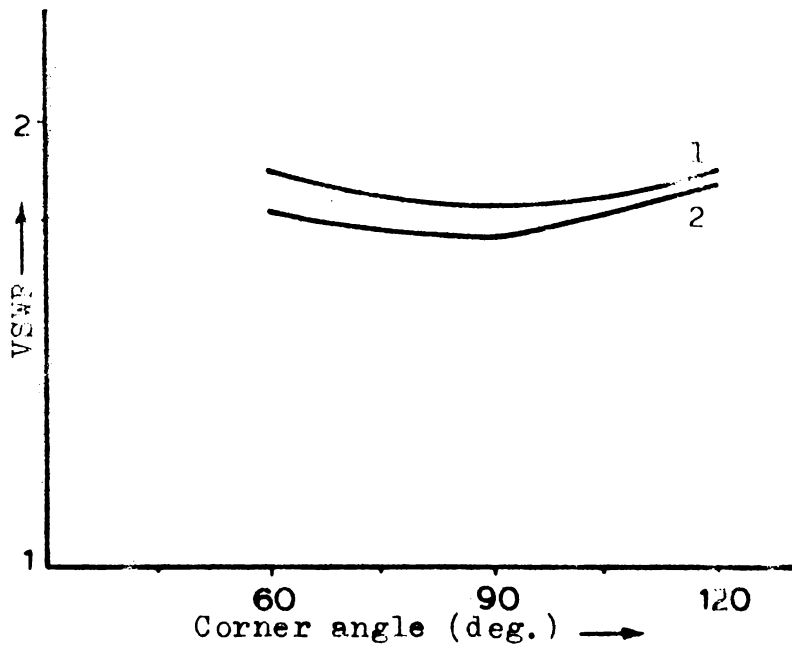

Fig.4.8(i)(d)   Variation of VSWR with corner angle when the
                dipole is kept at the O- and M-positions.
                1 - O-position, 2 - M-position, N = 0.8,
                Frequency = 8.67 GHz.

systems give minimum VSWR at a flange/corner angle of 90°. Eventhough the exact values of VSWR in the case of CR system are much less than those obtained with flanged horns, the general trend is such that the VSWR in both systems vary almost in a similar manner. The actual values of VSWR in both systems, under identical conditions, are different because the natural impedance of the primary feed in each case (horn or dipole as the case may be) will be different.

4.8(ii)   Change in VSWR with Corrugation Parameter

The corrugation parameter N is found to be strongly affecting the impedance conditions of the antenna systems. The VSWR at the 'Maximum' and 'Minimum' positions are measured for different flanges and reflectors and its dependence on the corrugation parameter is studied.

Figs.4.8(ii)(a) and (b) present the variation in VSWR with changes in corrugation parameter N for flanged sectoral horns at two different frequencies. It can be seen from these figures that the value of VSWR at the 'Optimum position' is lower than that at 'Minimum' for every value of corrugation parameter N. Figs.4.8(ii)(c) and (d) show the variation in VSWR with corrugation parameter N of the reflector elements, obtained in the case of corrugated CR systems. Comparing the results observed in the case of

Fig.4.8(ii)(a)   Variation of VSWR with corrugation parameter
N when the flanges are kept at the O- and
M-positions. 1 - O-position, 2 - M-position,
$2\beta = 90^{\circ}$, Frequency = 10.18 GHz.

Fig.4.8(ii)(b)   Variation of VSWR with corrugation parameter
N when the flanges are kept at the O- and
M-positions. 1 - O-position, 2 - M-position,
$2\beta = 90^{\circ}$, Frequency = 8.67 GHz.

Fig.4.8(ii)(c) Variation of VSWR with corrugation parameter N
when the dipole is kept at the O- and M-positions.
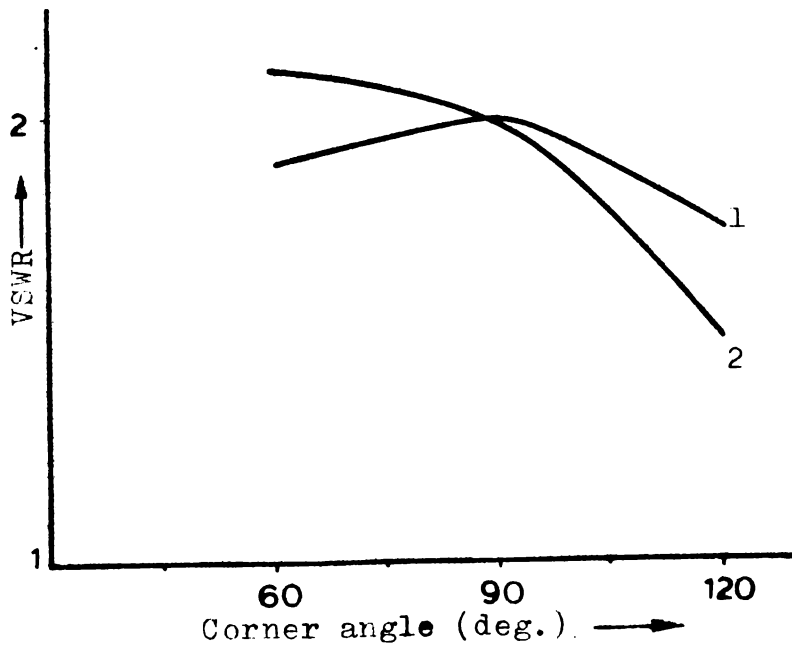1 - O-position, 2 - M-position, $2\beta = 90^\circ$,
Frequency = 10.18 GHz.

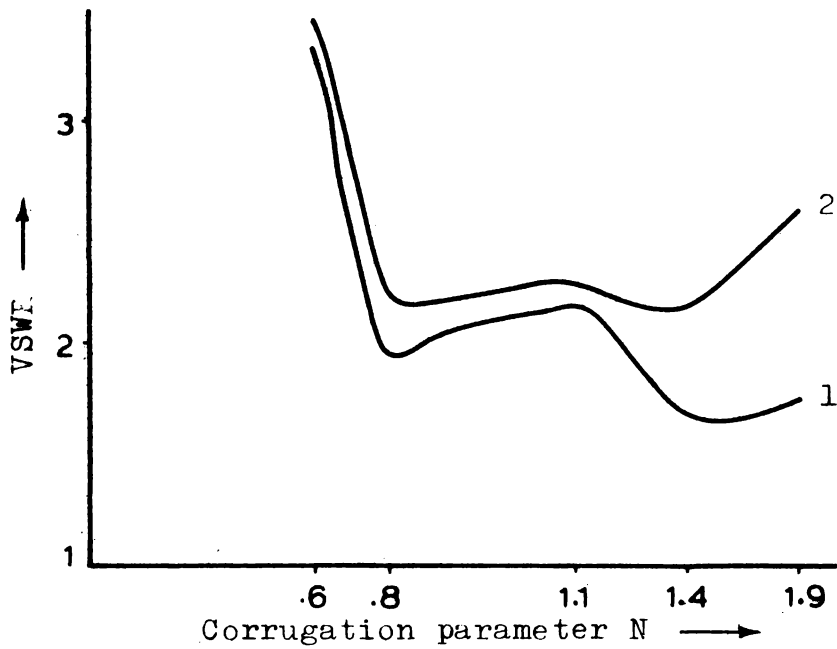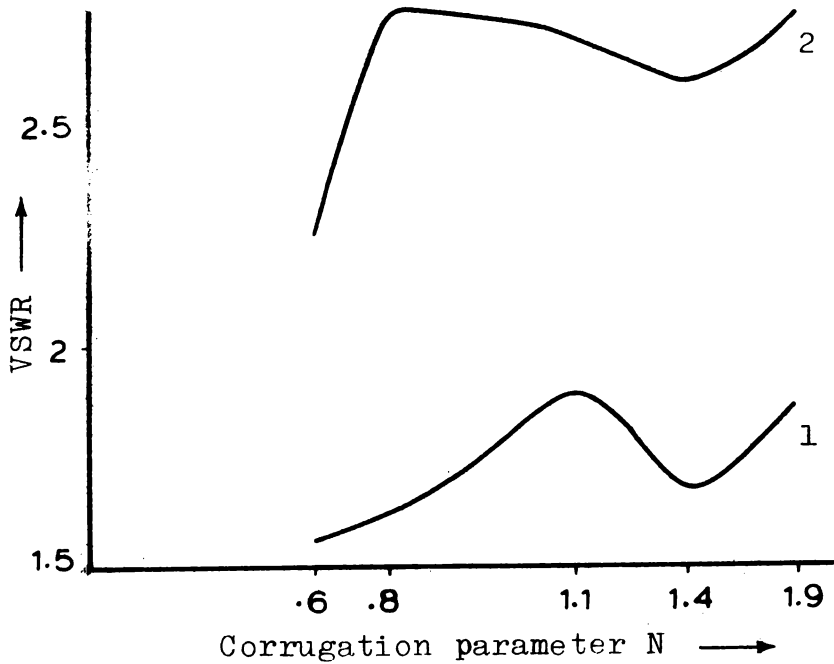Fig.4.8(ii)(d) Variation of VSWR with corrugation pa₃ meter N
when the dipole is kept at the O- and M-positions.
1 - O-position, 2 - M-position, $2\beta = 90^\circ$,
Frequency = 8.67 GHz.

CR system to that of flange system, it can be found that under identical conditions, the variation in impedance conditions of CR system closely resemble that of flanged sectoral horns. In the corrugated CR system also, the values of VSWR at 'O-position' are less than those at 'M-position' for almost all values of corrugation parameter N. Eventhough there are some slight discrepancies at certain portions of the graph, as can be seen from Figs.4.8(ii)(a) and (c), the general trend is such that the VSWR variation of the CR system closely follow that of flange system.

4.8(iii)   Dependence of VSWR on Frequency of Operation

When the frequency of operation of the antenna varies, the impedance of both systems were found to be changing. The VSWR at the positions of the primary feed giving maximum and minimum on-axis power (ie., O-position and M-position) were measured for both systems and the results are presented in Figs.4.8(iii)(a)-(d).

A comparative analysis of the results obtained with the two systems, show that the effect of frequency variation on VSWR are almost same for both systems. This is found to be true for all angles of corrugated flanges and CR system. Comparing Figs.4.8(a) and (c), it can be observed that the general nature of graphs have some

Fig.4.8(iii)(a)   Variation of VSWR with frequency when the
                  flanges are kept at the O- and M-positions.
                  1 - O-position, 2 - M-position, $2\beta = 90^{\circ}$,
                  N = 1.9.
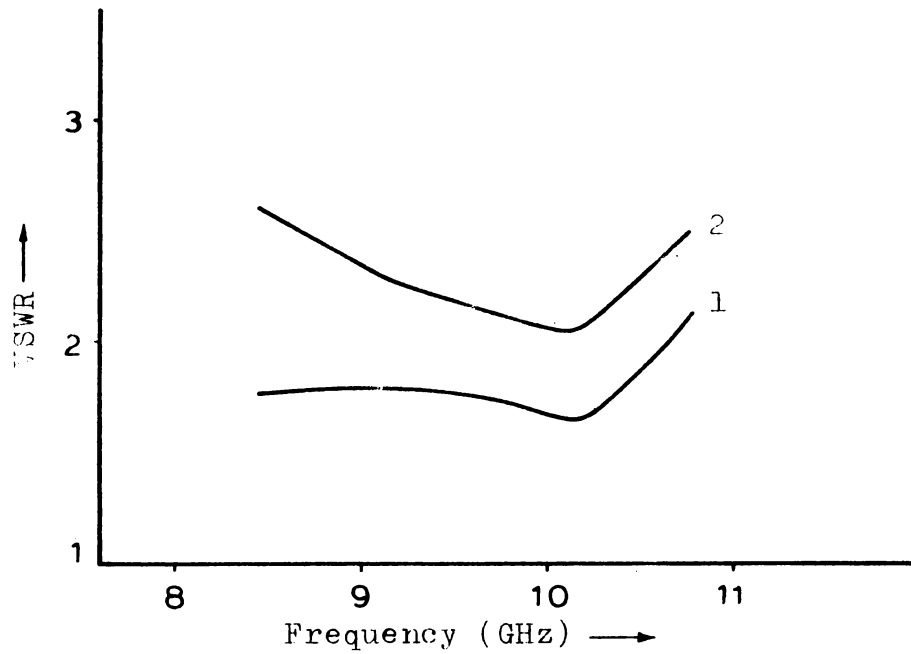
Fig.4.8(iii)(b)   Variation of VSWR with frequency when the
                  flanges are kept at the O- and M-positions.
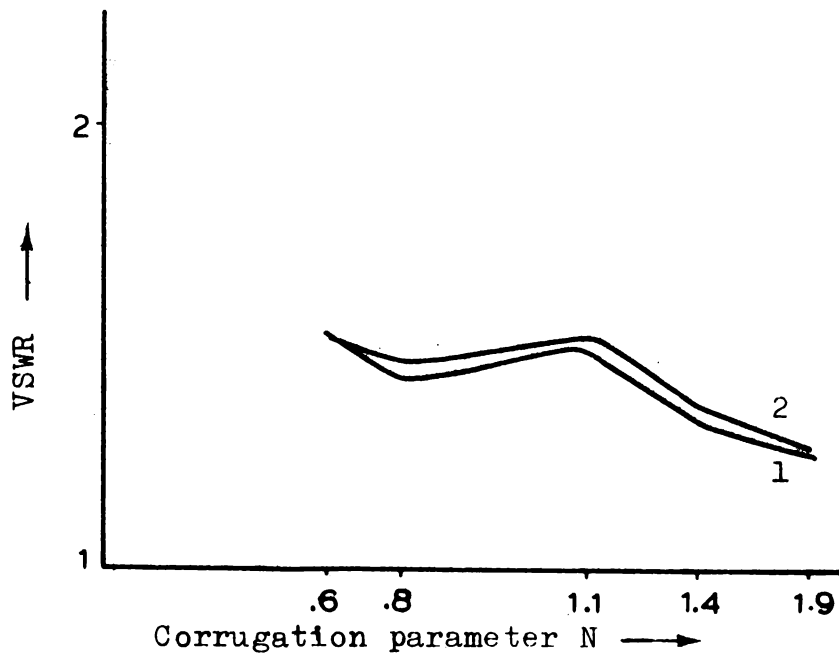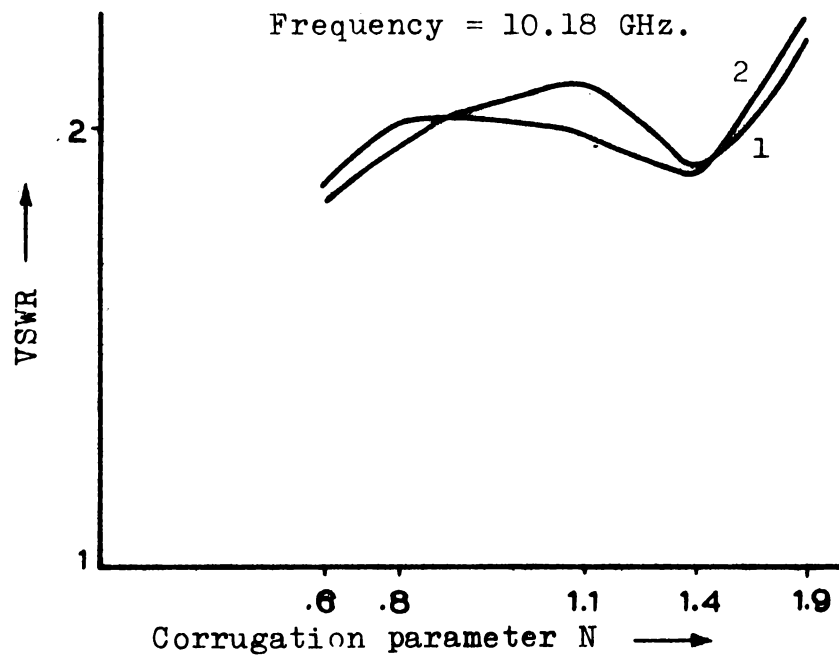   1 - O-position, 2 - M-position, $2\beta = 90^{\circ}$,
                  N = 1.4.

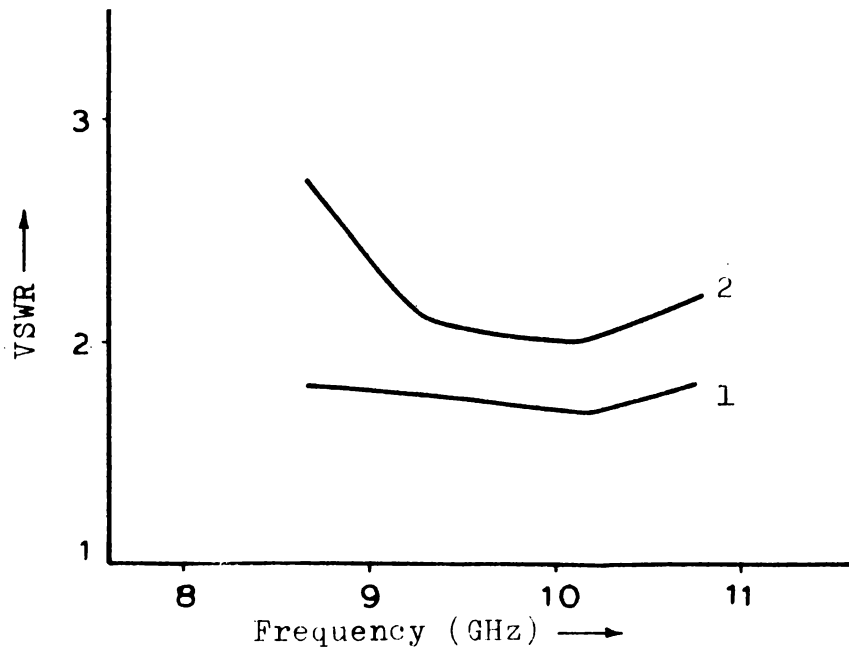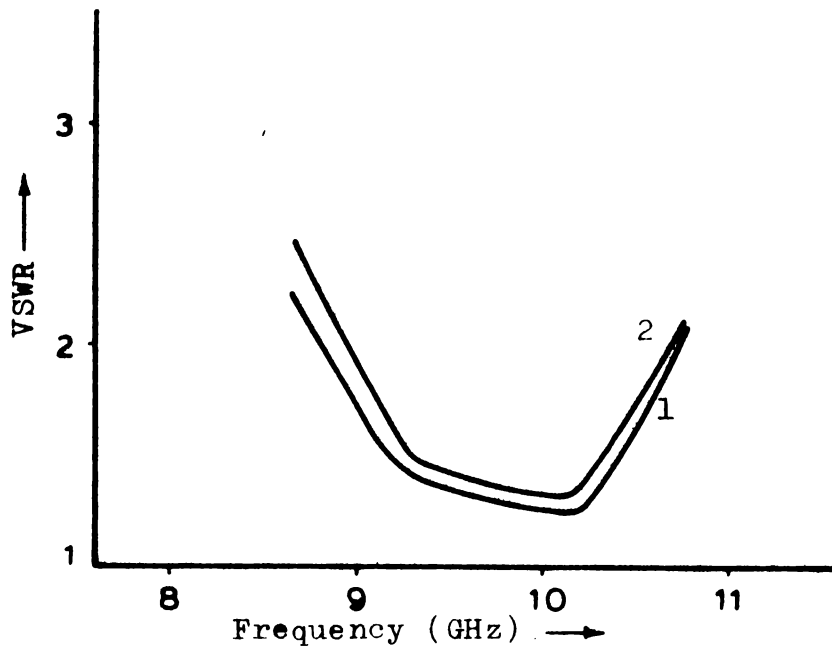**Fig.4.8(iii)(c)** Variation of VSWR with frequency when the dipole is kept at the O- and M-positions. 1 - O-position, 2 - M-position, $N = 1.9$, $2\beta = 90^{\circ}$.
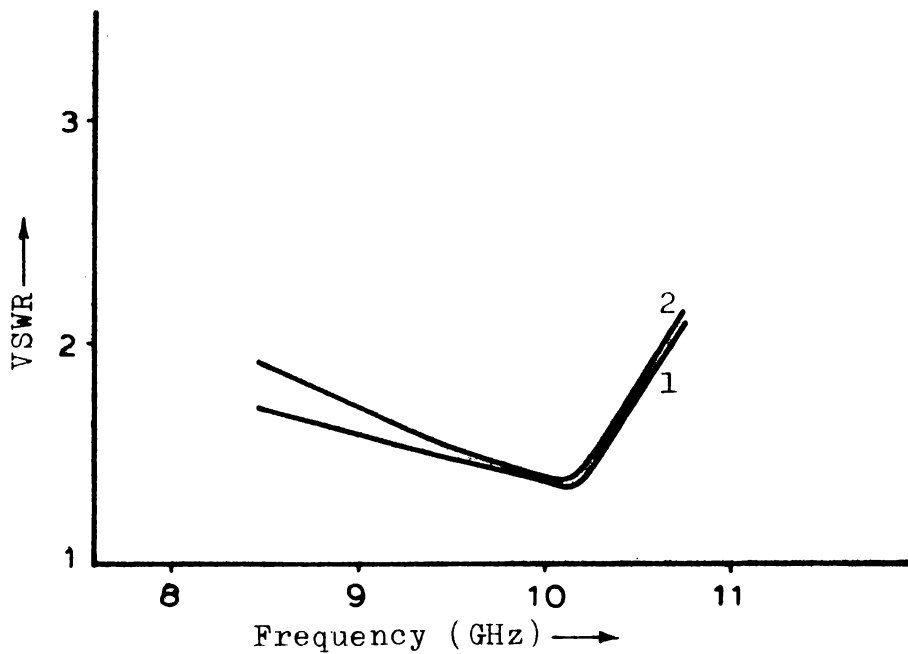
Fig.4.8(iii)(d) Variation of VSWR with frequency when the dipole is kept at the O- and M-positions. 1 - O-position, 2 - M-position, $N = 1.4$, $2\beta = 90^{\circ}$.

similarity in their shape, eventhough the change in VSWR at the O-position is very large for the CR system. When the frequency of operation changes, the length of dipole deviates from a half wavelength and this causes an increase in mismatch, and this can be the reason for the observed fluctuations in VSWR for the CR system. Again, the figures show that for both systems, the VSWR at the minimum position is higher than that at the maximum position. The frequency of operation giving the minimum VSWR under identical conditions, is also found to be the same for both flanged horns and CR systems.

4.8(iv)   Effect of Position of Primary Feed on VSWR

The position of the primary feed (horn or dipole) is found to influence the VSWR of both systems appreciably. Figs.4.8(iv)(a) and (b) show the variation of VSWR with distance of primary feed from apex of flange/reflector.

In the case of flanged horns, the maximum VSWR was observed at a distance of 3.2 cm of primary feed from apex of flange for a corrugation parameter of $N = 1.4$. Fig.4.8(iv)(b) shows that the corresponding distance, giving maximum VSWR, for corrugated CR system is 3.4 cms. Thus the figure illustrates that the variation in VSWR in both systems under identical conditions are almost similar.
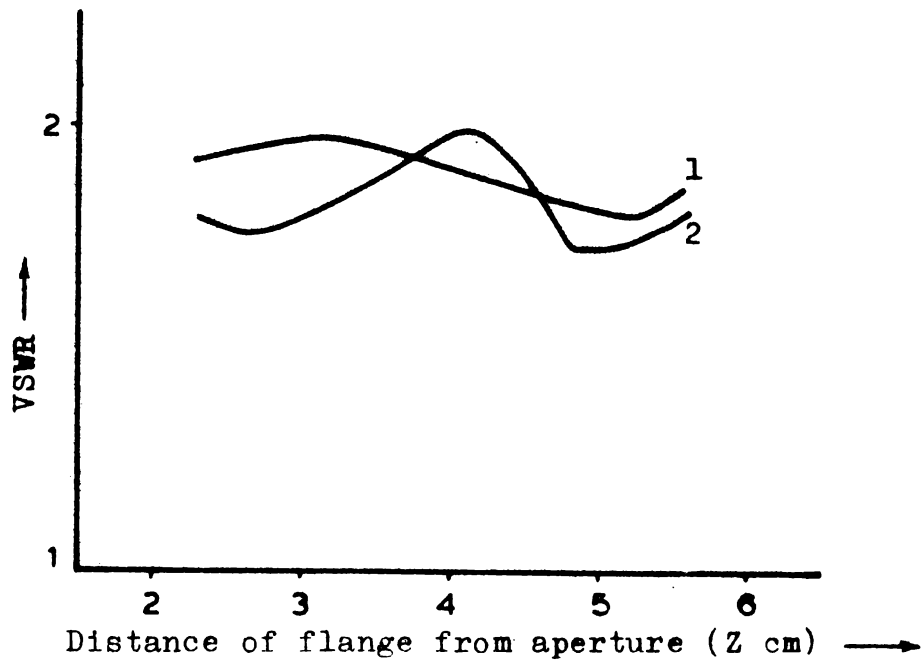
Fig.4.8(iv)(a)   Variation of VSWR with flange position.
1 - N = 1.4, 2 - N = 1.9, Frequency = 9.3 GHz,
$2\beta = 90^{\circ}$.
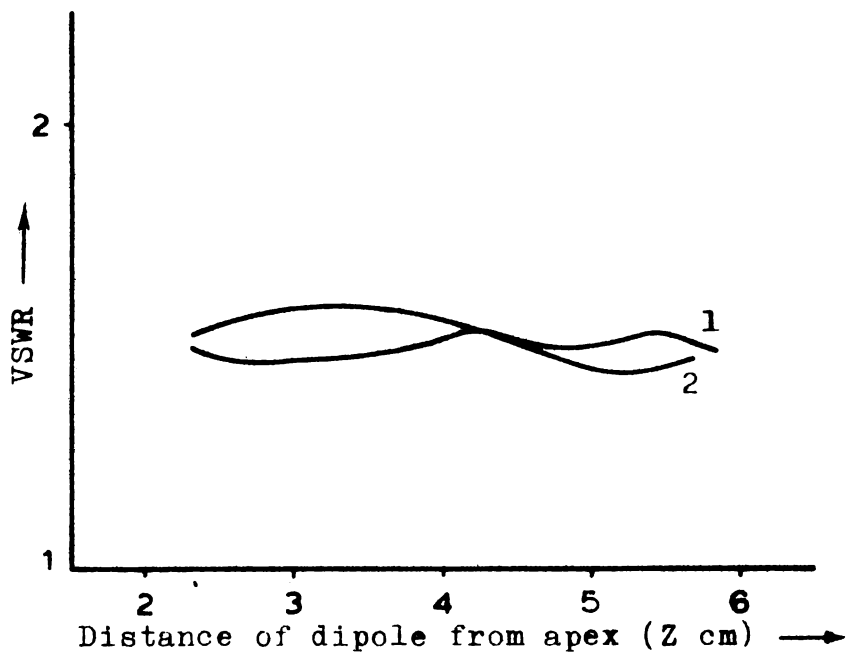
Fig.4.8(iv)(b)   Variation of VSWR with position of dipole of
the CR system. 1 - N = 1.4, 2 - N = 1.9,
Frequency = 9.3 GHz, $2\beta = 90^{\circ}$.

99

For a comparative analysis of the behaviour of two systems, the positions giving maximum and minimum VSWR for both systems are tabulated in table 4.8(iv)(I).

When the distance of the primary feed is varied, the phase difference of the reflected wave reaching the primary feed from the edges of the corrugations (which act as secondary radiators) will also change. This causes the variations observed in the matching conditions of both systems, with the position of the primary feed. For explaining a lower VSWR observed in the CR system, the point given in Section 4.8(i) can be used.

4.9 Beam Shaping by Corrugated Flanges/Corner Reflectors

The most important effect of corrugated flanges/ corner reflectors lies in their ability to control the radiation patterns. Corresponding to the variations in the on-axis power density of the system, the radiation pattern of the antenna also changes. Hence the various antenna parameters affecting the on-axis power density, strongly influence the beam pattern of the antenna systems.

4.9(i) Effect of Position of Primary Feed on Radiation Pattern

Many changes occur to the radiation pattern of flanges and CR systems when the position of primary feed

Table 4.8(iv)(I)

Positions giving minimum and maximum VSWR for corrugated flanged horns and corrugated CR systems

Flange/ corner angle 2β	Number of corrugations/cm (N)	Distance of primary feed giving minimum VSWR (cm)		Distance of primary feed giving maximum VSWR (cm)	
		Flanged horn	CR system	Flanged horn	CR system
90°	0.6	2.45	2.7	4	4.1
90°	0.8	2.7	2.9	4.8	4.9
90°	1.1	2.6	2.8	4	4.2
120°	0.6	2.9	3.15	1.8	2
120°	0.8	3	3.2	2.1	2.4

relative to the apex of the system is varied. The variations
in the beam patterns are similar to those observed in the
case of plane flanges and CR systems. In the case of corru-
gated systems also, the antenna pattern sharpens at the
0-position and splits at the M-position. At any other posi-
tion the radiation pattern obtained is a slightly broadened
one.

The methods of measurement and experimental details
for plotting the radiation patterns of both systems have
already been discussed in detail in the previous chapter.
The plotted radiation patterns of corrugated flanged sector-
al horns at 0-position and M-position are shown in
Fig.4.9(i)(a). It is observed that the property of beam-
focusing and splitting by corrugated flanges is true for all
flange angles, corrugation parameters and frequency of
operation. The patterns obtained for a corrugated CR
system at their 0- and M-positions are presented in Fig.
4.9(i)(b). Comparing Figs.4.9(i)(a) and (b), it can be
observed that both systems give almost similar patterns,
under identical conditions.

Tips of corrugations on the flange/reflector
elements act as secondary radiators excited by the primary
radiator (horn or dipole as the case may be) and the far
field radiation pattern obtained is a result of the

O-posn.   M-posn.

N=0.4
(4.2 GHz)

N=1.4
(10.18 GHz)

N=1.1
(10.18 GHz)

N=0.8
(10.18 GHz)
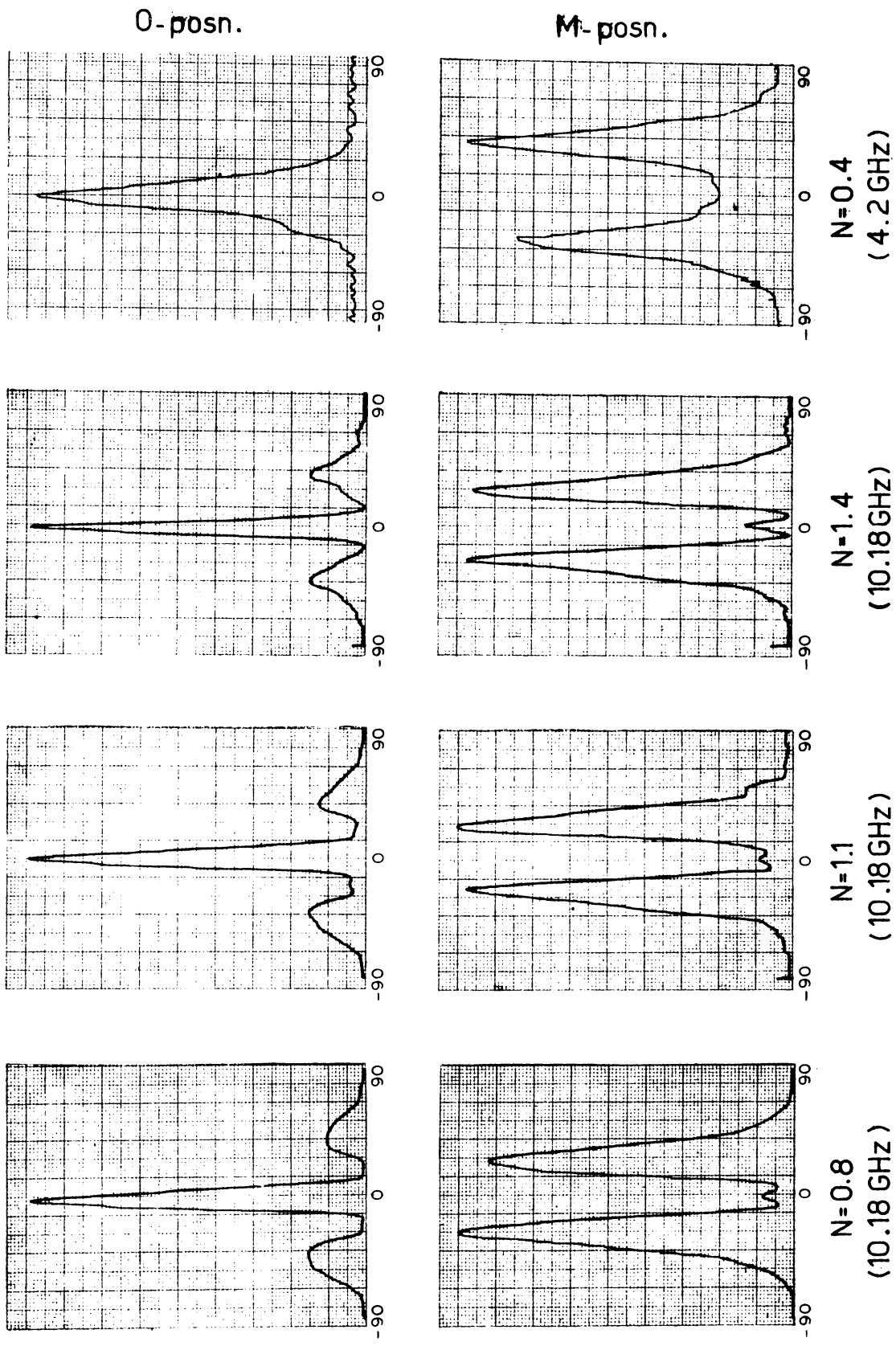
Fig. 4.9 (i)(a) Radiation patterns due to corrugated flanges. $2\beta = 90°$.

103

O - posn.

M - posn.

N = 0.4
(4.2 GHz)

N = 1.4
(10.18 GHz)

N = 1.1
(10.18 GHz)

N = 0.8
(10.18 GHz)
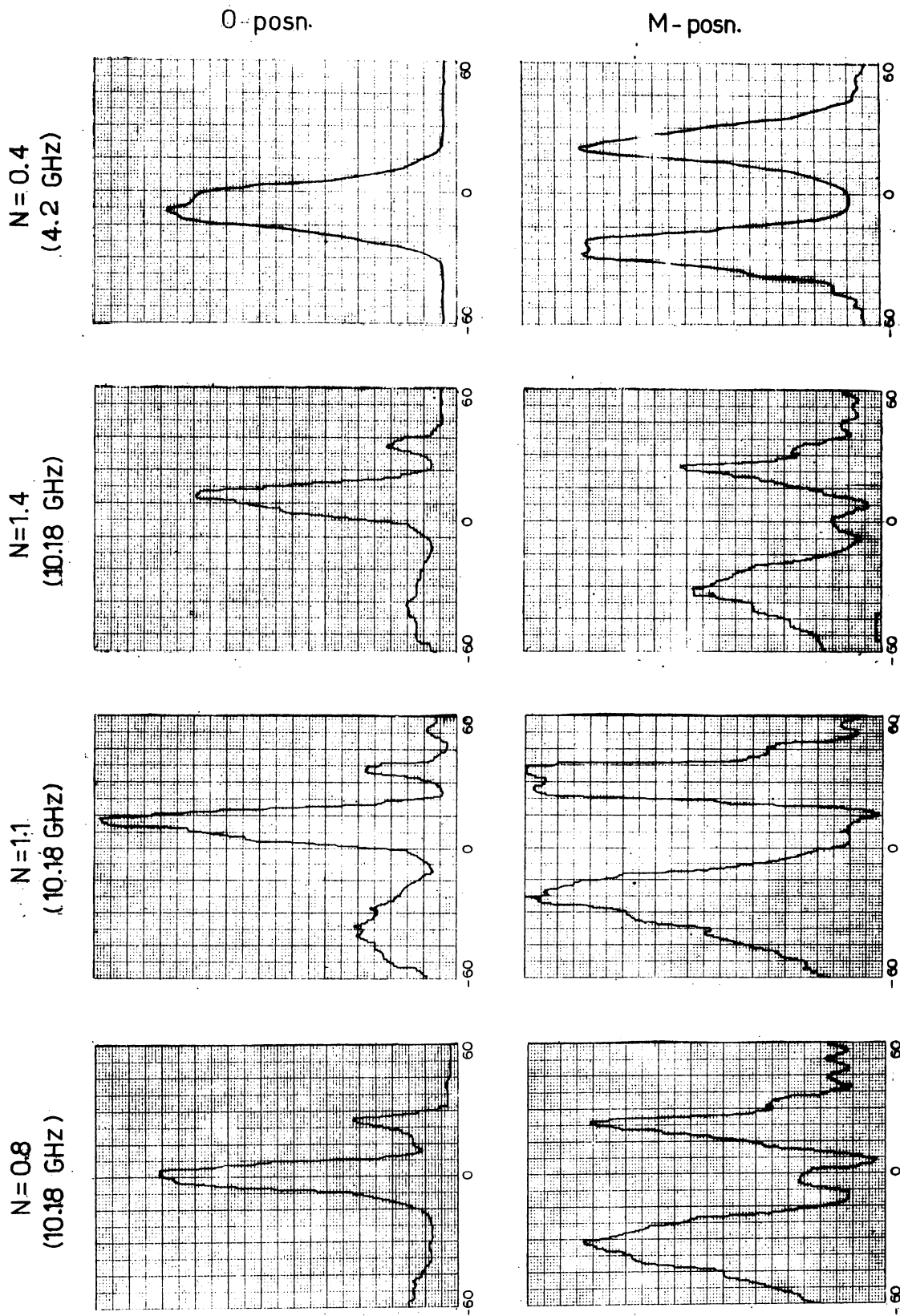
Fig. 4.9(i)(b). Radiation patterns of corrugated, CR system. $2\beta = 90°$.

104

superposition of the fields from all these radiating elements. When the distance of primary feed from the apex changes, the phase difference of waves from these radiators also varies and this causes a change in the resultant radiation pattern of the system. Thus the variation in the position of primary feed results in a change in the beam shape of the antenna system. Since the individual radiation patterns of sectoral horn and dipole (which will definitely affect the resultant radiation pattern of the antenna system) are different, the patterns observed using both systems will not be strictly identical in every respect.

Since the radiation patterns are closely related to the Half Power Beam Width (HPBW) and gain of the systems, the dependence of these characteristics on the different flange/reflector parameters like corrugation parameter, flange (corner) angle etc. is studied in detail. These results are presented in the following sections.

4.10 Half Power Beam Width (HPBW)

An important effect that follows, due to the variations in the radiation patterns of antennas, is the changes produced in the Half Power Beam Width. Since HPBW is directly related to the directivity and gain of the

systems,the study of its variations in respect of the various parameters will give an insight to the performance of the antennas.

4.10(i) Change in HPBW with Distance of Primary Feed from Apex of the System

As pointed out in the earlier section, the radiation patterns of both the systems undergo drastic changes with the position of the primary feed and this causes corresponding changes in the HPBW. Evidently, at the O-position, where the beam is very narrow, the beam width will be least. When the beam broadens, the half power beam width also increases. Thus the position of primary feed strongly affect the HPBW of the antennas. Since the change in radiation pattern with the position of primary feed for both systems are the same, the corresponding variations in HPBW also will be similar.

4.10(ii) Dependence of HPBW on Corrugation Parameter

Since corrugation parameter is the most important parameter of a corrugated system, the dependence of HPBW on it is studied in this section. The HPBW at both O- and M-positions are obtained for various corrugated flanges/ corner reflectors from their radiation patterns at these

positions. Figs.4.10(ii)(a) and (b) show the variation of HPBW with corrugation parameter N for a flange/corner angle of 90° at 0- and M-positions for both systems. Comparing the two figures, it can be seen that the values of N, giving maximum and minimum HPBW, are the same for both systems. Further, the general nature of the graphs also show a similarity in their shape.

4.10(iii) Variation of HPBW with Flange/Corner Angle

The effect of flange/corner angle on the beam width is studied for both systems and the results are presented in Figs.4.10(iii)(a) and (b). The analogous behaviour of both flanged horns and CR systems can be observed in this case also. The change in HPBW at both 0- and M-positions are presented and it shows that the beam width is least at 90° for a corrugation parameter of $N = 1.1$ for both systems. The figures again illustrate that the angle corresponding to maximum beam width also is the same in both cases.

4.11 Antenna Gain

The different changes effected in the radiation patterns of the systems due to variations in the different parameters, produce corresponding changes in the gain of
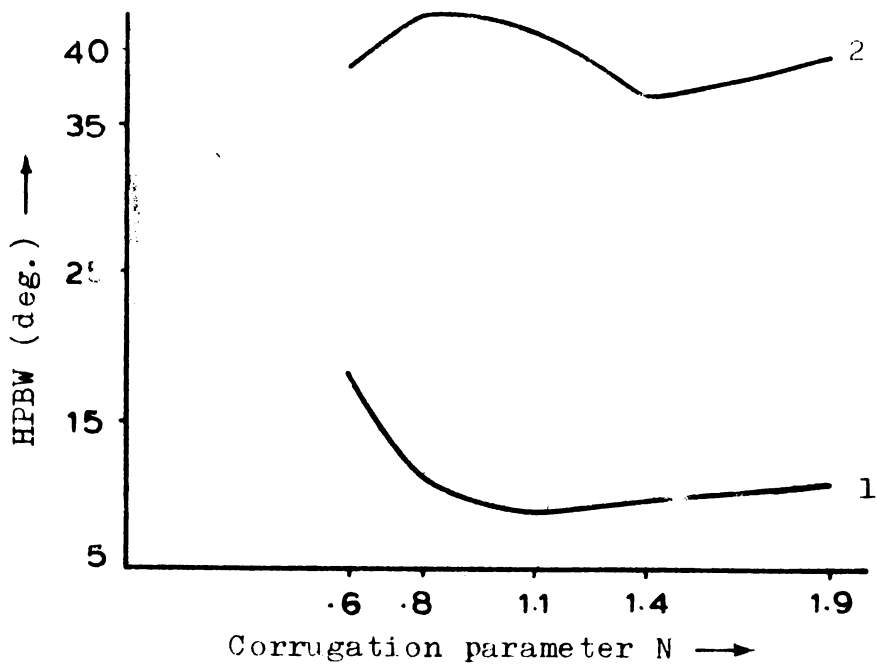
Fig.4.10(ii)(a) Variation of HPBW with corrugation par:meter N
                 wh.n the flanges are kept at the O- and M-positir .s.
                 $2\beta = 90^{o}$, Frequency = 10.76 GHz.

Fig.4.10(ii)(b) Variation of HPBW with corrugation parame!:r N
                 when the dipole is kept at the O- and M-positions.
                 $2\beta = 90^{o}$, Frequency = 10.76 GHz.

Fig.4.10(iii)(a)   Variation of HPBW with flange angle when the
                    flanges are kept at the O- and M-positions.
                    N = 1.1, Frequency = 9.3 GHz, 1 - O-position,
                    2 - M-position.
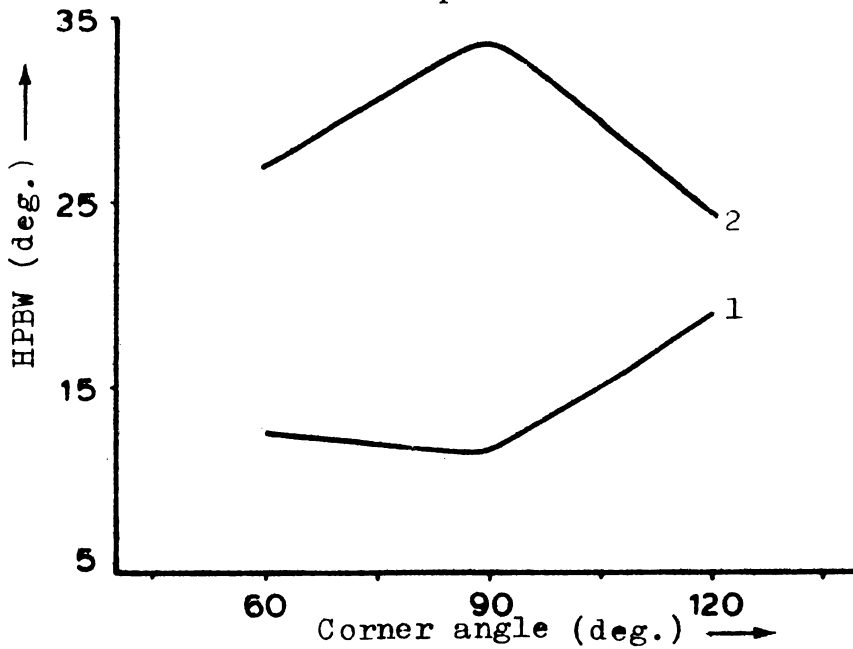
Fig.4.10(iii)(b)   Variation of HPBW with corner angle when the
                    dipole is kept at the O- and M-positions.
                    N = 1.1, Frequency = 9.3 GHz, 1 - O-position,
                    2 - M-position.

the system also. The flanges and reflectors can produce
changes in the radiation pattern in one plane, without
affecting the pattern in the other principal plane. Since
flanged H-plane sectoral horns and horizontally oriented
CR systems are used for modifying the E-plane pattern, the
comparison between the two systems is made by considering
the gain in that plane alone. The antenna gain in each case
is calculated using the numerical integration method
described in Section 3.4.

4.11(i)   Change in Antenna Gain with Position of Primary
          Feed

From the radiation patterns recorded at various
positions of the primary feed, the gain of the antennas were
calculated. At positions giving narrow radiation patterns,
the gain of the system is large and the gain reduces when
the beam width increases. Again, the gain of the system,
as can be seen from the numerical integration method depends,
to a great extent, on the radiation pattern of the antenna.
Hence the resemblances, already established between the two
systems regarding the radiation patterns, clearly show that
corresponding variations in gain may also exhibit resemblances.

4.11(ii) Variations in Gain with Corrugation Parameter

As in the case of other antenna characteristics already described, the gains of the system also depend much on the corrugation parameters of the flanges/corner reflectors used. The effects observed by the use of different types of flanges/corner reflectors having different corrugation parameters were studied. The variations in the gains of the antennas at both 0- and M-positions were taken for the purpose of comparison between flanged horns and CR systems. Figs. 4.11(ii)(a) and (b) show the variations obtained using flanged horns and CR system at a frequency of 9.3 GHz and having an included angle $2\beta = 90^{\circ}$. It can be observed from the graphs that the gains of the antennas at the 0-position has a maximum value for a corrugation parameter of N = 0.8. This is found to be true for both systems.

4.11(iii) Change in Gains of Both Systems with Flange/CR Angle

The included angle of the flanges/reflector elements also have considerable effect on the antenna gain of the systems. Fig.4.11(iii)(a) shows the variation of gain with flange angle at 0- and M-positions for a flange of corrugation parameter N = 1.1. Fig.4.11(iii)(b) gives the corresponding graph obtained in the case of corrugated CR system. The figures clearly indicate that the angle giving maximum
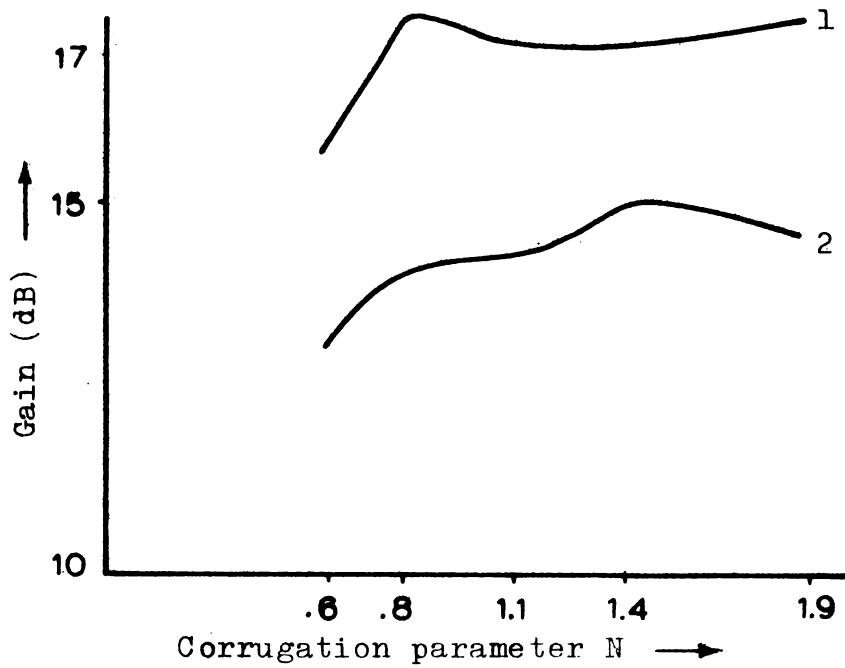
Fig.4.11(ii)(a)   Variation of gain with corrugation parameter N
                  when the flanges are kept at the O- and M-
                  positions.   2β = 90°, Frequency = 9.3 GHz.
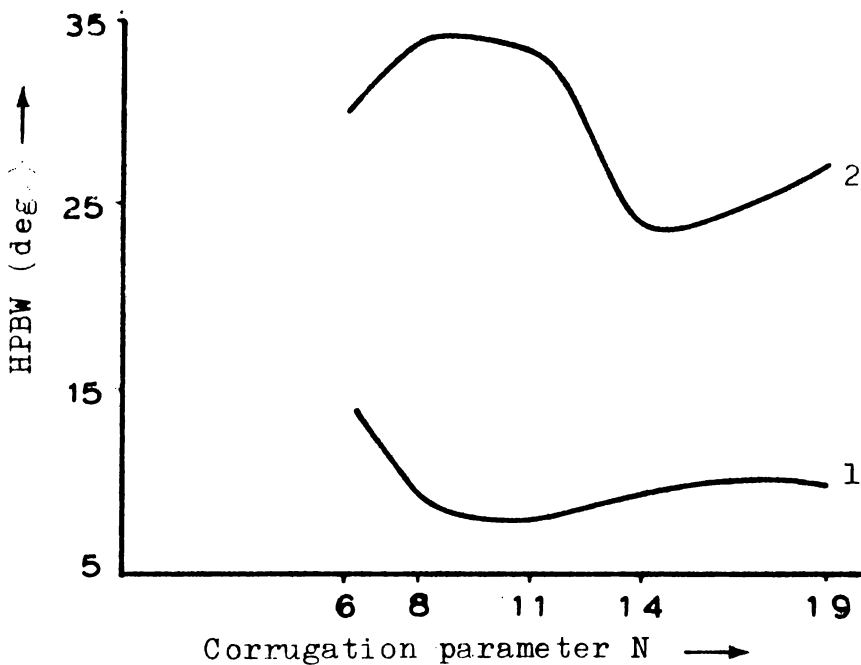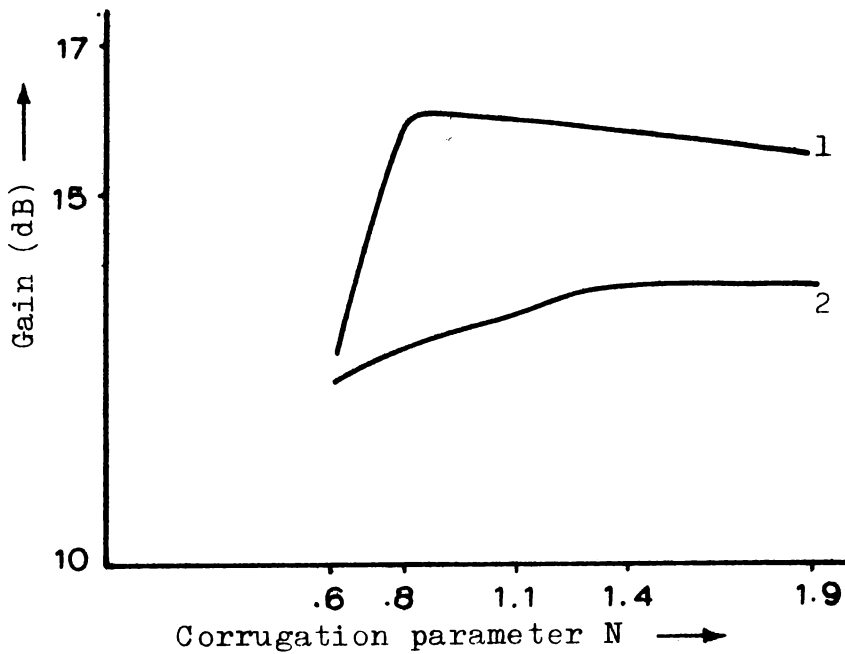

Fig.4.11(ii)(b)   Variation of gain with corrugation parameter N
                  when the dipole is kept at the O- and M-
                  positions.   2β = 90°, Frequency = 9.3 GHz.
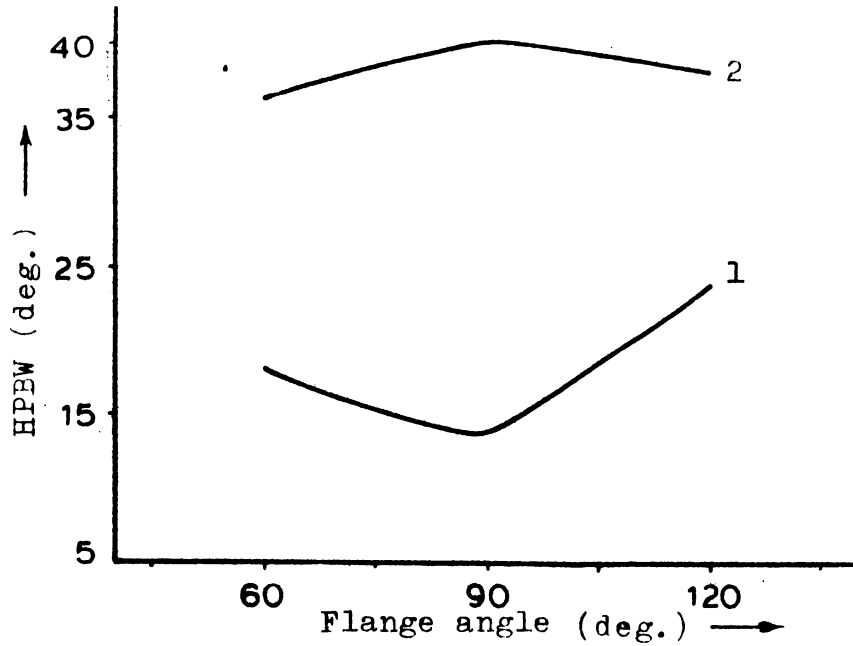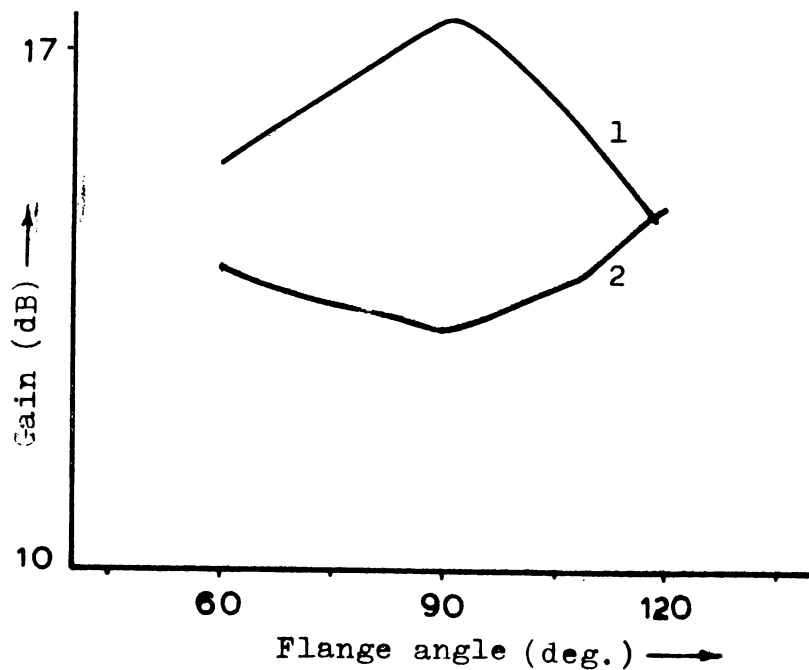
Fig.4.11(iii)(a) Variation of gain with flange angle when the flanges are kept at the O- and M-positions. N = 1.1, Frequency = 9.3 GHz, 1 - O-position, 2 - M-position.
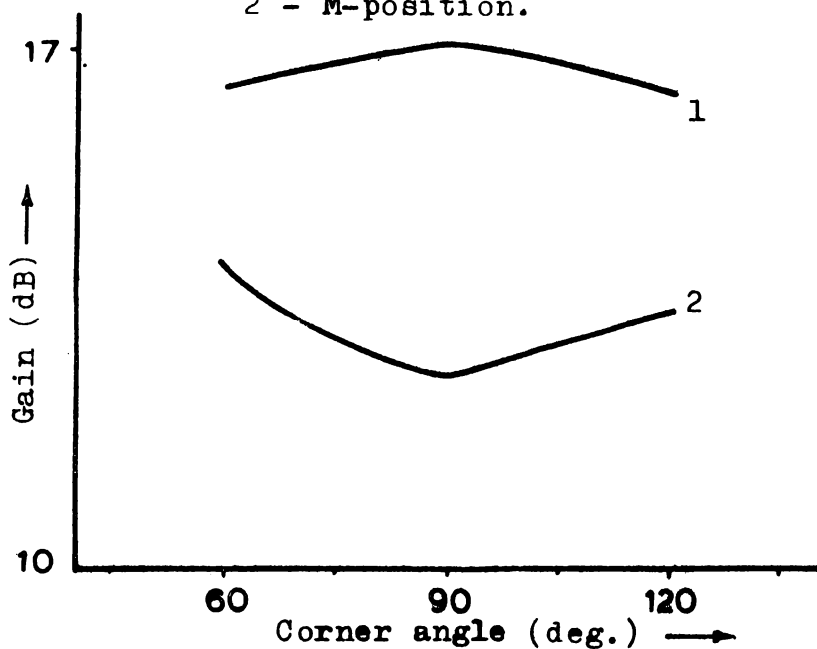
Fig.4.11(iii)(b) Variation of gain with corner angle when the dipole is kept at the O- and M-positions. N = 1.1, Frequency = 9.3 GHz, 1 - O-position, 2 - M-position.

113

and minimum gain at O- and M-positions are the same for both systems. Thus the analogy in the behaviour of corrugated flanged sectoral horns and corrugated CR systems already observed for other antenna characteristics, is found to be true in this case also.

Part III   Inclined Corrugated Flanges/Reflectors for
          Producing Elliptically and Circularly
          Polarized Radiation from Horns/CR Systems

This section presents the results of an attempt to produce elliptically and circularly polarized radiations using inclined corrugated flanges and reflectors. In the case of CR systems, investigations are carried out on the various characteristics like axial ratio, angle of tilt of the polarization ellipse etc. Eventhough an exhaustive study using the flange system has not been conducted, preliminary investigations reveal that the inclined corrugated flange system are also capable of producing elliptical and circular polarization.

4.12   Radiation Patterns of Horizontal and Vertical Field
       Components

Since a circularly polarized wave can be resolved into two mutually perpendicular linearly polarized waves, the horizontal and vertical field patterns in the azimuthal plane

of the antenna systems are plotted. Fig.4.12(a) shows the radiation patterns in the azimuth plane of vertical and horizontal field components obtained using inclined corrugated CR systems. The experimental techniques used in this study have already been described in the previous chapter. From the figures, it can be observed that the vertical and horizontal field patterns are almost similar, but with different peak values. This indicates that the radiation from CR system is elliptically polarized. This result may be true even in the case of partially polarized beam, which is impossible here since the dipole is giving plane polarized beam originally. Using the inclined corrugated flanges also, the radiation patterns of both vertical and horizontal field components were plotted and these are also given in Fig.4.12(a). This figure shows that the radiation from sectoral horns are also polarized elliptically by the use of inclined corrugated flanges. Thus, **from the** figure, it can be seen that the two systems give elliptical or circular polarizations when inclined corrugated flanges/ reflectors are used. A detailed study of the polarization properties of CR systems have been made and the results of this are presented in the subsequent sections.
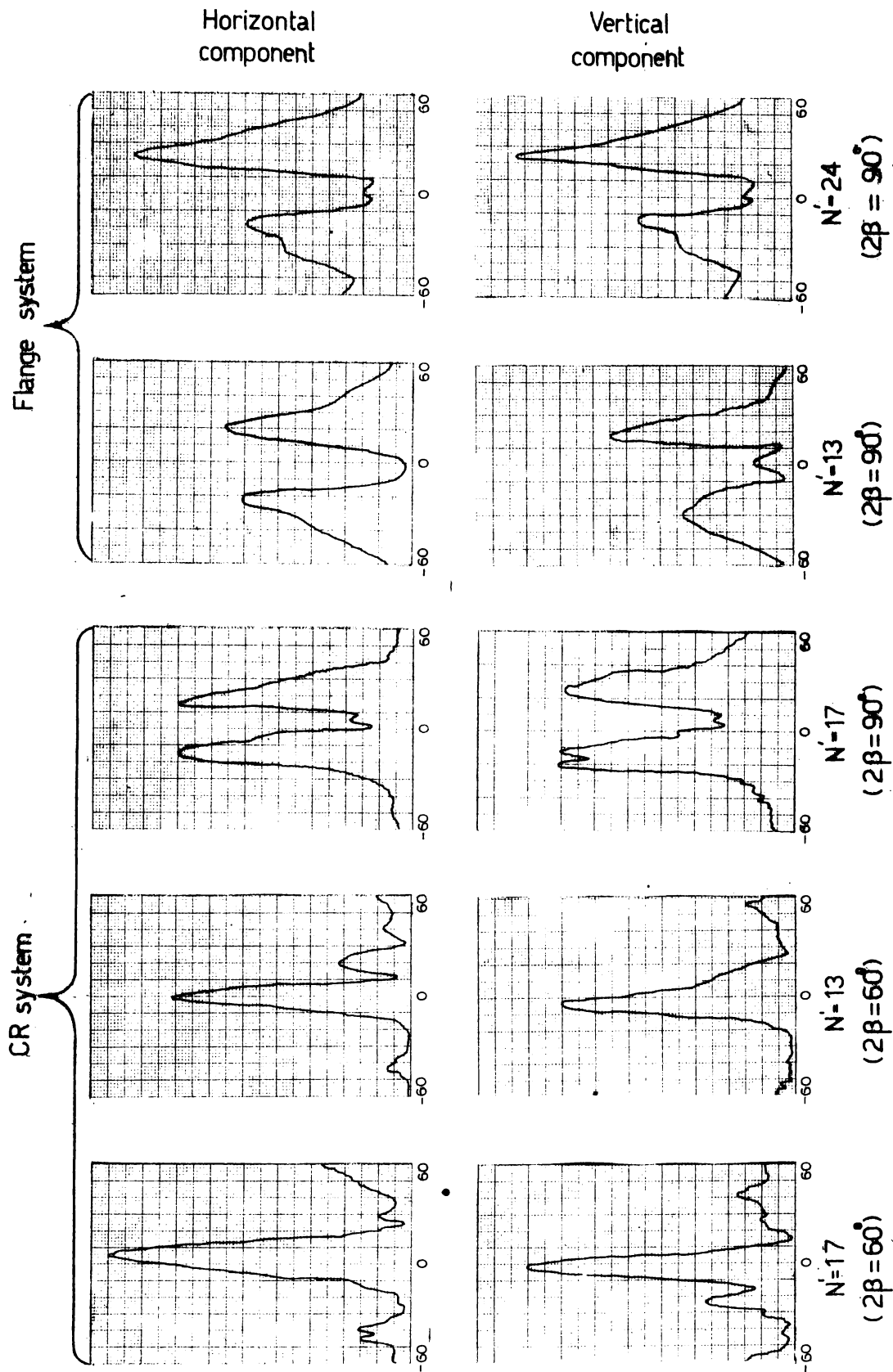
Fig. 4.12(a). Normalized patterns of vertical and horizontal field components obtained using inclined corrugated flange/CR systems. Frequency = 8.67GHz.

116

4.13   Axial Ratio

"Axial ratio" or "ellipticity" of the radiated
energy generally refers to the ratio of the major axis to
the minor axis of the polarization ellipse taken on the
axis of the radiated beam. This being an important chara-
cteristic of an elliptically polarized antenna, as pointed
out in chapter III, its dependence on the various parameters
of the CR systems have been studied in detail.

The variation of axial ratio of the radiated beam
with number of corrugations N'on the reflector elements have
been presented in Fig.4.13(a). The graph shows that the
radiated beam is clearly elliptically polarized for all
values of N'and on certain cases, it is circularly polarized
(example N'= 13). The axial ratio obtained using different
inclined corrugated flanges have been presented in Table
4.13(I). From this, it can be seen that the inclined
corrugated flange systems are also capable of producing
elliptically and circularly polarized beam. Fig.4.13(b)
gives the changes in axial ratio of the elliptically polarized
radiations for different corner angles. This figure indicates
that the axial ratio of the beam is dependent on the corner
angle of the CR system appreciably.

Fig.4.13(a)   Variation of axial ratio with number of corrugations
             N' on the inclined corrugated reflector elements.
             1 - 10.76 GHz, 2 - 8.67 GHz, 2β = 120°.
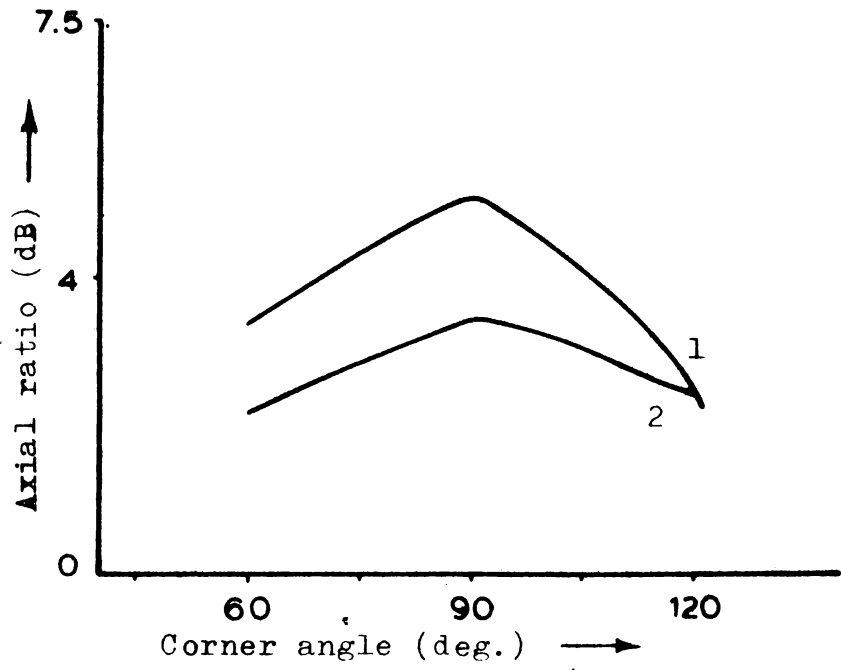
Fig.4.13(b)   Variation of axial ratio with corner angle of the
             inclined corrugated CR system. N' = 24, 1 - 8.67 GHz,
             2 - 10.18 GHz.

Table 4.13(I)

The axial ratio obtained using different inclined
corrugated flanges. Frequency = 8.67 GHz.

Flange Number	Number of corrugations N'	Axial ratio (dB)	
		$2\beta = 90^\circ$	$2\beta = 60^\circ$
1	6	7.5	5.5
2	13	7.2	4.2
3	17	1.1	2.1
4	24	0.6	2.7

4.14   Angle of Tilt of the Polarization Ellipse

The polarization ellipse is generally tilted in space and the angle of tilt above the horizontal is measured using a single linearly polarized directional antenna. The variations of this angle of tilt with different parameters of the CR system have been studied and the results are presented in this section.

Figs.4.14(a) and (b) present the changes in the angle of tilt with number of corrugations N' on the reflector elements for two different corner angles. From the figures it can be seen that the polarization ellipse has undergone drastic changes in its orientation when the corrugation parameters are varied. Further, the dependence of the angle of tilt on corner angle and frequency of operation are given in Figs.4.14(c) and (d) respectively. Hence, any of these parameters can be conveniently adjusted to obtain a desired angle of tilt of the polarization ellipse.

4.15   Impedance Conditions

Impedance matching of the inclined corrugated system is the next aspect taken for investigation. This important characteristic related to the radiation efficiency of the antenna, is studied by measuring the VSWR of the systems. The values of VSWR obtained using different inclined
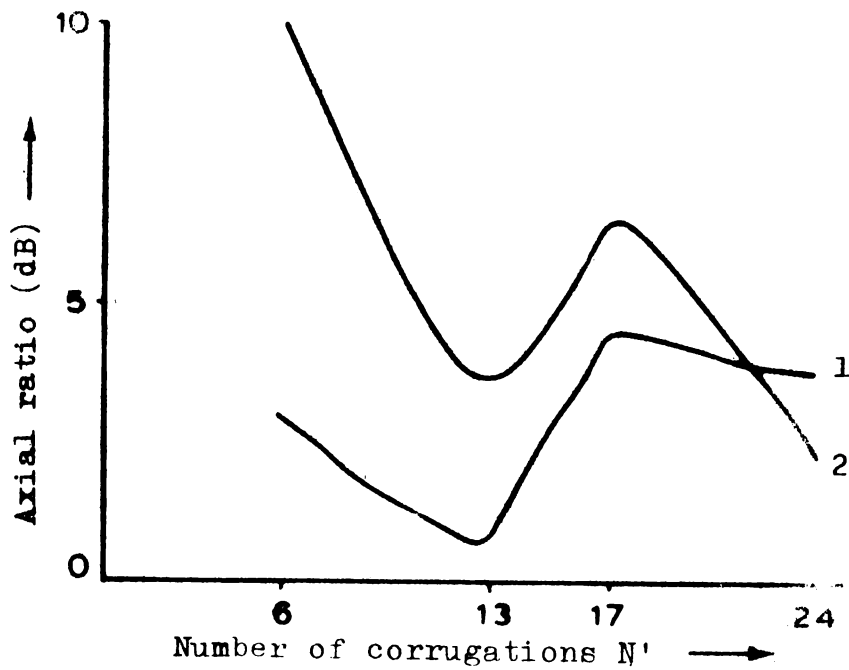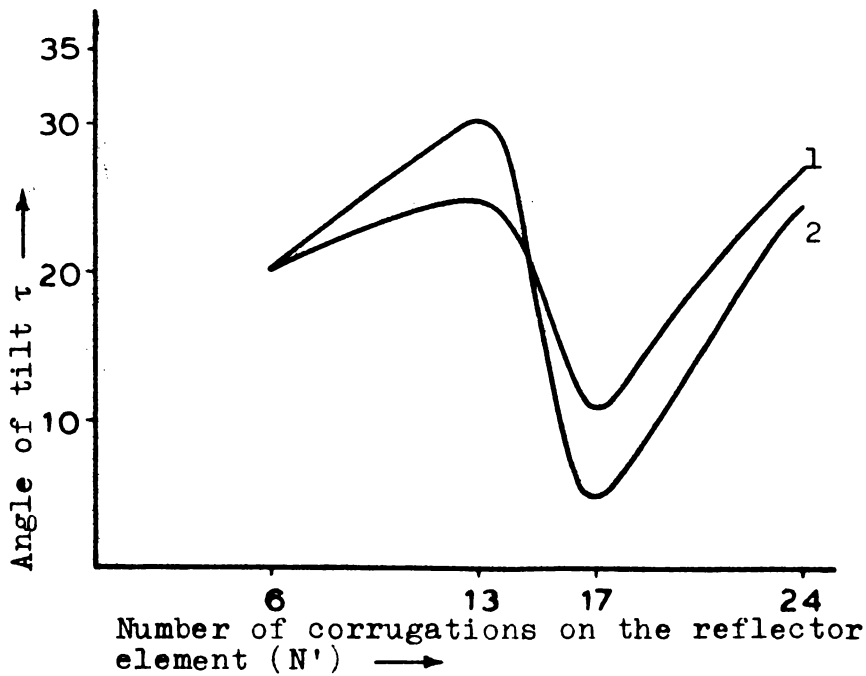
Fig.4.14(a)   Variation of angle of tilt with number of
              corrugations on the inclined corrugated
              reflector element. 1 - 10.76 GHz, 2 - 10.18 GHz,
              $2\beta = 90^{\circ}$.
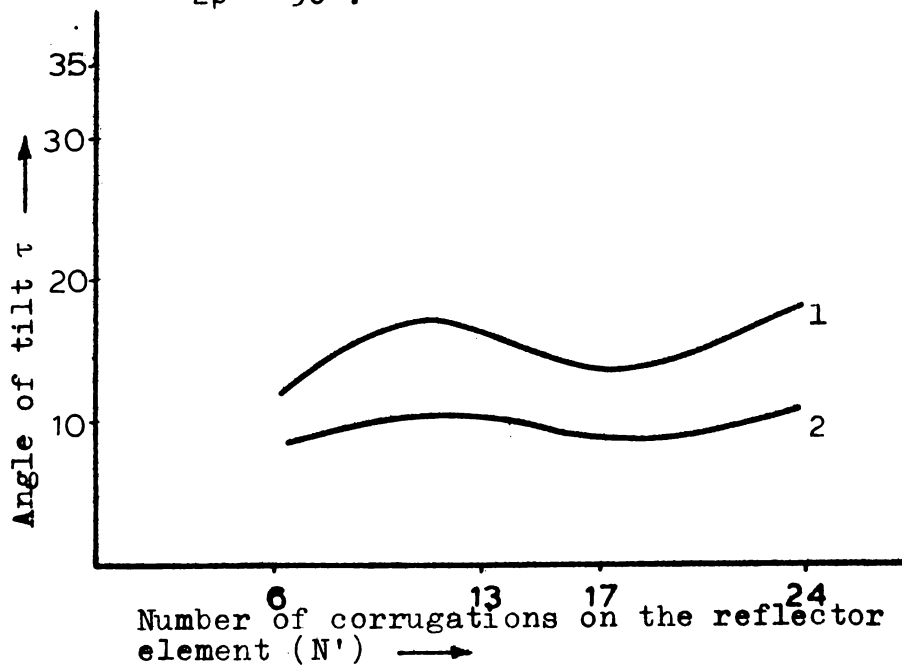
Fig.4.14(b)   Variation of angle of tilt with number of
              corrugations on the inclined corrugated
              reflector element. 1 - 10.76 GHz, 2 - 10.18 GHz,
 $2\beta = 120^{\circ}$.
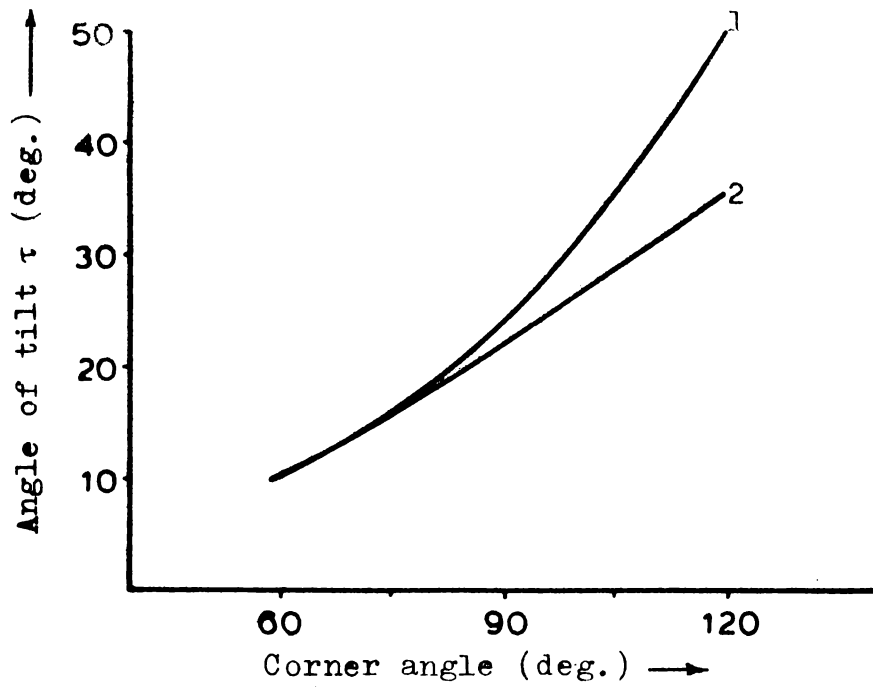
Fig.4.14(c)   Variation of angle of tilt with corner angle of the
inclined corrugated corner reflector system.
1 - N' = 17, 2 - N' = 13, Frequency = 10.76 GHz.
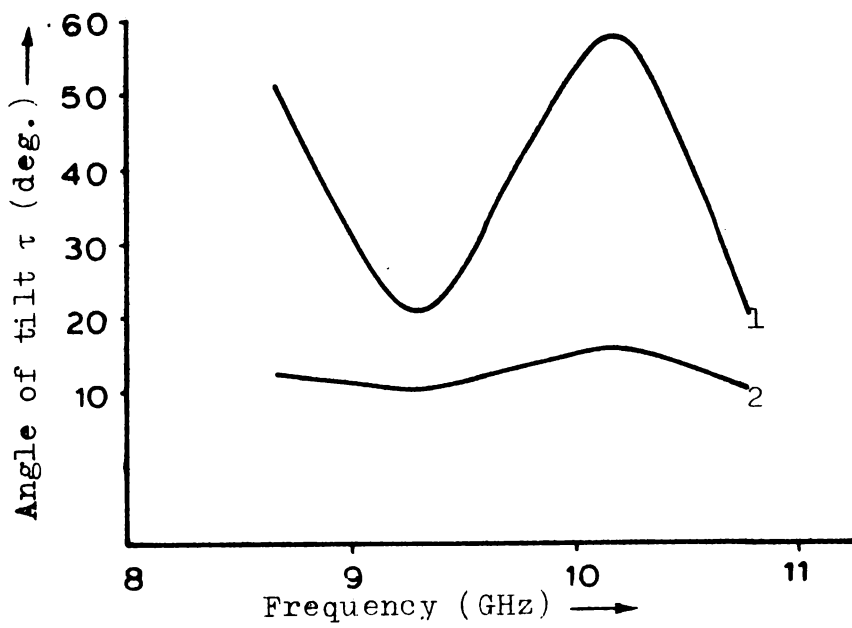
Fig.4.14(d)   Variation of angle of tilt with frequency.
1 - N' = 24, 2 - N' = 13, $2\beta = 60°$.

122

Table 4.15(I)

VSWR of the Inclined corrugated CR systems
Frequency = 10.76 GHz

Reflector Number	Number of corrugations N'	VSWR		
		$2\beta = 60°$	$2\beta = 90°$	$2\beta = 120°$
1	6	1.47	1.82	1.55
2	13	1.8	1.71	1.76
3	17	1.45	1.67	1.44
4	24	1.85	1.45	1.92

corrugated reflectors at various corner angles are presented
in Table 4.15(I). This table illustrates that the CR
systems giving elliptically or circularly polarized radiation
have a considerably low mismatch.

Thus, the results obtained using inclined corruga-
ted reflectors show that this system provides a simple
technique for producing elliptically and circularly polarized
radiation from linearly polarized CR antennas. A preliminary
investigation on sectoral horns has shown that the inclined
corrugated flanges also are capable of producing elliptically
polarized radiation. Hence the investigations using inclined
corrugated structures also show a similarity in behaviour
between flanged sectoral horns and CR systems.

A theoretical analysis of these experimental results
are discussed in the next chapter.

THEORETICAL ANALYSIS OF FLANGED SECTORAL HORN ANTENNAS
AND CORNER REFLECTOR SYSTEMS

A theoretical analysis of the experimental results described in the previous chapter, is presented here. The Line Source Theory, suggested by Owen and Reynolds[57] is used for explaining the effects of flanges on sectoral horns. The radiation from corner reflector systems has been analysed by employing the method of images[73]. In the case of corrugated systems, a detailed mathematical derivation for the power radiated to a point in the far field is presented. Numerical data computed on the basis of this theory is also given and a comparison is made between the theoretical results and experimental observations.

5.1(i) Theory of Plane Flanged Sectoral Horns

For deriving an expression for the radiated power at a point in the far field, the following two major assumptions, proposed by Owen and Reynolds[57] and later by Butson and Thompson[58] have been adopted.

(i) The narrow aperture of the sectoral horn may be approximated to a linear source.

(ii) The two edges of the plane flanges act as secondary radiators excited by the primary line source (aperture of horn).

Fig.5.1(i)(a) is the schematic diagram of a plane flange mounted H-plane sectoral horn. The geometry of the system is shown in Fig.5.1(i)(b). Here S is the primary radiator and S_1 and S_2, the two secondary radiators. Assuming that the intensity of field from the primary as unity, k is taken as the amplitude of field at P due to each of the secondary radiators. Now, magnitude of the secondary relative to the primary can be written as

$$V = ke^{-j(\frac{2\pi}{\lambda} \cdot \frac{B}{2})} = ke^{-j\frac{\pi B}{\lambda}}$$

$$= ke^{-j\varphi} \tag{5.1}$$

This phase difference is due to the separation $\frac{B}{2}$ between each secondary source and S.
The resultant of the secondary sources at O is given by

$$V_s = ke^{-j\varphi} \left[e^{j\frac{2\pi b}{\lambda}} + e^{-j\frac{2\pi b}{\lambda}} \right]$$

$$= 2ke^{-j\varphi} \cos\frac{2\pi b}{\lambda} \tag{5.2}$$
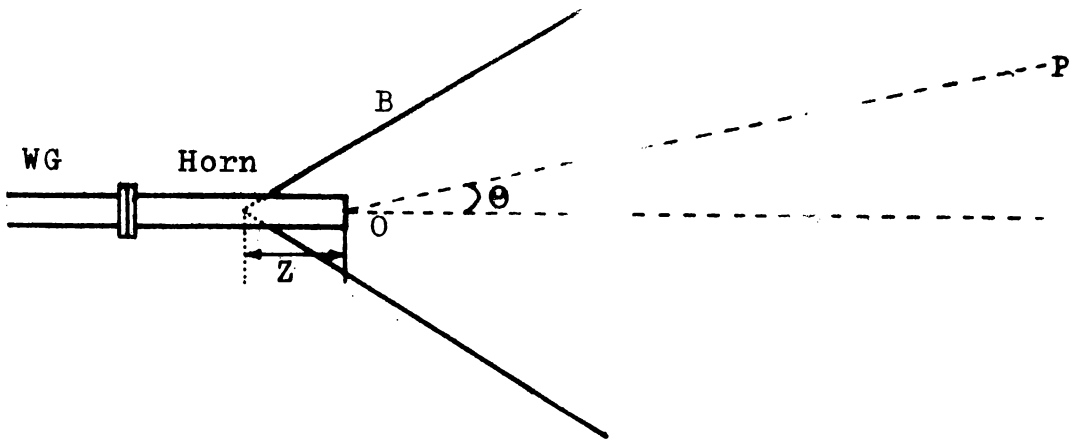
Fig.5.1(a)   Schematic diagram of plane flange mounted
             H-plane sectoral horn. O is the horn aper-
             ture, B is the width of flange, P is the
             distant point.
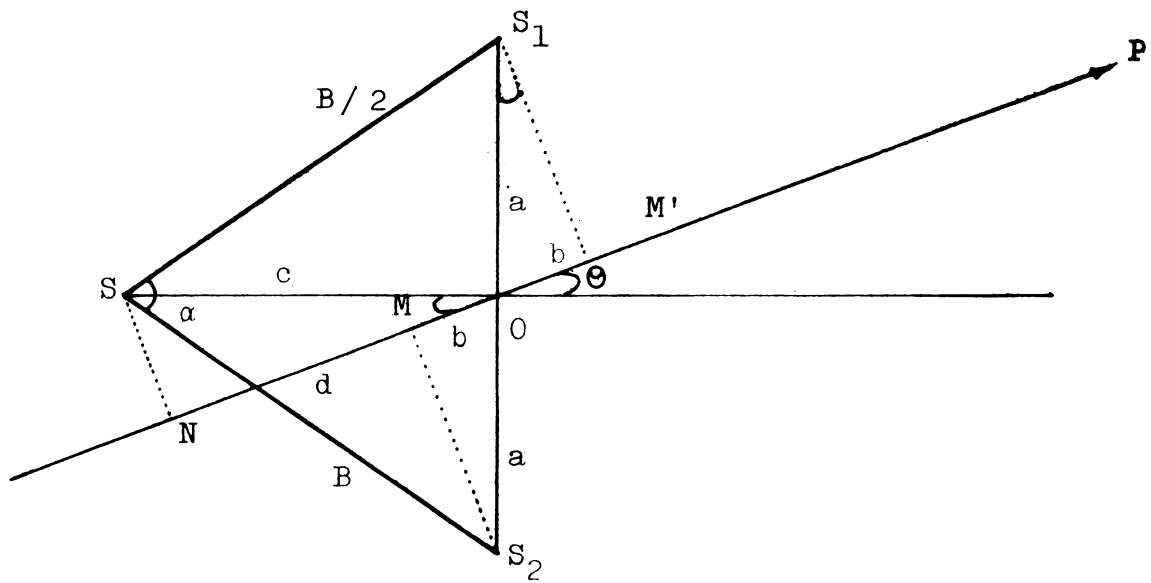
Fig.5.1(b)   Geometry of the plane flange system.
             S_1 and S_2 are the secondary sources.

127

Substituting $b = a \, \text{Sin} \, \theta$

where $a = \dfrac{B}{2} \, \text{Sin} \, \alpha$

Equation (5.2) can be written as

$$V_s = 2k e^{-j\varphi} \, \text{Cos} \left(\dfrac{\pi B}{\lambda} \, \text{Sin}\alpha \, \text{Sin} \, \theta \right)$$

$$= a_s e^{-j\varphi} \tag{5.3}$$

where

$$a_s = 2k \, \text{Cos} \left(\dfrac{\pi B}{\lambda} \, \text{Sin}\alpha \, \text{Sin} \, \theta \right) \tag{5.4}$$

which gives the amplitude of V_s.

Then, combining V_s with the field due to S (equal to unity) to give the resultant field V

$$V = 1 + a_s e^{-j\left(\dfrac{2\pi d}{\lambda} + \varphi \right)}$$

where $d = c \, \text{Cos} \, \theta$ and $c = \dfrac{B}{2} \, \text{Cos}\alpha$ as can be seen from figure. Then, by vector addition, power at the distant point P_θ is given by

$$P_\theta = 1 + a_s \left\{ 2 \, \text{Cos}\left(\dfrac{\pi B}{\lambda} \, \text{Cos}\alpha \, \text{Cos} \, \theta + \varphi \right) + a_s \right\} \tag{5.5}$$

Substituting for a_s from equation (5.4), we get

$$P_\Theta = 1 + 4k \cos\left(\frac{\pi B}{\lambda} \sin\alpha \sin\Theta\right) \left\{\cos\left(\frac{\pi B}{\lambda} \cos\alpha \cos\Theta + \varphi\right)\right.$$

$$\left. + k \cos\left(\frac{\pi B}{\lambda} \sin\alpha \sin\Theta\right)\right\} \qquad (5.6)$$

This expression gives the power at a distant point of an H-plane sectoral horn symmetrically mounted with plane flanges.

5.1(ii) Analysis of Plane CR System

Radiation from plane corner reflectors are generally analysed using the method of images. The mathematical model for the calculation of radiation field using this method requires the reflecting planes to be infinite in extent. Again the image theory suggested by Kraus[73] is applicable only for CR system having an included angle of π/n where n is an integer. Moullin[74] has shown that the directional pattern of a CR system with a vertically oriented dipole feed can be expressed in the form of a series of Bessel functions as

$$\frac{E}{E_o} = 4n(-1)^{n/2}[J_n(k) \cos n\Theta + J_{3n}(k) \cos 3n\Theta$$

$$+ J_{5n}(k) \cos 5n\Theta + \dots]$$

where n is even $\qquad (5.7)$

and $\dfrac{E}{E_o} = 4nj(-1)^{\frac{n-1}{2}} [J_n(k) \, Cos \, n\Theta - J_{3n}(k) \, Cos \, 3n\Theta$

$$+ \, J_{5n}(k) \, Cos \, 5n\Theta \, - \, ...]$$

when n is odd. $\hspace{3cm}$ (5.8)

Here E = Electric field at any point with bearing angle Θ ,

E_o $\hspace{1cm}$ = Maximum Electric field,

n $\hspace{1cm}$ = $\pi/2\beta$ where 2β is corner angle,

k $\hspace{1cm}$ = $\dfrac{2\pi}{\lambda}$ Z where Z is distance of dipole from apex.

When n is not an integer sufficient number of terms of the infinite series must be added in the expression given by

$$\dfrac{E}{E_o} = 4n[e^{\frac{nj\pi}{2}} \, J_n(k) \, Cos \, n\Theta \, + \, e^{\frac{3nj\pi}{2}} \, J_{3n}(k) \, Cos \, 3n\Theta$$

$$+ \, ...] \hspace{1cm} (5.9)$$

For a horizontally oriented dipole fed CR system, described in terms of a spherical co-ordinate system (R, Θ, φ) Klopfenstein[84] has shown that the electric field at a point P in the far field is

$$E_\varphi = \dfrac{\mu \lambda}{2\beta} \dfrac{e^{jkR}}{R} \sum_{n=0}^{\infty} \varepsilon_n \, exp[(-\dfrac{jn\pi}{2\beta}) \dfrac{\pi}{2}] \cdot$$

$$Cos(\dfrac{n\pi\varphi_o}{2\beta}) \, Cos \, (\dfrac{n\pi\varphi}{2\beta}) \, J'_{\frac{n\pi}{2\beta}} \, (k\rho_o \, Sin\Theta) \hspace{1cm} (5.10)$$

where R and Θ are the spherical co-ordinates of point P.
ε_n is a constant depending upon the values of n. $\varepsilon_n = \frac{1}{2}$
for n = 0 and ε_n = 1 for all other values of n. 2β is the
corner angle, and k = $\frac{2\pi}{\lambda}$.

The Line Source Theory suggested for flanged horn
antennas in the earlier section can explain the behaviour of
flanged H-plane sectoral horns only. Since the experimental
results have shown an analogy between the two systems, the
corner reflector theory for a vertically oriented dipole fed
CR system can be used to explain the effect of flanges on
E-plane sectoral horns (In this case the electric vector is
parallel to the apex of the flanges). Thus the difficulty
in explaining the bahaviour of flanged E-plane sectoral horns
can be solved by considering it as a CR system.

5.2   Corrugated-Flange-Mounted Sectoral Horns and Corrugated
      CR Systems

(i)   Expression for Power Density at a Point Due to Corrugated
      Flange Mounted Sectoral Horn Antenna

For analysing the radiation patterns of corrugated
flange system, an expression for the power radiated to a
point in the far field is derived. The assumptions made for
the plane flange system, are used in this case also.

Fig.5.2(i)(a) shows the geometry of the system.
P is a distant point of angular deviation Θ from the common axis. 2β is the included angle of the flange system. Z is the distance of the flange from aperture of horn. $n\lambda$ is the separation between two corrugations and B_p is the distance of pth radiator S_p from the aperture of horn. O is the aperture of horn and O' and O'' are the images of the primary radiator formed by the plane surface of the flange elements on both sides.

The relative amplitude of each secondary source is taken as $\dfrac{k}{B_p^2}$ where k is a constant[58] indicating the amplitude of excitation. From Fig.5.2(i)(a),

$$B_p = [Z^2 + (pn\lambda - \tfrac{h}{\tan\beta})^2 - 2Z(pn\lambda - \tfrac{h}{\tan\beta}) \, Cos\beta]^{\frac{1}{2}} \quad (5.11)$$

Now the path difference between the waves from primary and the pth secondary radiator on one flange element, when it reaches the point P is

$$[Z + (pn\lambda - \tfrac{h}{\tan\beta})^2 - 2Z(pn\lambda - \tfrac{h}{\tan\beta}) \, Cos\beta]^{\frac{1}{2}}[1 - Cos(\alpha_p - \Theta)]$$

Hence the phase difference η_p between the waves can be written as

$$\eta_p = \frac{2\pi}{\lambda} B_p[1 - Cos(\alpha_p - \Theta)] \quad (5.12)$$
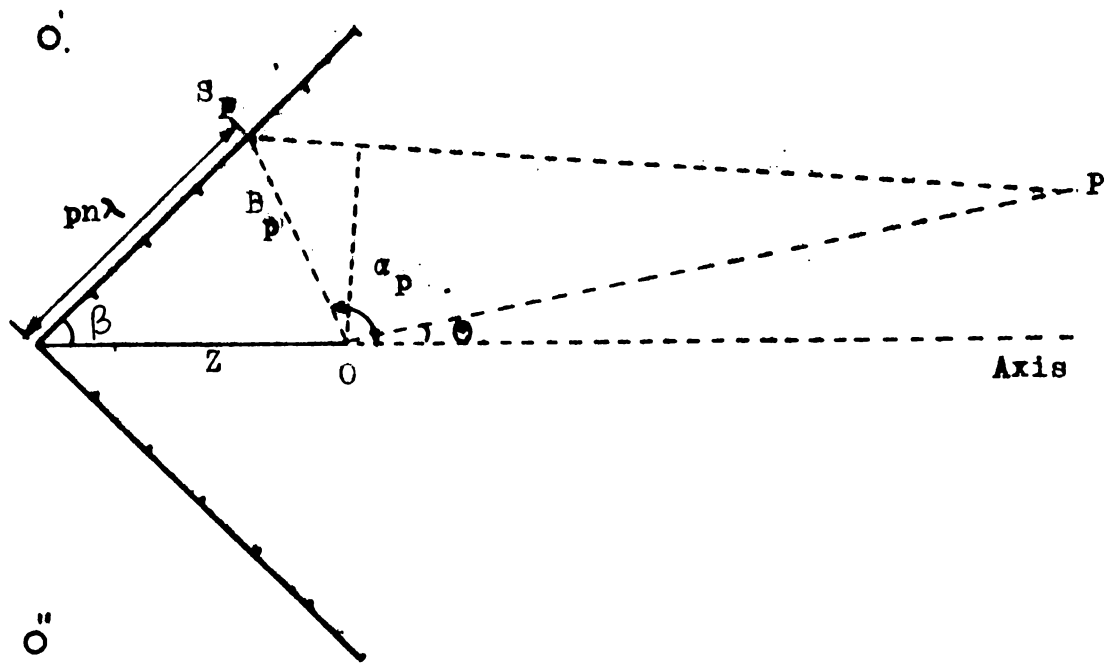
Fig.5.2(i)(a)   Geometry of the corrugated flange mounted
                sectoral horn.   O is the horn aperture.
                S_p is the pth element and the flange
                surface. B_p is the distance of the pth
                element from the aperture.   Z is distance
                of flange from aperture of horn.

133

By a similar method, the phase difference of pth radiator on the second flange element η'_p can be derived as

$$\eta'_p = \frac{2\pi}{\lambda} B_p[1 - \cos(\alpha_p + \Theta)] \qquad (5.13)$$

Let there be N_1 corrugations on each flange element. The total field at P due to these N_1 radiators can be obtained by taking the vector sum of the fields of all the radiators. If K is the resultant amplitude of this total field and φ is the resultant phase, then,

$$K = \left\{ \left[\frac{k}{B_1^2} \sin \eta_1 + \frac{k}{B_2^2} \sin \eta_2 + \ldots + \frac{k}{B_{N_1}^2} \sin \eta_{N_1} \right]^2 \right.$$

$$\left. + \left[\frac{k}{B_1^2} \cos \eta_1 + \frac{k}{B_2^2} \cos \eta_2 + \ldots + \frac{k}{B_{N_1}^2} \cos \eta_{N_1} \right]^2 \right\}^{\frac{1}{2}} \qquad (5.14)$$

This can be written as

$$K = \left\{ \left[\sum_{p=1}^{N_1} \frac{k}{B_p^2} \sin \eta_p \right]^2 + \left[\sum_{p=1}^{N_1} \frac{k}{B_p^2} \cos \eta_p \right]^2 \right\}^{\frac{1}{2}} \qquad (5.15)$$

The relative phase of the resultant is

$$\varphi = \tan^{-1}\left[\frac{\sum_{p=1}^{N_1} \frac{k}{B_p^2}\ \mathrm{Sin}\ \eta_p}{\sum_{p=1}^{N_1} \frac{k}{B_p^2}\ \mathrm{Cos}\ \eta_p}\right] \qquad (5.16)$$

By a similar method, the amplitude of the resultant field due to the N_1 radiators on the second flange element K' can be written as

$$K' = \left\{\left[\sum_{p=1}^{N_1} \frac{k}{B_p^2}\ \mathrm{Sin}\ \eta_p'\right]^2 + \left[\sum_{p=1}^{N_1} \frac{k}{B_p^2}\ \mathrm{Cos}\ \eta_p'\right]^2\right\}^{\frac{1}{2}}$$

$$(5.17)$$

The relative phase φ' of this resultant is

$$\varphi' = \tan^{-1}\left[\frac{\sum_{p=1}^{N_1} \frac{k}{B_p^2}\ \mathrm{Sin}\ \eta_p'}{\sum_{p=1}^{N_1} \frac{k}{B_p^2}\ \mathrm{Cos}\ \eta_p'}\right] \qquad (5.18)$$

The resultant field at P due to the two field vectors K and K' can now be obtained by adding them vectorially.

ie., $E = K\ \underline{/\varphi} + K'\ \underline{/\varphi'}$

The amplitude of this resultant is multiplied by an overall space factor which satisfies the limiting condition $E = 0$ when $\theta = \beta$.

Thus

$$E_\theta = \left\{ \left[(K \, \text{Sin} \, \varphi + K'\text{Sin} \, \varphi')^2 + (K \, \text{Cos} \, \varphi + K'\text{Cos} \, \varphi')^2 \right] \right.$$
$$\left. \left(\frac{\text{Cos}\theta}{\text{Cos}\beta} - 1 \right) \right\}^{\frac{1}{2}} \qquad (5.19)$$

when $\theta \rangle \beta$, $\left(\frac{\text{Cos}\theta}{\text{Cos}\beta} - 1 \right)$ will become negative and E_θ becomes imaginary. Since we are concerned with the actual field distribution, only the real values of E_θ are taken. The effective phase of E_θ is given by

$$\varepsilon = \tan^{-1} \left[\frac{K \, \text{Sin} \, \varphi + K'\text{Sin} \, \varphi'}{K \, \text{Cos} \, \varphi + K'\text{Cos} \, \varphi'} \right] \qquad (5.20)$$

Now, taking into consideration the image sources of the primary, each of amplitude unity, the relative phase of $0'$ is

$$\delta = \frac{2Z \, 2\pi}{\lambda} \, \text{Sin}\beta \, \text{Sin}(\beta - \theta) \qquad (5.21)$$

and that of $0''$ is

$$\delta' = \frac{2Z \, 2\pi}{\lambda} \, \text{Sin}\beta \, \text{Sin}(\beta + \theta) \qquad (5.22)$$

The sum of the fields due to the primary and the two images O' and O" can be written as

$$E_\theta' = \left\{ 3 + 2\,Cos(\delta-\delta') + 2[Cos\,\delta(1+Cos(\delta-\delta')) \right.$$
$$\left. + Sin\,\delta\,Sin(\delta-\delta')] \right\}^{\frac{1}{2}} \tag{5.23}$$

and its phase is

$$\epsilon' = tan^{-1}\left[\frac{Sin\delta + Sin\,\delta'}{1+ Cos\,\delta+Cos\delta'} \right] \tag{5.24}$$

The resultant effective power distribution P_θ of a sectoral horn with a symmetric corrugated flange system can now be obtained by the vector addition of E_θ and E_θ'.

Then

$$P_\theta = \left\{ [E_\theta\,Sin\,\epsilon + E_\theta'\,Sin\,\epsilon']^2 + [E_\theta\,Cos\,\epsilon \right.$$
$$\left. + E_\theta'\,Cos\,\epsilon']^2 \right\} (1 + Cos\theta) \tag{5.25}$$

where $(1 + Cos\,\theta)$ is taken as the overall space obliquity factor for the directional antenna system. This expression can be used to calculate the power at the point P of a corrugated flange mounted sectoral horn.

(ii) Radiation from Corrugated CR System

A theoretical analysis has been carried out for a corrugated CR system excited by a horizontally oriented dipole, on the basis of the line source theory[58] and the method of images[73]. Klopfenstein[84] has suggested that in the theoretical analysis of CR systems, the half-wave dipole, usually used in the experimental studies, can be approximated to be an infinitesimal one.

Now, for analysing the antenna operation by the method of images, let the corner angle subtended by the plane surfaces of the corrugated elements be 2β. The horizontally oriented dipole will produce symmetrical images with currents flowing as in a continuous loop[84]. The image representation for a typical case of corner angle 60° is shown in Fig.5.2(ii)(a). Consider a point P in the far field of angular deviation Θ from the common axis. In this case also, the primary radiator (dipole) is assumed to have unit amplitude.

Using Fig.5.2(ii)(a) the path difference between the waves from the primary dipole radiator and the nth image from one plane surface, when it reaches the point P can be derived as

$$\left(Z + \frac{h}{\text{Sin } \beta} \right) \frac{\text{Sin } 2n\beta}{\text{Cos } n\beta} \text{ Sin } (n\beta - \Theta) \qquad (5.26)$$
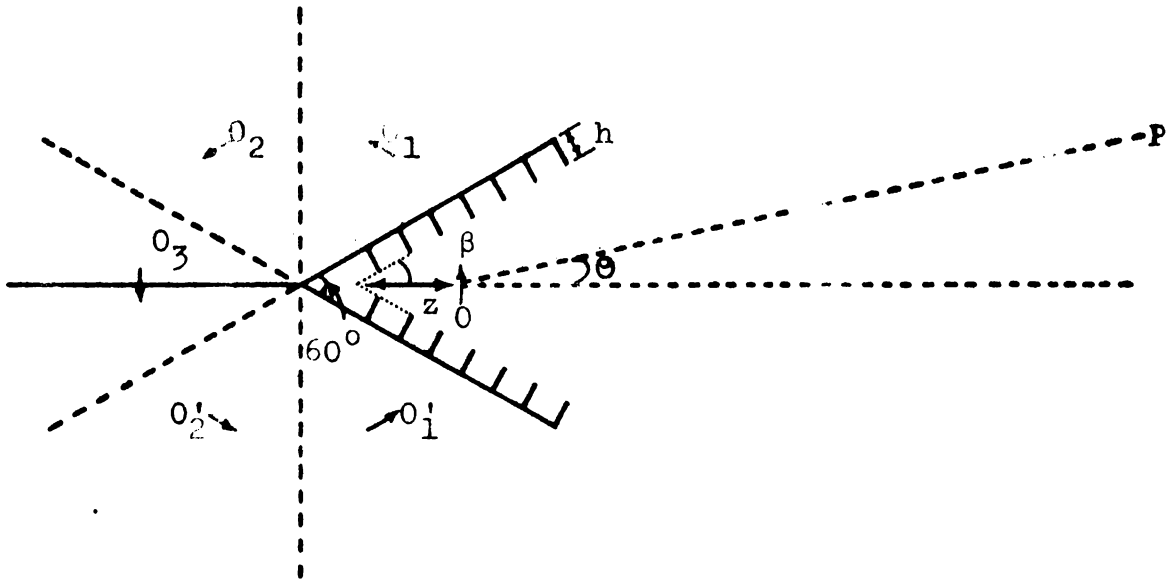
Fig.5.2(ii)(a)   Image representation for a typical case of
60° CR system. O_1, O_2 etc. are the images
of the dipole O due to one plane surface of
the CR system. O_1' and O_2' are images due to
the other plane surface. P is a distant
point having an angular deviation θ from
the common axis.

139

Since the nth image itself has an initial phase difference of 2nβ with the primary, the phase difference δ_n between the waves can be written as

$$\delta_n = \frac{2\pi}{\lambda} \left(Z + \frac{h}{\sin \beta}\right) \frac{\sin 2n\beta}{\cos n\beta} \sin (n\beta - \theta) + 2n\beta \qquad (5.27)$$

By a similar method, the phase difference δ_n' between the wave from the primary and the nth image due to the second plane surface of the reflector elements can be written as

$$\delta_n' = \frac{2\pi}{\lambda} \left(Z + \frac{h}{\sin \beta}\right) \frac{\sin 2n\beta}{\cos n\beta} \sin (n\beta + \theta) - 2n\beta \qquad (5.28)$$

The vector sum of the fields at P due to the primary and the images can be found by combining the contributions from all these radiators. For a corner angle of even submultiple of 2π (as in the case shown in Fig.5.2(ii)(a)) the number of images due to one plane surface will be $\frac{\pi}{2\beta}$, and due to the other plane surface it will be $(\frac{\pi}{2\beta} - 1)$. Hence, the field at P due to the dipole and its images can be written as

$$E_e' = \left\{ \left[\operatorname{Sin} \delta_0 + \operatorname{Sin} \delta_1 + \ldots + \operatorname{Sin} \delta_{\left(\frac{\pi}{2\beta}\right)} \right. \right. +$$

$$\left. \operatorname{Sin} \delta_1' + \operatorname{Sin} \delta_2' + \ldots + \operatorname{Sin} \delta'_{\left(\frac{\pi}{2\beta} - 1\right)} \right]^2$$

$$+ \left[\operatorname{Cos} \delta_0 + \operatorname{Cos} \delta_1 + \ldots + \operatorname{Cos} \delta_{\left(\frac{\pi}{2\beta}\right)} \right. +$$

$$\left. \left. \operatorname{Cos} \delta_1' + \operatorname{Cos} \delta_2' + \ldots + \operatorname{Cos} \delta'_{\left(\frac{\pi}{2\beta} - 1\right)} \right]^2 \right\}^{\frac{1}{2}}$$

$$(5.29)$$

This can be expressed in the form

$$E_e' = \left\{ \left[\sum_{n=0}^{\frac{\pi}{2\beta}} \operatorname{Sin} \delta + \sum_{n=1}^{\frac{\pi}{2\beta} - 1} \operatorname{Sin} \delta_n' \right]^2 + \right.$$

$$\left. \left[\sum_{n=0}^{\frac{\pi}{2\beta}} \operatorname{Cos} \delta_n + \sum_{n=1}^{\frac{\pi}{2\beta} - 1} \operatorname{Cos} \delta_n' \right]^2 \right\}^{\frac{1}{2}} \quad (5.30)$$

The relative phase of this field with the primary radiator is

$$\epsilon' = \tan^{-1} \frac{\displaystyle\sum_{n=0}^{\frac{\pi}{2\beta}} \operatorname{Sin} \delta_n + \sum_{n=1}^{\frac{\pi}{2\beta} - 1} \operatorname{Sin} \delta_n'}{\displaystyle\sum_{n=0}^{\frac{\pi}{2\beta}} \operatorname{Cos} \delta_n + \sum_{n=1}^{\frac{\pi}{2\beta} - 1} \operatorname{Cos} \delta_n'} \quad (5.31)$$

For corner angles of odd submultiples of 2π, the number of images due to each plane surface will be $(\frac{\pi}{2\beta} - \frac{1}{2})$. Hence, in that case, the upper limit in the above summation series becomes $(\frac{\pi}{2\beta} - \frac{1}{2})$.

In order to consider the effect of corrugations, let there be N_1corrugations on each reflector element. Tips of the corrugations are assumed to be acting as secondary radiators excited by the waves from the dipole radiator. The relative amplitude of each secondary radiator is taken as k/B_p^2 where k is a constant indicating the amplitude of excitation[58] and B_p is the distance of the pth element from the primary radiator (dipole). Now, proceeding in a similar manner discussed in the earlier case of corrugated flanges, the amplitude of the resultant field due to all $2N_1$secondary radiators at the point P can be derived as

$$E_\Theta = \left\{ [(K \; Sin\varphi + K'Sin\varphi')^2 + (K \; Cos\varphi + K'Cos\varphi')^2] \right.$$
$$\left. (\frac{Cos\Theta}{Cos\beta} - 1) \right\}^{\frac{1}{2}} \qquad (5.32)$$

and its phase is

$$\varepsilon = tan^{-1} \; [\frac{K \; Sin\varphi + K'Sin\varphi'}{K \; Cos\varphi + K'Cos\varphi'}] \qquad (5.33)$$

where K and K' are the amplitude of the resultant field of

N_1 secondary radiators in the first and second reflector elements respectively, and φ and φ' are their relative phases. The resultant power distribution of the corrugated CR system at a point P in the far field can now be written as

$$P_\theta = \left\{ [E_\theta \operatorname{Sin} \varepsilon + E'_\theta \operatorname{Sin} \varepsilon']^2 + [E_\theta \operatorname{Cos} \varepsilon + E'_\theta \operatorname{Cos} \varepsilon']^2 \right\}$$

$$(1 + \operatorname{Cos} \theta) \qquad (5.34)$$

Here also $(1 + \operatorname{Cos} \theta)$ is taken as overall space obliquity factor.

5.3 Results of Numerical Computation

Radiation patterns of both corrugated flange system and corrugated CR system were computed using the theoretical expressions derived in the earlier sections. The theoretical radiation patterns were computed using TDC 316 and Micro 78 computers. The theoretical values are compared with the experimental data and the results are presented.
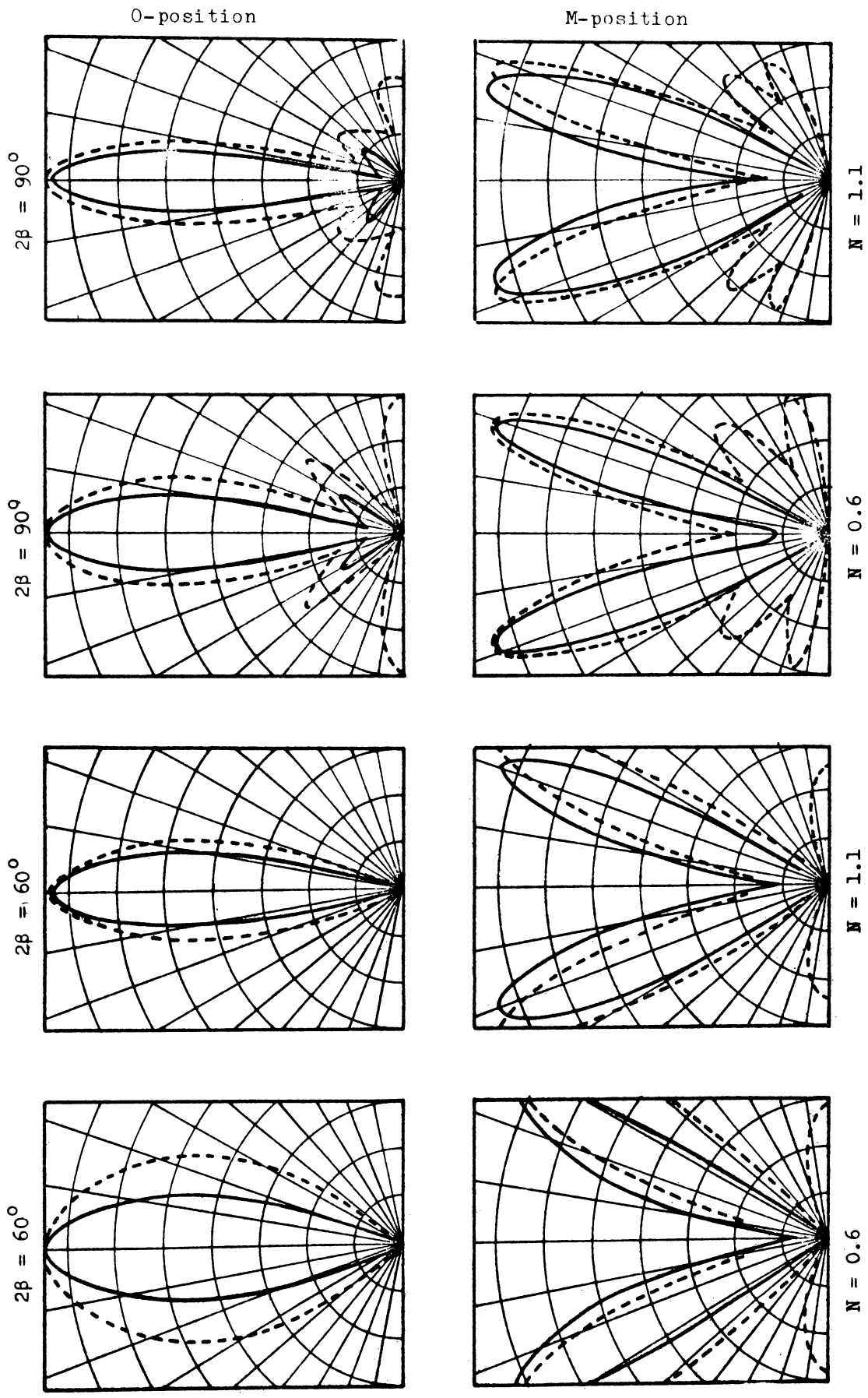
5.3(i) Radiation Patterns of Corrugated Flange System

Using equation (5.25), the radiated power in the far field is calculated for various values of θ. Then the normalized radiation patterns are plotted manually. The

patterns plotted in polar coordinates are shown in Fig. 5.3(i)(a). The experimental radiation patterns are also shown along with this. The results show a fairly good agreement between theoretical values and experimental data.

5.3(ii) Radiation from Corrugated CR System

In order to study the variation of on-axis power density with dipole position, the value of θ in equation (5.34) is put equal to zero. The values of P_0 are then calculated for different values of Z, ranging from 0.2 to 6. From this result, the positions giving maximum and minimum on-axis power density are noted. Table 5.3(ii)(I) shows the experimental and theoretical values of the positions giving maximum and minimum on-axis power density. It can be seen from the table that the experimental and theoretical results show considerable agreement in almost all cases.

Radiation patterns were plotted using equation (5.34). These are shown as dotted lines in Fig.5.3(ii)(a) and (b). The experimental radiation patterns are also presented in this figure. The HPBW obtained from the theoretical and experimental radiation patterns are tabulated in table 5.3(ii)(II). The presented figures and table illustrate the validity of the theoretical prediction.

O-position   M-position

$2\beta = 90^\circ$ $2\beta = 90^\circ$ $2\beta = 60^\circ$ $2\beta = 60^\circ$

N = 1.1   N = 0.6   N = 1.1   N = 0.6

Fig.5.3(i)(a)   Radiation patterns of corrugated flanged horn at O- and M-positions.
Frequency = 9.3 GHz.   —— Experimental   .... Theoretical.

149

Table 5.3(ii)(I)

Positions giving maximum and minimum on-axis power
density for different corrugated reflectors

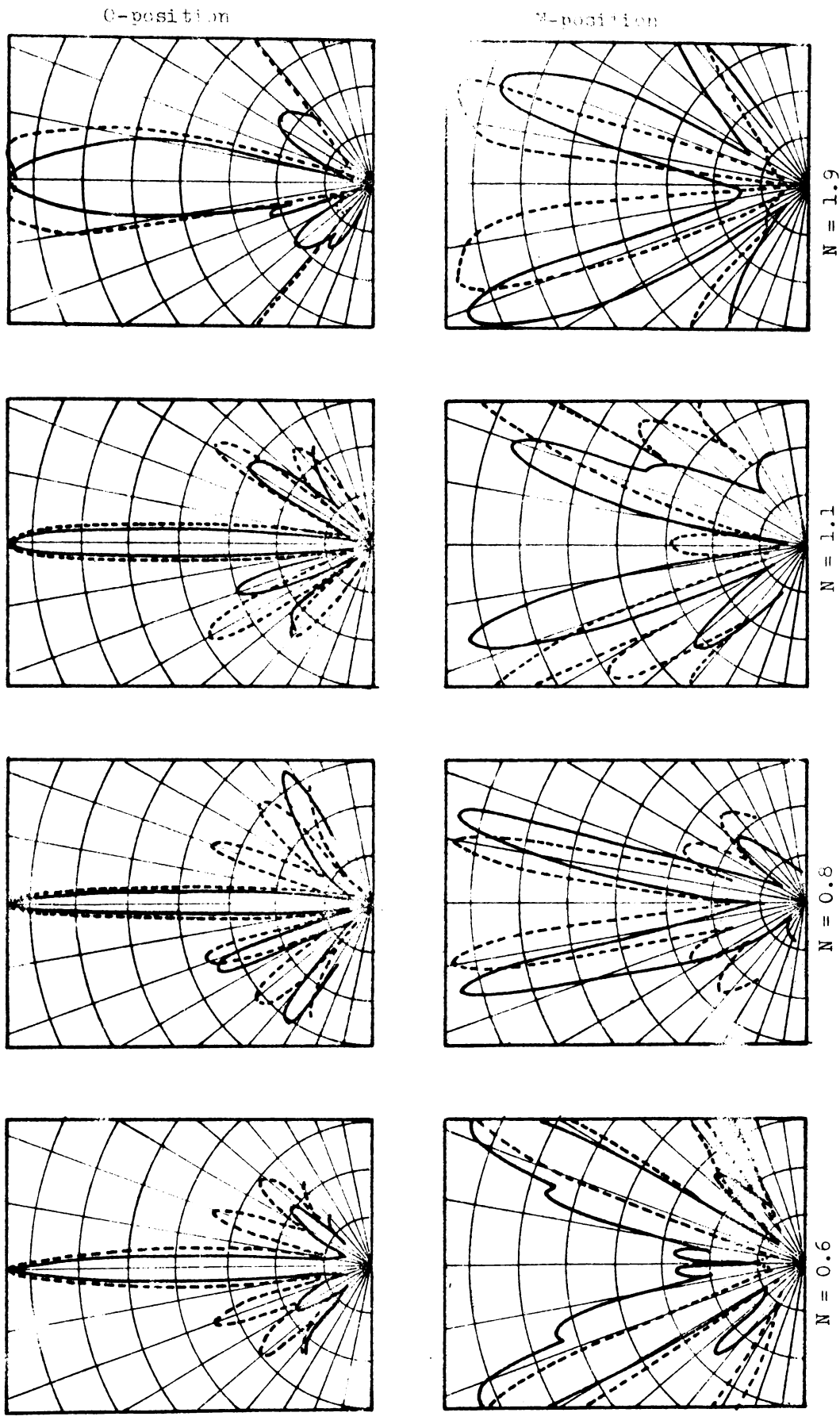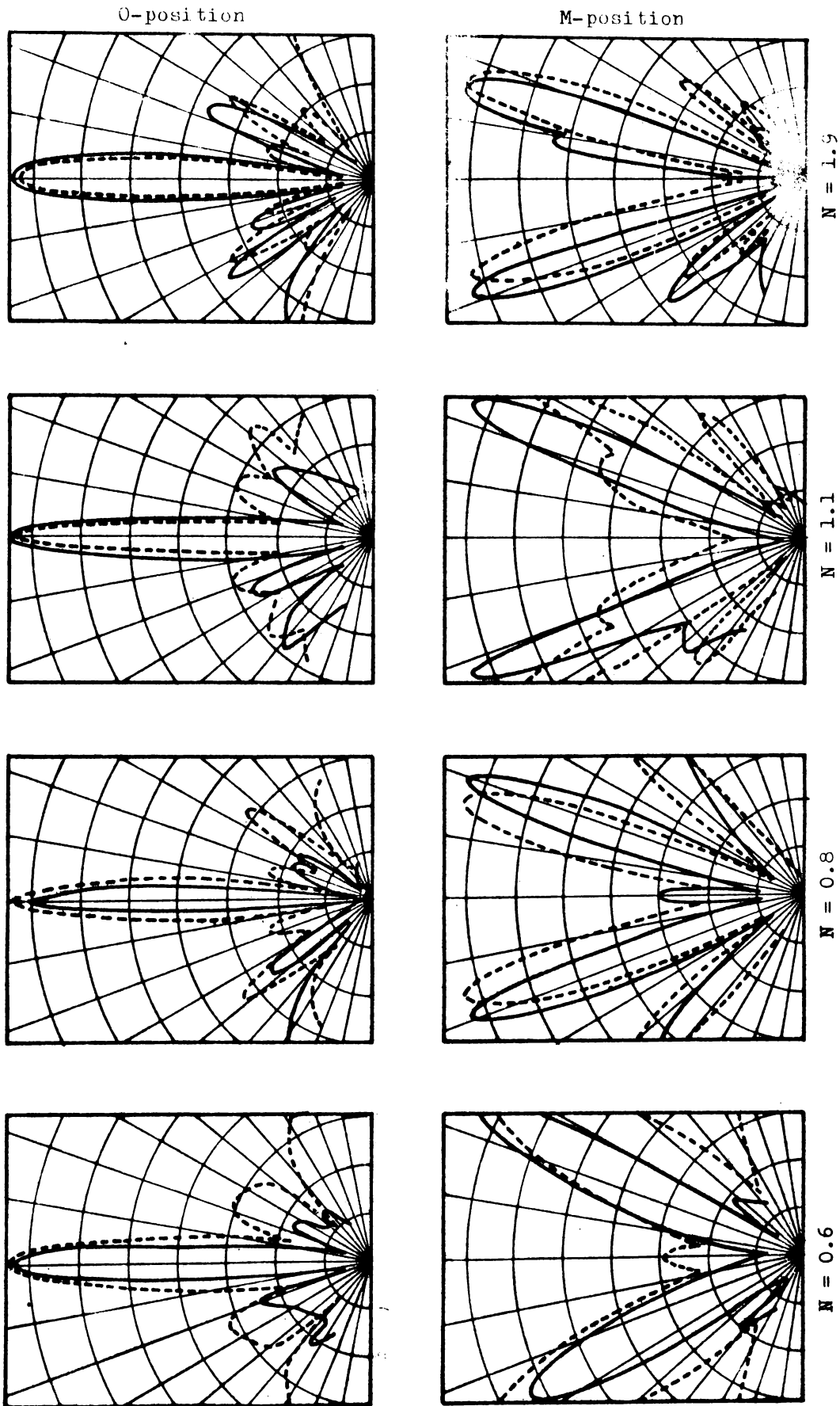| Corner angle 2β	Number of corrugations/cm (N)	Distance of primary feed from apex giving maximum on-axis power (Z_o cms)		Distance of primary feed from apex giving minimum on-axis power (Z_m cms)	
		Theoretical	Experimental	Theoretical	Experimental
60°	0.6	6.2	6.2	0.6	0.4
	0.8	4.2	4.2	2.8	2.6
	1.9	4.2	4.4	3.6	3.4
120°	0.6	6	5.8	5.1	4.8
	1.4	7	6.8	9	9.2
	1.9	5.7	6	9	9.3

N = 0.6

N = 0.8

N = 1.1

N = 1.9

Fig.5.3(ii)(a) Radiation patterns of corrugated CR system at O- and M-positions.
$2\beta = 60^\circ$, Frequency = 9.3 GHz. ——— Experimental ....Theoretical.

147

O-position   M-position

N = 1.5

N = 1.1

N = 0.8

N = 0.6

Fig.5.3(ii)(b) Radiation patterns of corrugated CR system at 0- and M-positions.
2β = 120°, Frequency = 9.3 GHz. ——— Experimental .... Theoretical.

148

Table 5.3(ii)(II)

HPBW at Optimum and Minimum positions for different corrugated reflectors

	Number of corruga-tions/cm (N)	Corner Angle 2β			
		60°		120°	
		Half Power Beam Width			
		Theoreti-cal	Experi-mental	Theore-tical	Experi-mental
Optimum position	.6	11°	10.5°	11°	8.5°
	.8	12.5°	11°	9.8°	9.1°
	1.9	19°	17.9°	13.2°	15°
Minimum position	.6	26°	28.5°	39°	28.5°
	.8	28°	25.5°	26°	24.6°
	1.1	29°	26.8°	25°	23.9°
	1.4	39.5°	37°	24.5°	23.2°
	1.9	34°	32°	30°	28°

An analysis of the radiation from flange mounted sectoral horns and CR systems have been attempted on the basis of line-source theory and method of images. Expressions for the radiated power were derived for the corrugated systems and a comparison is made between the numerical results and experimental data. Small differences between the theoretical and experimental results are due to the inadequacy of the approximations made in the theoretical analysis.

In the case of inclined corrugated flange/CR systems, the tips of corrugations, inclined at 45° to the E-vector, will act as secondary radiators which will be having components in both planes. In certain cases, the resultant vertical and horizontal field components due to the primary and secondary radiators will be equal and in phase quadrature, and thus give a circularly polarized radiation. A detailed mathematical analysis of the phenomenon has not been attempted here and is left out for future work.

CHAPTER VI

CONCLUSIONS

Results of the exhaustive experimental and
theoretical investigations carried out on flanged horns
and corner reflector systems have been discussed in the
foregoing chapters. The conclusions drawn from these
results are given in this chapter.

6.1 Analogy Between Flanged Horns and CR Systems

In part I of the experimental results, the
effect of various parameters on the radiation characteri-
stics of plane flanged sectoral horns and plane CR systems
have been described. Results presented in Sec.4.1 reveal
that on-axis power density of both systems are strongly
affected by the variations in different antenna parameters.
The presented tables and figures show that the behaviour
of both systems, under identical conditions, are almost
the same.

The matching conditions of both systems are
found to be depending on the position of the primary feed,
flange/CR angle and the frequency of operation. The
measured fluctuations in VSWR with these antenna parameters

151

were also found to be indicating an analogy between the behaviour of flanged horns and CR systems.

The radiation patterns presented in Sec.4.3 show that both systems give focusing and splitting of the radiated beam at their O- and M-positions respectively. The HPBW and gain of both flanged horns and CR systems at these positions were also observed to be varying in an analogous manner by the different antenna parameters. As in the case of flanged horn, the corner reflector also was found to give tilting of the antenna beam, due to the different asymmetries imposed on the system.

The various experimental investigations performed with corrugated flange/CR systems have been described in sections 4.7 through 4.11. The results obtained indicate that the analogy between corner reflectors and flanged horns, observed in the case of plane flange/CR systems, is exhibited by corrugated systems also. From the results presented in Sec.4.7, it can be seen that, for both systems, the on-axis power density can be considerably increased by a proper choice of the corrugation parameter. It has been observed that the presence of corrugations on the flange/CR elements has improved the impedance conditions of both systems.

Results described in Sec.4.9 indicate that the analogy between the two corrugated systems is valid for the radiation patterns of the antenna at the Optimum and Minimum positions. The curves drawn for HPBW and gain show that both these characteristics are strongly dependent on the corrugation parameters. This is found to be true for both the systems. It can be seen from the results presented in Sec.4.11 that the corrugations always increase the gain of both flanged horns and CR systems in a plane perpendicular to the direction of corrugations.

Investigations reported in part III show that flanged horns and CR systems can be designed to produce elliptically polarised radiation by the use of inclined corrugated flanges/reflectors. By an appropriate selection of the different flange/reflector parameters, both these systems can be converted even into a circularly polarised radiator.

Thus the exhaustive experimental studies clearly indicate the close resemblance between the flanged horns and CR systems with respect to the various antenna characteristics, including their polarization properties.

6.2 Analysis of the Radiation Patterns

The Line Source Theory, used for analysing the radiation from flanged sectoral horn can be employed only

in the case of flanged H-plane sectoral horns, because it requires the Electric vector to be perpendicular to the flange edges. The difficulty, thus encountered for flanged E-plane sectoral horns, can be solved by considering it as a CR system. The image theory has been used for analysing the radiation from CR systems.

In the case of corrugated systems expressions have been derived, based on the Line Source Theory and image theory, and numerically computed patterns have been presented in Sec.5.3. A fairly good agreement between the theory and experiment, shown by the graphs and tables in sections 5.3(i) and (ii), illustrates the validity of the theoretical approach. For both the systems, a major cause for discrepancies between the theory and experiment is the approximation of the primary source as a linear radiator. The error due to the approximation of the half wave dipole to an infinitesimal one, also causes some discrepancies in the case of CR systems. However, the theoretical computations show a general agreement with the experimental data for almost all cases.

6.3 Some Practical Applications

Flanged horns and corner reflectors find some important applications in beacons and radar systems. When

horns are used as transmitting antennas in small airborne radars, the beams from the horns should be properly focused. Metallic plane flanges or corrugated flanges of suitable parameters can be used for obtaining this focused beam from the horn antenna. Horns employed for illuminating secondary reflector antennas usually produce considerable mismatch due to normal reflection from the secondary reflector. The flange system attached on the horns at the 'Minimum position' gives a split beam which has little power along the axial direction. This may reduce the normal reflection and enhance the matching conditions of the antenna. Again, the beam tilting property of asymmetric flange system can be used for aligning the primary horn with the secondary reflector antenna.

The corner reflector antenna provide an effective and simple directional antenna system suitable for point to point communication. By suitably adjusting the various parameters of plane and corrugated CR system, a split double beam can be produced, which finds extensive application in radio range beacon and airport runway localizer. A suitable inclined corrugated CR system, acting as a circularly polarized radiator, can be used for transmitting signals to places where the polarization of the receiving antenna is unknown.

6.4   Scope for Further Study

The results presented in this thesis offer much scope for further investigations in this field.

A detailed theoretical analysis of corrugated CR systems has to be attempted for calculating the radiation patterns of corner reflectors having arbitrary apex angle. A mathematical analysis for the variations in impedance conditions also can be considered.

Experimental investigations on inclined corrugated flange/CR systems for producing circularly polarized radiation, have to be studied in detail, taking into account the different antenna parameters. A mathematical model for this system also is to be developed.

The use of CR systems as primary feeds for secondary reflectors can be taken as a topic for further investigation. The various radiation and polarization characteristics of the primary antenna may have considerable effect on the radiation from the secondary antenna.

The effect of change in orientation of dipole feed of the corrugated CR system also can be taken as a problem for further work.

APPENDIX I

FABRICATION OF AN ANTENNA POSITIONER (TURN-TABLE) WITH REMOTE CONTROL SYSTEMS

Antenna radiation pattern measurements are generally made by rotating the antenna under test about its axis and noting the received power. An antenna positioner (turn-table) is employed for this. The turn-table is essentially a rotating platform on which the antenna under test is mounted. The platform rotates at a conveniently low speed.

The studies reported in this thesis were performed inside a microwave anechoic chamber, the construction and details of which are given in Appendix II. The operator cannot remain inside the anechoic chamber while making antenna measurements, since human bodies will act as reflectors and scattering sources. Hence the turn-table used had to be equipped with remote control facilities, so that it could be operated from outside the anechoic chamber. Such an antenna positioner was designed and fabricated, the details of which are presented here.

AI.1 Design of the Positioner

While designing the positioner, the important factors which had to be decided were its speed of rotation and its load capacity.

157

AI.1(i)   Speed

The speed of rotation of the platform was chosen
to be 1 rpm.   This speed was selected taking into considera-
tion the very sharp radiation patterns expected and the
writing speed of the pattern recorder used in conjunction
with the turn-table.   At one rpm, the antenna covers one
degree in approximately 0.17 sec.   The Hewlett Packard model
7047A X-Y Recorder can record every peaks falling in this
range.   The recorder could be set at a writing speed of
97 cm/sec.

The turn-table is powered by an electric motor
with oil immersed worm gear systems to reduce its speed to
the required value.   Precise gear systems are used to avoid
jerks and uneven rotation.

AI.1(ii)   Loading

Only medium sized antennas are intended to be
tested using this turn-table.   This has been designed to
take a maximum load of 300 kgs.   Even with overhanging loads,
this would rotate smoothly.   A two H.P. three phase A.C.
motor was used as the power source.   This provides a very
high and uniform torque at the output shaft of the gear
box, rotating at 1 rpm.   The three phase AC motor used is

electrically reversible. Fig.AI.1(i)(a) shows a sketch of
the turn-table, showing its design.

AI.2   Main Features and Facilities Incorporated

To provide ease in operation and maximum flexibi-
lity and adaptability in use, certain additional features
were incorporated in the design.   The following are the
major features.

AI.2(i)   Azimuthal Position Indicator

As described earlier, the antenna radiation
pattern is a plot of the distribution of the radiated energy
as a function of the angle.   Hence, to plot the radiation
pattern using an X-Y recorder, information regarding the
azimuthal position of the antenna also has to be fed to the
recorder.

For providing an X-input proportional to the angle
through which the antenna has rotated, a wire wound linear
potentiometer whose wiper-stopper had been removed, is coupled
to the shaft of the turn-table.   A steady D.C. is applied
across the potentiometer. When the turn-table shaft rotates,
the wiper of the potentiometer also rotates, and the
potential at the wiper contact is proportional to the angle
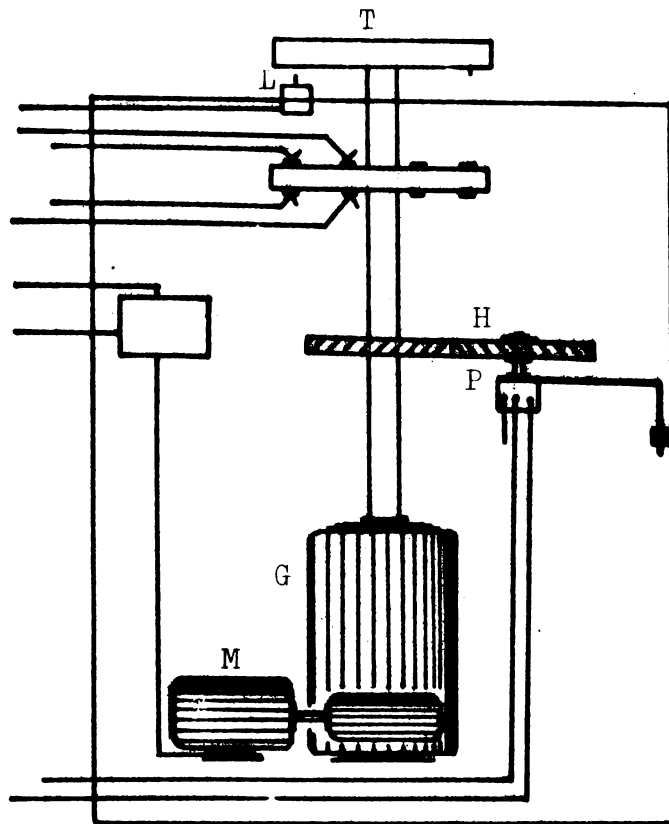through which the shaft has rotated.   This is fed to the

Fig.AI.1(i)(a)   Schematic diagram of the antenna turn-table.
T - Turn table platform, L - Limit switch,
P - Potentiometer for position indicator,
H - Gear arrangement for rotating the shaft
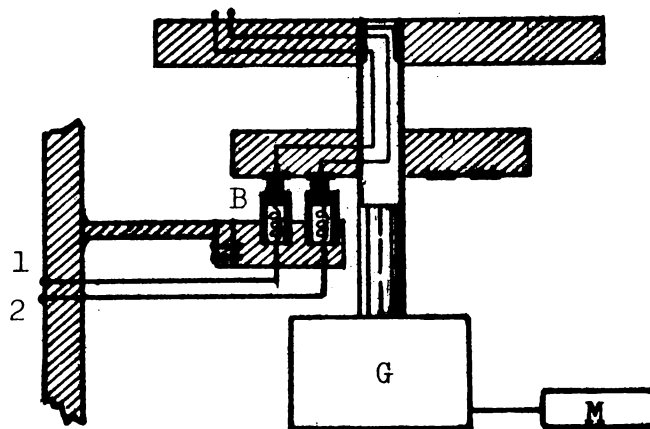of potentiometer, G - Gear box, M - Motor.

Fig.AI.2(ii)(a)   Schematic lay out of the Brush and Ring
arrangement. B - Brush and Ring contact.
1,2 - Signal connections from the receiv-
ing antenna to the recorder. G - Gear box,
M - Motor.

X-input of the recorder. Alternatively, this can be fed to a meter to read the analog voltage in degrees on the control panel. This is used for initial alignments and settings.

AI.2(ii) Brush and Ring Contacts

The output from the antenna is fed to the pattern recorder using cables. As the table rotates, these cables may twist and break off. Hence brush and ring contacts are provided to the rotating shaft. It may be noted that only rectified output from the detector is fed to the recorder. Two sets of brush and ring contacts are incorporated, one set for tapping the microwave signal pick up and the other for providing a 220 V A.C. power supply to the platform to use ancilliary instruments. Fig.AI.2(ii)(a) shows the lay out of the system.

AI.2(iii) Limit Switch

To avoid the platform rotating beyond the necessary scan, limit switches were provided to the turn-table. The angle through which the platform has to be rotated is programmed by inserting a peg in the required holes on the platform. As the platform rotates, the peg strikes against the limit switch lever, which in turn, cuts off the starter relay circuit. This switches turn off the starter and stop

162

the motor. The motor can be started with another parallel switch on the control panel. Thus, both manual and remote control facilities are provided. By passing the limit switches with parallel short circuiting switches on the control panel, continuous rotation also may be given to the turn-table, if necessary.

AI.2(iv) Motor Control

The three phase AC motor used in the turn-table is overload protected using a motor control relay. The direction of rotation of the motor can be altered using anyone of the Forward/Perverse (F/P) Switches, one on the control panel and the other on the turn-table frame. The latter one is to provide ease in aligning and making initial adjustments when the operator is inside the chamber.

The two F/R switches are connected, in series. Hence, reversing anyone of the two will reverse the direction of rotation irrespective of the indicator. Hence it became necessary to develop a method to sense the direction of rotation. A very simple circuit has been developed for this purpose. Fig.AI.2(iv)(a) gives the circuit details. It can be seen from the diagram that depending on the position of both the switches either one of the lamps gets connected across two different phase supplies and 'sees' a voltage
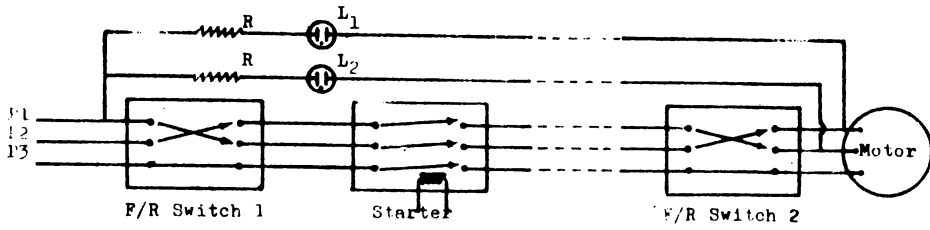
Fig.AI.2(iv)(a)   A simple circuit for sensing the direction of rotation of motor
of the turn-table.   Pl – Phase 1, P2 – Phase 2, P3 – Phase 3,
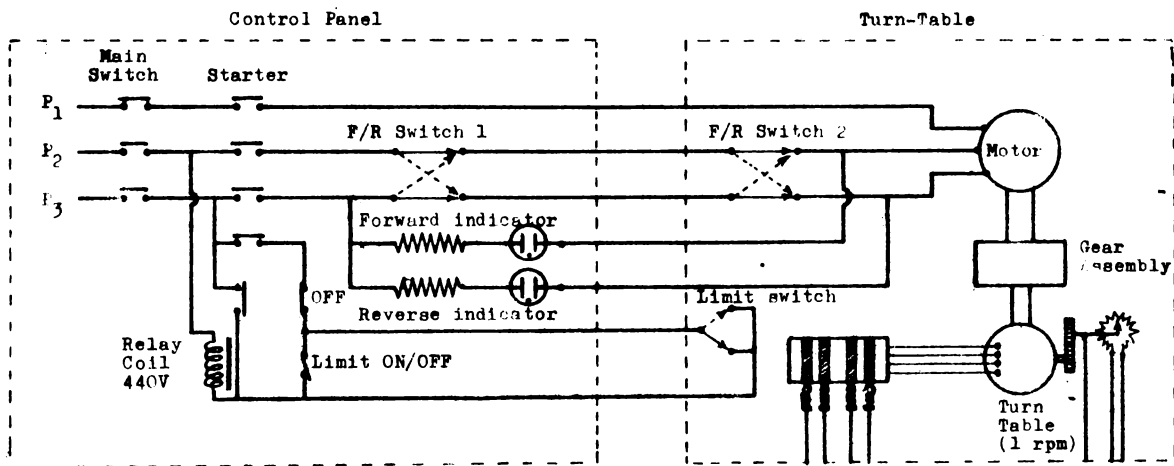L_1 – Lamp 1, L_2 – Lamp 2.

Fig.AI.3(ii)(a)   The detailed circuit diagram of the turn-table and control pan   assembly.

163

which is the vector sum of the voltages in each line. The
other lamp would not 'see' any voltage. When either of the
two switches is reversed, the states of the lamps get
reversed. This gives a visual indication of the direction
of rotation of the turn-table.

AI.3 Control Panel

The turn-table control panel is kept in the
anechoic chamber control room. The turn-table and control
panel are shown in Figs.AI.3(a), (b) and (c). The following
are the main controls.

AI.3(i) Motor ON/OFF

This is an ordinary motor starter relay. An
overload protection relay is also incorporated. The starter
relay coil is connected through the limit switch on the turn-
table. Hence when the limit switch is switched off, the relay
coil is de-energized and releases the contacts, which stops
the motor. The limit switch can be shorted by another switch
on the control panel, in which case the limit switch would
become non-operative.

AI.3(ii) Clock-wise/Anti-clock-wise Rotation Control

An ordinary Forward/Reverse switch in which the
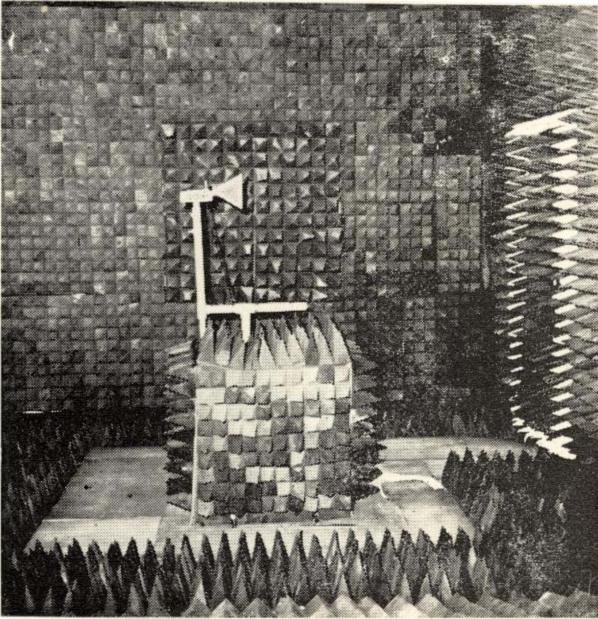two phase connections are interchanged by throwing the

Fig.AI 3(a)

THE QUIET ZONE AND THE ANTENNA POSITIONER:

The back wall and the walk-ways. The 'target area' in the back wall's central portion is covered with pyramidal absorbers of 8 x 8 cm. base and 40 cm. height. The antenna positioner (also called the turn-table) is placed at the centre of the quiet-zone. Its metallic frame is covered with pyramidal absorbers at the time of observation, to avoid exposed reflecting surfaces in the chamber. Around the turn-table, the walk-ways can be seen. The entrance door can be located by the white lined pyramids on the edges of the shutter.
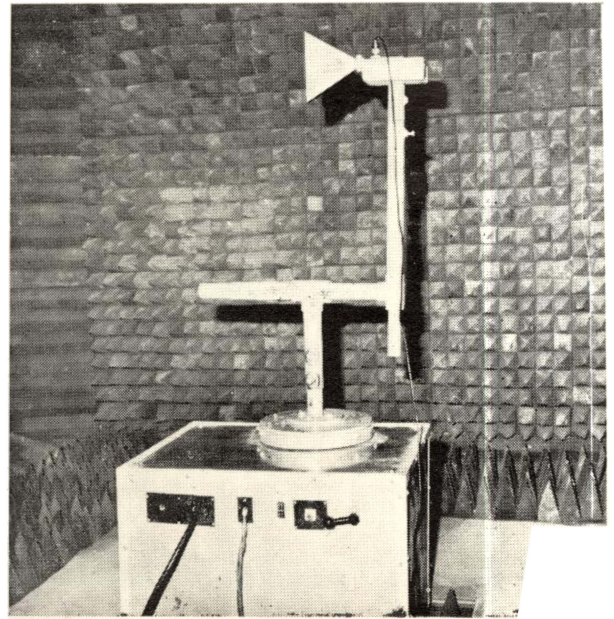
Fig.AI.3(b)

THE ANTENNA POSITIONER (TURN-TABLE):

At the time of observation, the metallic surfaces of the positioner will be covered with pyramidal absorbers. The positioner can be controlled either from inside of the chamber or from the control room. The system is fully automatic. It scans the azimuth at a speed of 1 rpm. Limit switch is provided to stop at 0 and 180 degrees. Its position will be indicated on a meter in the control pannel.

Fig.AI.3(c)

THE CONTROL ROOM OF THE ANECHOIC CHAMBER:

The remote control unit, the X-Y/t recorder, microwave source for transmitting horn and the power supplies can be seen in the figure. The transmitting horn antenna is located at the apex of the tapered portion of the chamber, inside the terminal box.

lever to either sides, is used for direction control.
Since this would reverse the phase sequence in a three
phase circuit, the direction of rotation of the motor also
would be changed.

As described earlier, another identical switch
is kept on the turn-table. These two switches are put in
series. Hence, reversing any one of them will reverse the
direction of rotation. A direction indicator is also kept
on the control panel. The detailed circuit diagram of the
turn-table and control panel assembly are shown in Fig.
AI.3(ii)(a).

AI.3(iii) Position Indicator

The power supply for the position indicator is
kept in the control unit. This is a stabilised d.c. source.
The controls for this include the ON/OFF switch, calibrator
meter, output jacks and selector switch.

AI.3(iv) Meters

Two meters are on the control panel, one of which
is calibrated to read the azimuthal position of the antenna.
Alternately, this information can be fed to the X-input of
the recorder, while plotting radiation patterns. The second
meter indicates the antenna output. This is to be used for
initial alignments.

Cables carrying power, the control leads and the signal leads running between the control unit and the turn-table are separately shielded and are running through separate metallic pipes, to avoid EMI problems.

This turn-table has been used for plotting the radiation patterns of horn antennas for the investigations presented in this thesis. The performance of the fabricated system was highly satisfactory.

APPENDIX II

PERFORMANCE EVALUATION OF A MICROWAVE ANECHOIC CHAMBER

Antenna measurements, scattering experiments etc. have to be conducted in an environment free from radio signal interference. Generally the major source of interference in these experiments will be energy reflected from nearby objects and ground. Hence specially prepared 'environment' is used for conducting these experiments. These are generally called 'antenna test ranges'.

A test range is a space specially prepared to minimise any sort of reflection or interactions from the surroundings. These are broadly classified into two groups as "outdoor test ranges" and "indoor test ranges". Outdoor test ranges consume a large amount of space. They require high towers or if available, two nearby hills separated by a distance of a few kilometers. On the other hand, the indoor test ranges are comparatively very small. They are constructed as big halls, the geometry and dimensions of which are chosen according to the type of application required. The inside enclosure is then covered with a radiowave absorber to reduce reflections. Such an enclosure is called an "anechoic chamber".

A major part of the work reported in this thesis was carried out inside an anechoic chamber. The author was involved in the design, fabrication and testing of this chamber. The chamber was subjected to detailed test and analysis to evaluate its performance. The test procedures employed and their results are presented here.

AII.1 Construction of the Chamber

As mentioned earlier, the most important part of the chamber is the absorbing material used for its constru- ction. In this chamber, polyurethane foam based absorbers are employed. This consists of the absorbing material dispersed in a foamy base. The foamy base helps to keep the density of the material very low. A very low density is required to avoid the reflection from the surface of the material. Another requirement to avoid the surface reflect- ion is a very slow variation in density in the air-absorber boundary. There are two methods to achieve this. One is to cut the material into pyramids or wedges and align the tips of all the pyramids facing the advancing wave. As the wave advances, it 'sees' only a very little absorbing material at first, and as it goes in further, the amount of absorbing material per unit volume increases. Hence, a slow transfer of absorber density from zero to maximum is attained. Another
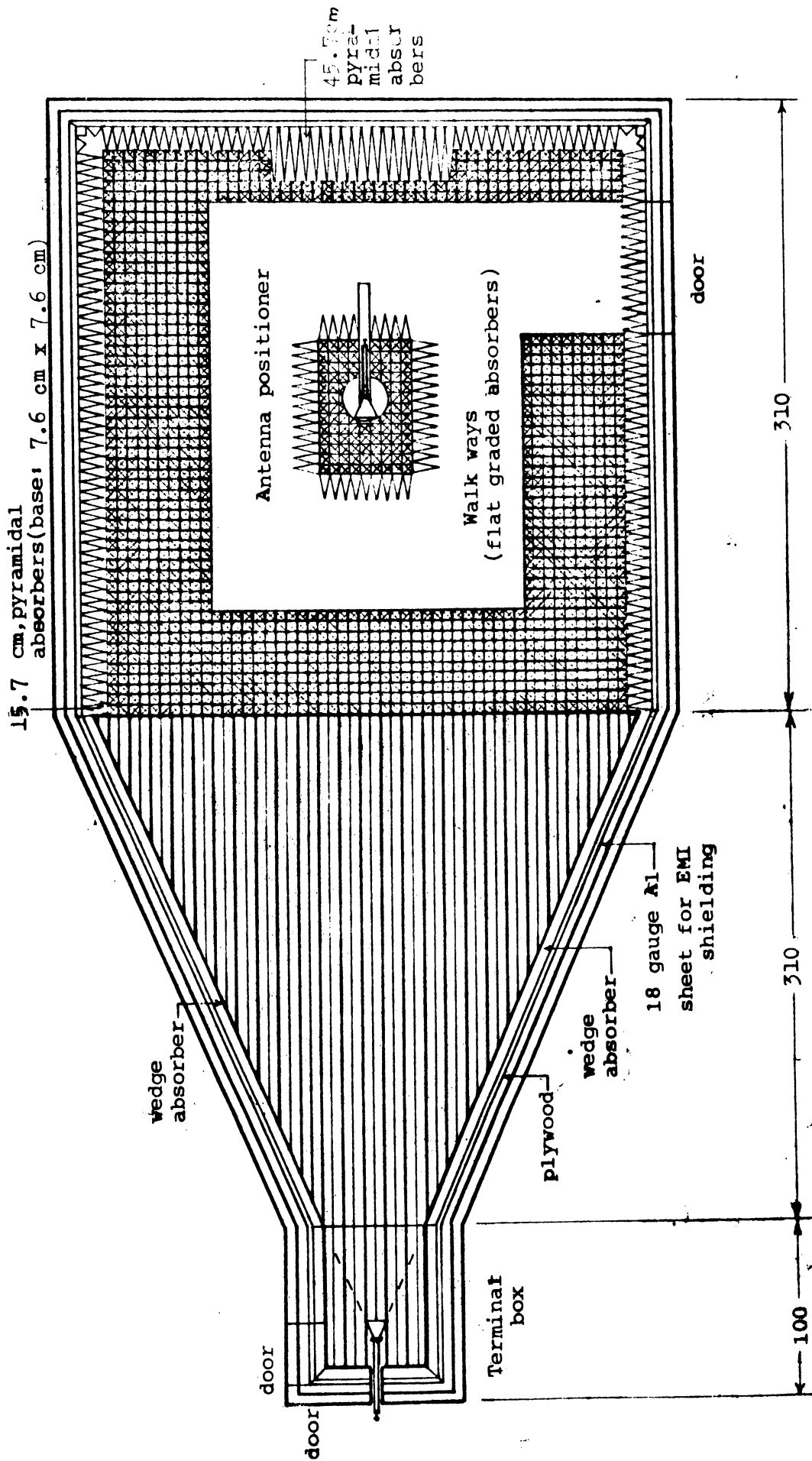
method is to vary the amount of absorbing material dispersed in the foam slowly from one end to the other. This is equivalent to stacking different layers of absorbing material with different absorber density so that the least denser one comes on top and the most denser one at the bottom. This arrangement also gives a slow variation in absorber density. This is called the "flat, layered absorber".

In this chamber, absorbing materials of flat layered type, wedge type and pyramidal type are employed. Fig.AII.1(a) is a sketch of the chamber showing its construction. The flat layered material is used in the walkways where the operator has to stand, to align the antenna on the turn-table. The wedge absorber is used in the tapered portion which does not 'see' the main lobe from the antenna. Pyramidal absorber is used in other places, from where there are greater chances of reflection occurring. As shown in the diagram, the portions of the back wall which receives the full impact of the main beam from the transmitter (called the target area) is covered with very long pyramids of 40 cm height to give greater absorption.

This is a tapered anechoic chamber. The tapered geometry was adopted for the following reasons.

171

COCHIN UNIVERSITY MICROWAVE ANECHOIC CHAMBER
[VIEW FROM THE TOP]

15.7 cm, pyramidal absorbers(base: 7.6 cm x 7.6 cm)

45.7cm pyramidal absorbers

door

Antenna positioner

Walk ways (flat graded absorbers)

door

310

wedge absorber

wedge absorber

plywood

18 gauge Al sheet for EMI shielding

door

door

Terminal box

310

100

(All dimensions are in cm.)

-Fig.AII.1(a)

1. A tapered geometry straightens the wavefront much faster than the rectangular geometry as shown in diagram AII.1(b)[86]

2. The tapered geometry results in a smaller surface area which in turn, reduces the quantity of absorbing material required to cover it,and hence the cost. Fig.AII.1(a) shows the dimensions and the main features of the chamber.

An E.M.I. shielding is provided to the chamber to avoid coupling between the interior and the external regions. Aluminium sheets of gauge 28 were employed for this purpose. A view of the different portions of the chamber is shown in Figs.AII.1(c), (d) and (e). The antenna positioner kept inside the chamber is fully automatic and it has got remote control option.

AII.2 Evaluation of the Chamber

AII.2(i) Reflectivity of the Material Used

Prior to the construction of the anechoic chamber, the absorbing material to be used was tested to ensure its suitability. The 'Arch method' was employed for this[87] evaluation. Fig.AII.2(i)(a) is a schematic diagram of this set up. As shown in the diagram, the transmitting and receiving horns are arranged along the arc of a circle,

Rectangular Chamber   **Tapered Chamber**
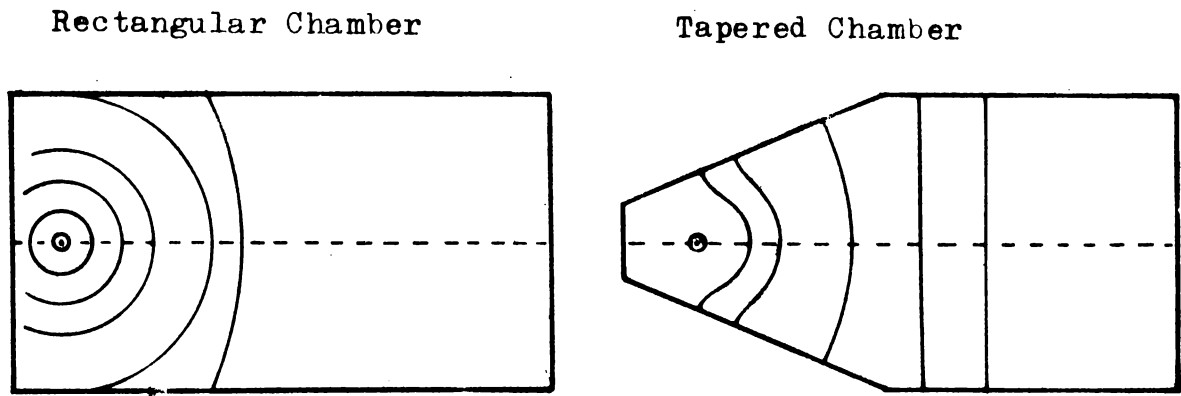
Fig.AII.1(b)   Propagation of wavefront in rectangular and tapered chambers.
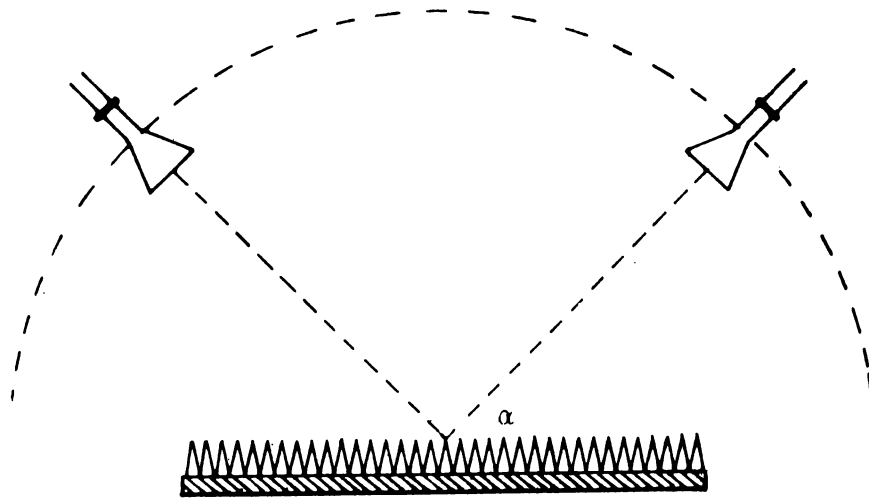
Fig.AII.2(i)(a)   Schematic diagram of the experimental set up for 'Arch Method' used to test absorber samples. α is the angle of incidence.
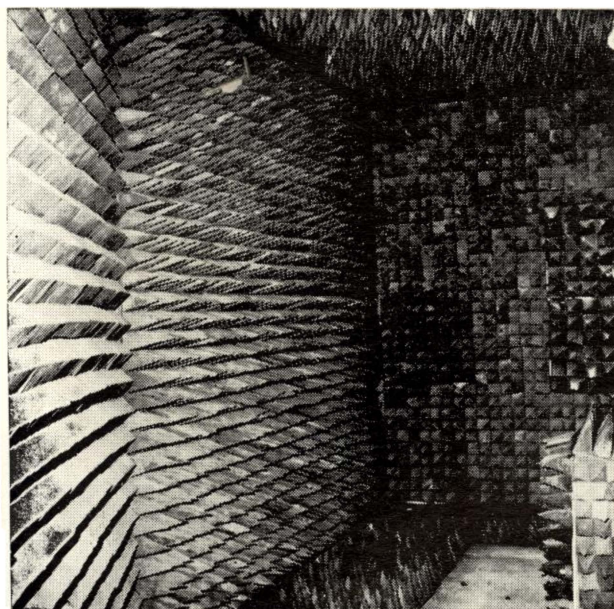
Fig.AII.1(c)
INTERIOR VIEW OF THE ANECHOIC CHAMBER:
Wedge absorbers lined in the tapered portion, pyramidal absorbers in the cubical portion and on the turn-table frame, and layered-flat absorbers paved in walk-ways around the turn-table can be seen.
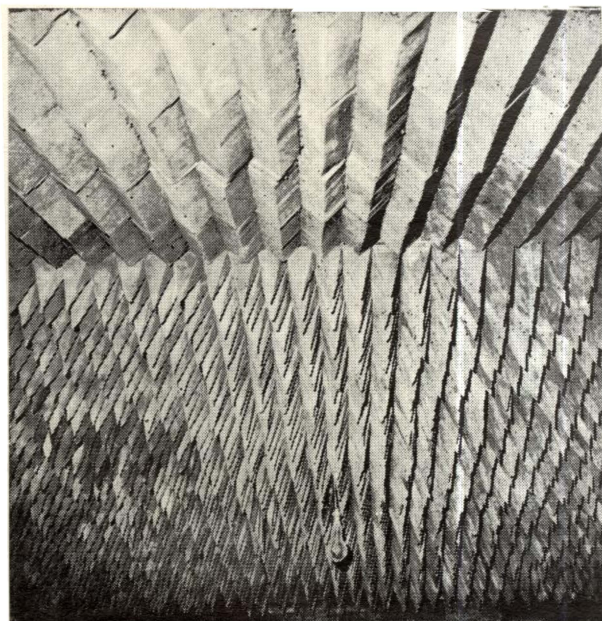
Fig.AII.1(d)
ROOF OF THE ANECHOIC CHAMBER:
Interior view of the roof: Wedge absorbers are on the tapered portion.
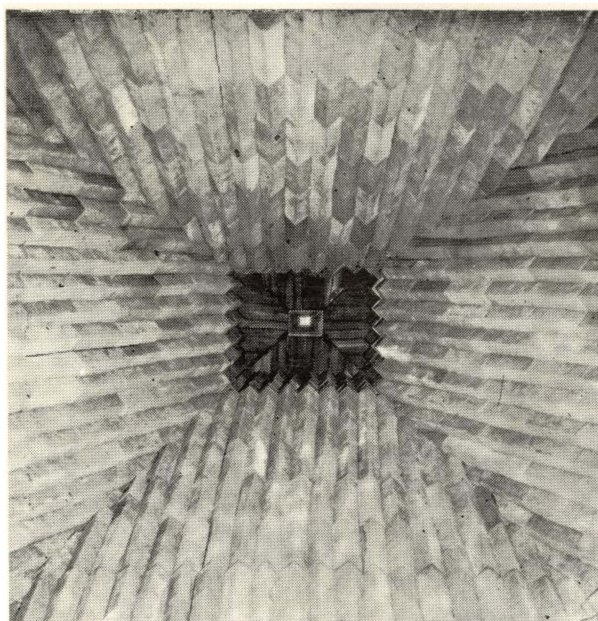
Fig.AII.1(e)
VIEW OF THE TAPERED PORTION FROM THE QUIET ZONE:
The small rectangular block at the centre is a pyramidal horn, situated exactly at the apex of the taped portion. This will function as a standard transmitter of microwave signal at the time of operation. The black portion around the standard transmitting antenna is the interior of the terminal box of the chamber.

both pointing towards its centre. A conducting sheet is kept at the centre of the arc, the transmitting and receiving horn making an angle α with the normal to line at the centre. The reflected power is noted as P_o. This is the reference power. The conducting sheet is then replaced with absorbing material, covering the same area as the sheet. Due to the absorption by the material, the reflected power in this case will be much smaller. Let this be P_r. The reflectivity of the material can be calculated as

$$R_{dB} = 10 \log_{10} \frac{P_r}{P_o} \ dB.$$

The advantage of this method is that the reflectivity at different angles of incidence can be determined very easily. The reflectivity values obtained for the large and small pyramidal absorbers were -30 dB and -27 dB respectively. For the flat layered and wedge type absorbers, the reflectivity was found to be -20 dB and -25 dB respectively.

AII.2(ii) Measurement of Chamber Reflectivity

While making antenna measurements, the test antenna is kept at the 'quiet zone' in an anechoic chamber. The quiet zone is the region inside an anechoic chamber, where the reflection from the chamber surfaces are below

the direct radiation from the transmitter by a certain specified amount. In other words, the quiet zone is the region which is free from reflected energy and hence an undistorted wavefront will be available. Generally, it is a spherical volume, the centre of which falls on the chamber axis. This region occurs at some distance from chamber wall, and is centered about the antenna stand.

The chamber reflectivity is defined as the average reflectivity level measured in the quiet zone. Of the many different techniques for measuring the reflectivity[88,89] the antenna pattern comparison technique was employed since it is the most widely accepted and convenient one. Moreover, this technique gives an idea about the quality of the chamber, because the small reflection depict themselves as perturbation in the antenna patterns.

Fig.AII.2(ii)(a) is a schematic diagram of the experimental set up. The transmitting antenna is kept at the apex of the tapered portion. The receiving antenna is mounted on the antenna turn-table and is kept at the centre of the quiet zone. The receiving and transmitting antennas were standard pyramidal horns. The radiation pattern of the receiving antenna was plotted for a 360° scan. This was taken as the reference pattern. The turn-table was moved through a distance of 15 cms to a new position, along
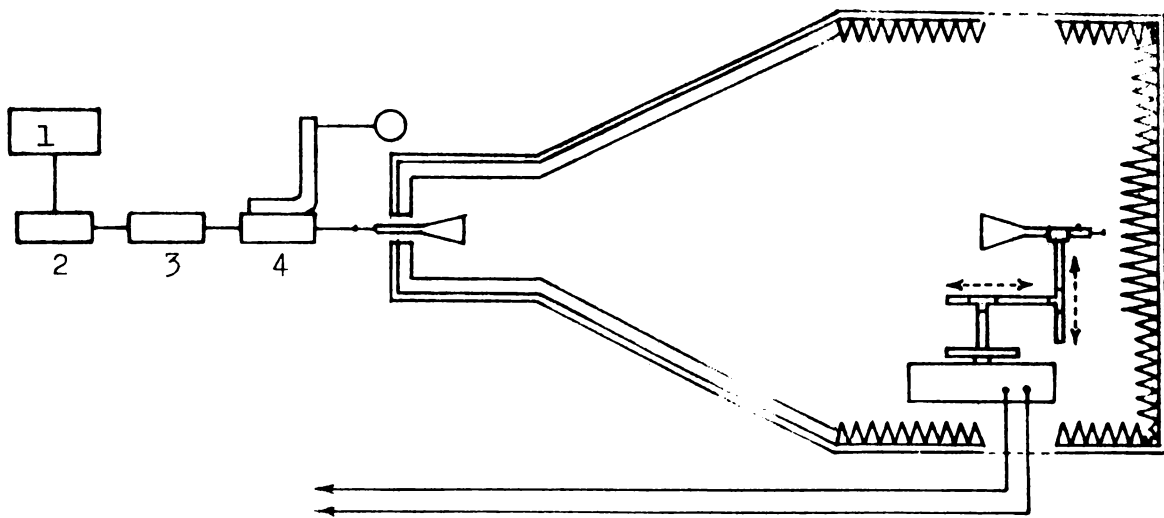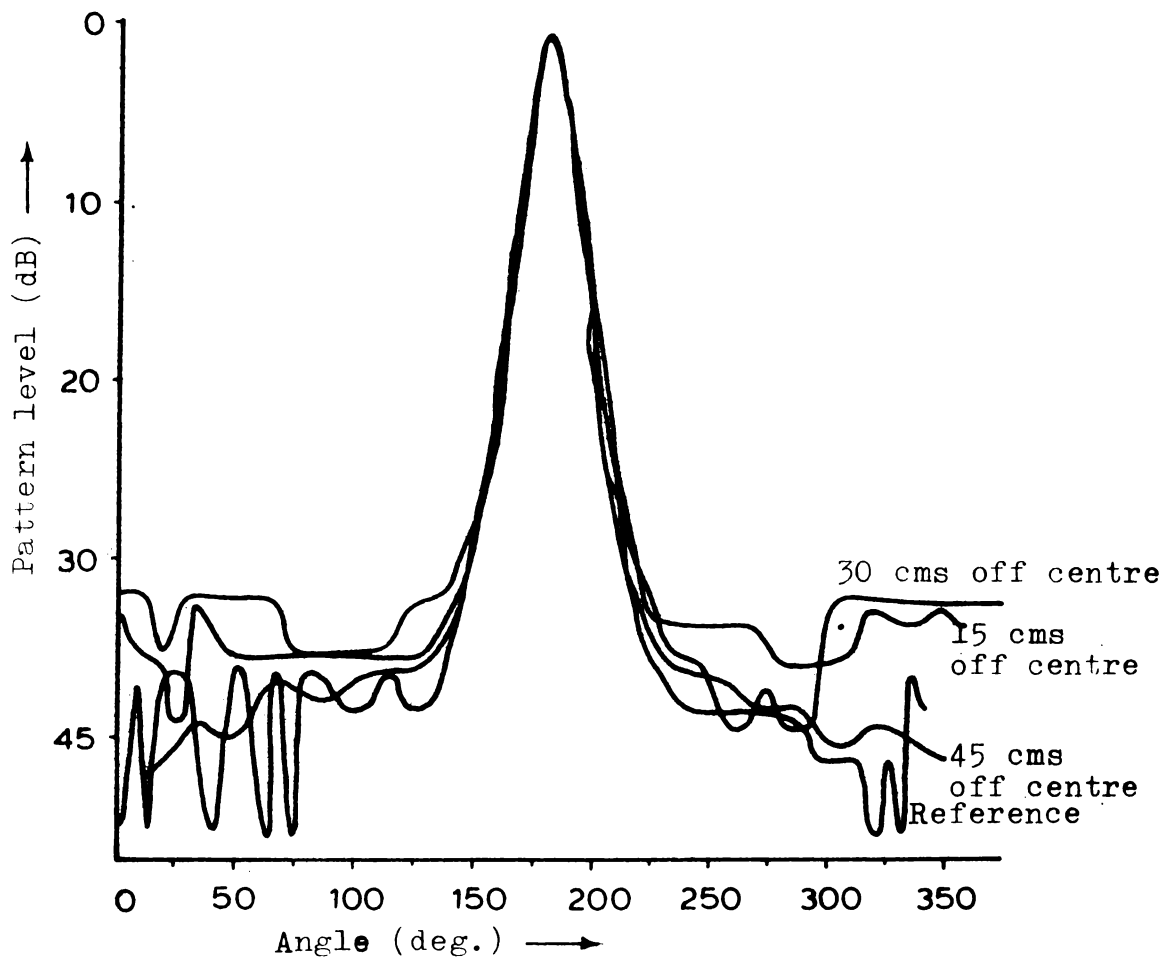
Fig.AII.2(ii)(a)　Experimental set up used for measuring chamber reflectivity. 1 - Gunn power supply, 2 - Gunn Source, 3 - Isolator, 4 - Directional coupler.

AII.2(ii)(b)　Radiation pattern plotted for pattern comparison method of evaluation.

a direction perpendicular to the chamber axis. The radiation
pattern of the same antenna at this new position is super-
imposed over the reference pattern, so that their main lobe
peaks coincide. This is repeated at different positions
along transverse and longitudinal directions from the centre
of the quiet zone.

Fig.AII.2(ii)(b) shows some of the patterns
recorded by the above method. Here it is seen that at pat-
tern levels well below the main lobe peaks, there exist
differences between the two patterns at reference and new
positions. As the patterns are plotted in dB scale, the
difference between the two patterns at specified pattern
levels, say -15dB, -20dB, -25dB etc., below the main lobe
peak are noted and plotted as a function of the distance
from the centre of the quiet zone. Fig.AII.2(ii)(c) shows
this deviation curve. It is seen here that this deviation
curve fluctuates between maximum and minimum values. The
peak to peak excursion of this deviation curve is noted at
each pattern level. The chamber reflectivity can then be
obtained from a standard curve described by Buckley[89].
Fig.AII.2(ii)(d) has been reproduced from the above refer-
ence. The chamber reflectivity can be readily obtained from
the curves presented here. The average reflectivity of this
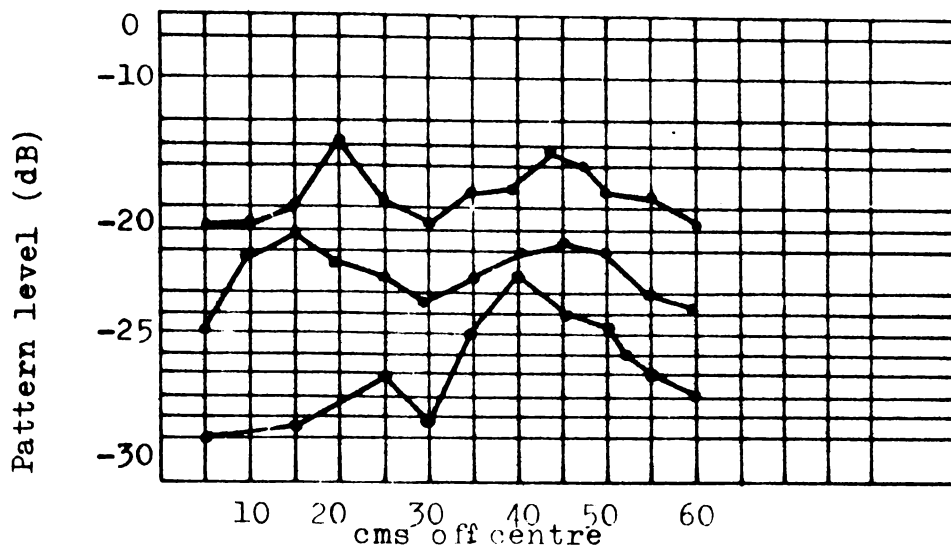chamber, determined by this method, has been found to be
32dB at 8.7 GHz.

Fig.AII.2(ii)(c)   The deviation at each **reference-pattern**
                        level with radial distance between
                        chamber centre and test point.
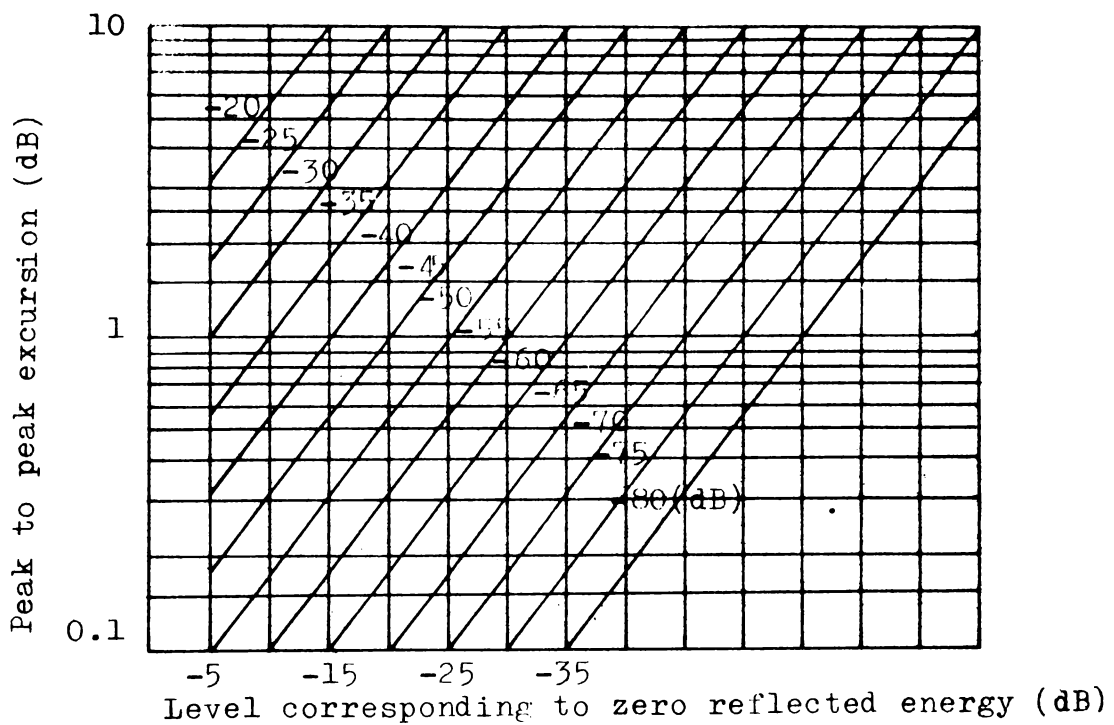

Fig.AII.2(ii)(d)   The standard curve used for determining
                        reflectivity of quiet zone (Ref.89).

179

AII.2(iii) Measurement of Termination VSWR of the Chamber

As the self impedance of the antennas have to be measured, the termination VSWR of the chamber becomes important. Under such circumstance, the chamber acts as a large free space termination.

The termination VSWR of the chamber will be very small. Hence the conventional method of measuring the VSWR with a slotted section cannot be adopted, since the mismatch introduced by the probe in the slotted section itself may be of the order of the mismatch in this termination. Therefore the moving termination technique[89,92] was adopted.

Here a standard pyramidal horn antenna is employed as the transmitter. The probe in the slotted section is kept stationary. The system as a whole is moved along a longitudinal axis and the probe output is recorded. The termination VSWR of the chamber is calculated from this.

It may be noted here that the directivity of the horn and its positioning has an effect on the measured value of the termination VSWR. The antenna was pointed along the axis of the chamber, a manner in which the test antenna would be mounted during actual observation.

The measured values of termination VSWR from different parts of the chamber were found to be below 1.05.

AII.2(iv)   Amplitude Uniformity in the Chamber

Reflections in a chamber can cause the field to vary in amplitude at the test antenna aperture. In order to determine the amplitude uniformity, the chamber is illuminated with a small pyramidal horn placed at the apex of the tapered portion. Another small pyramidal horn which is used as the test antenna, is mounted on the turn-table at the centre of quiet zone. The test antenna is oriented along the axis of the transmitter.

The value of the received power at the above position of the test antenna is noted as the reference power level. The turn-table is moved about 15 cm from the centre in a transverse direction perpendicular to the chamber axis and the new value of power is noted. By moving the turn-table from one end of the side wall to the other end, the power values are recorded at every 15 cm. The experiment is repeated by moving the test antenna along the longitudinal direction of the chamber axis and along the vertical direction from the centre of quiet zone. Fig.AII.2(iv)(a) gives the amplitude, variation along the transverse, longitudinal and vertical directions from the centre of the quiet zone. The amplitude variations measured along the transverse and vertical directions were found to be less than
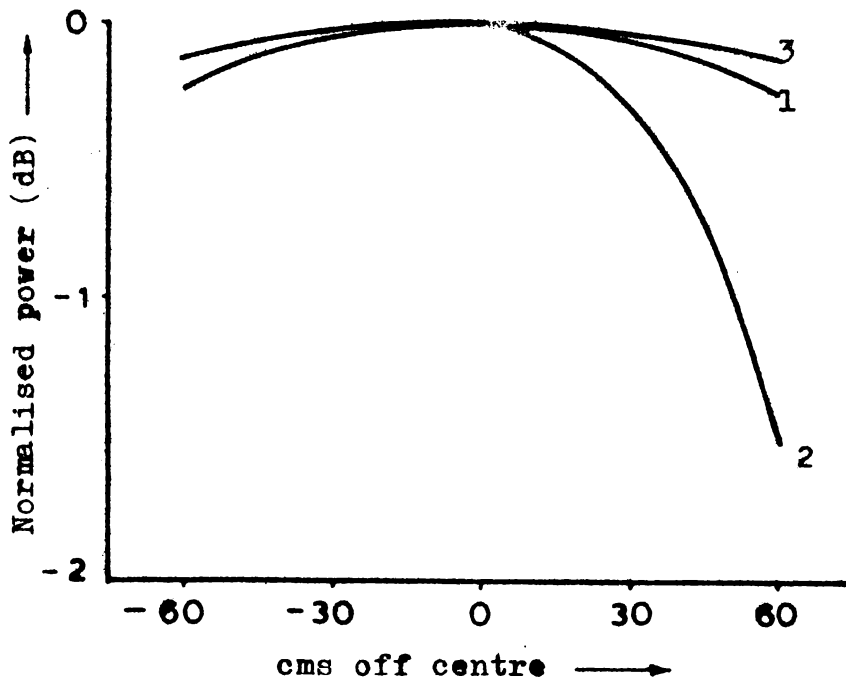
Fig.AII.2(iv)(a) Amplitude variation along the transverse,
longitudinal and vertical directions from
the centre of the quiet zone. 1 - Transverse
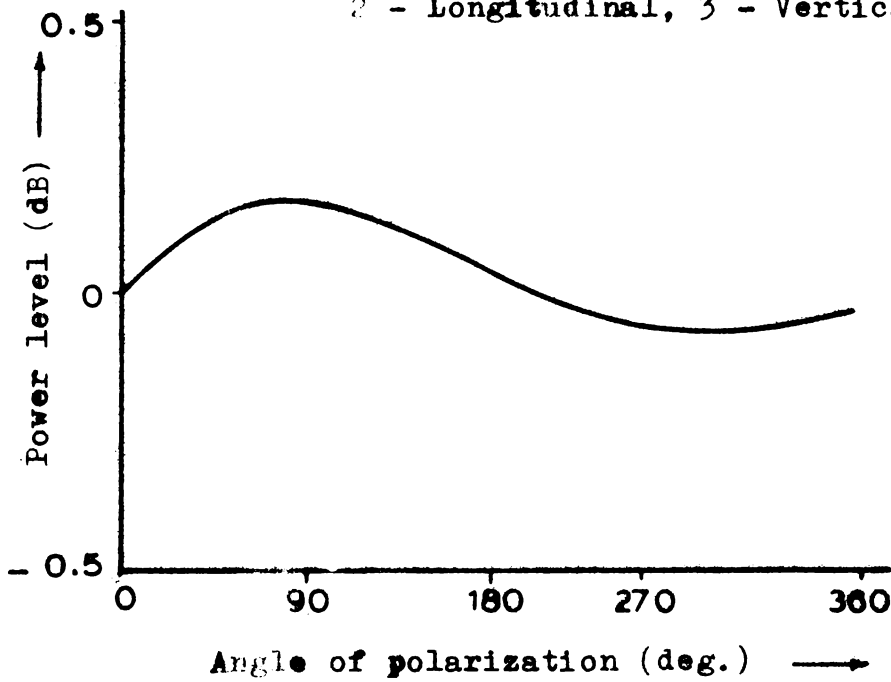2 - Longitudinal, 3 - Vertical.

Fig.AII.2(v)(a) Variation in transmission losses for
different polarization of the transmitted
signal.

0.25dB in the quiet zone. The longitudinal variations were found to be slightly high (nearly 2dB) because of the R^2 variation of power.

AII.2(v) Measurement of Path Loss Uniformity

Vertically and horizontally polarized signals should be transmitted down the chamber with the same transmission loss. For measuring the path loss uniformity, the chamber is illuminated with a small pyramidal horn. The test antenna, mounted on the turn-table, is placed at the centre of the quiet zone and oriented at 0° (on axis). The received power is recorded as the reference power. Both the transmitting and receiving antennas are rotated synchronously, on-axis maintaining the same plane of polarization from 0° to 180°. Power level at every 15° increment are recorded. Fig.AII.2(v)(a) shows the variation in transmission losses for different polarization of the transmitted signal. It can be seen that the path loss difference is within ± 0.2dB of the reference level. This limit is considered to be satisfactory for a good anechoic chamber[87].

A microwave anechoic chamber was constructed and its performance was evaluated. Some of the important chamber-performance characteristics like reflectivity of the

chamber, termination VSWR, amplitude uniformity and path loss uniformity were measured. The values obtained were found to be very well within the requirements for which the chamber was designed. These are well in match with international standards of such microwave anechoic chambers.

REFERENCES

1. G.C. Southworth, "Hyper-frequency waveguides--general
considerations ", Bell Syst. Tech. J., vol.15,
pp.284-309, Apr. 1936.

2. W.L. Barrow, "Transmission of electromagnetic waves in
hollow tubes of metal ", Proc. IRE, vol.24,
pp.1298-1328, Oct. 1936.

3. W.L. Barrow and F.D. Lewis, "The sectoral electromag-
netic horn ", Proc. IRE, vol.27, pp.41-50, Jan. 1939.

4. W.L. Barrow and L.J. Chu, "Theory of the electromagnetic
horn ", Proc. IRE, vol.27, pp.51-64, Jan. 1939.

5. G.C. Southworth and A.P. King, " Metal horns as directive
receivers of ultra short waves ", Proc. IRE, vol.27,
pp.95-102, Feb. 1939.

6. L.J. Chu and W.L. Barrow, "Electromagnetic horn design",
Trans. AIEE, vol.58, pp.333-338, Jul. 1939.

7. L.J. Chu, "Calculation of radiation properties of hollow
pipes and horns", J. Appl. Phys., vol.11,
pp.603-610, Sep. 1940.

8. N.M. Rust, "The phase correction of horn radiators ",
J. Inst. Elec. Eng., vol.93, pt. III A, pp.50-51,
Mar.-May 1946.

9. D.R. Rhodes, "An experimental investigation of the
radiation pattern of electromagnetic horn antennas ",
Proc. IRE, vol.36, pp.1101-1105, Sep. 1948.

10. H.S. Bennett, "Transmission-line characteristics of the sectoral horn", Proc. IRE, vol.37, pp.738-743, Jul. 1949.

11. C.W. Horton, "On the theory of the radiation patterns of electromagnetic horns of moderate flare angles", Proc. IRE, vol.37, pp.744-749, Jul. 1949.

12. A.P. King, "The radiation characteristics of conical horn antennas", Proc. IRE, vol.38, pp.249-251, Mar. 1950.

13. M.G. Schorr and F.J. Beck, Jr., "Electromagnetic field of the conical horn", J. Appl. Phys., vol. 21, pp.795-801, Aug. 1950.

14. W.C. Jakes, "Gain of electromagnetic horns", Proc. IRE, vol.39, pp.160-162, Feb. 1951.

15. E.H. Braun, "Gain of electromagnetic horns", Proc. IRE, vol.41, pp.109-115, Jan. 1953.

16. E.H. Braun, "Some data for the design of electromagnetic horns", IEEE Trans. Antennas Propagat. vol.AP-4, pp.29-31, Jan. 1956.

17. James J. Epis, "Compensated electromagnetic horns", Microwave J., vol.4, pp.84-89, May 1961.

18. K.L. Walton and V.C. Sundberg, "Broadband ridged horn design", Microwave J., vol.7, pp.96-101, Mar. 1964.

19. P.M. Russo, R.C. Rudduck, and L. Peters, Jr., "A method for computing E-plane patterns of horn antennas , IEEE Trans. Antennas Propagat., vol.AP-13, pp.219-224, Mar. 1965.

20. Y.S. Yu, R.C. Rudduck, and L. Peters, Jr., "Comprehensive analysis for E-plane of horn antennas by edge diffraction theory", IEEE Trans. Antennas Propagat. vol.AP-14, pp.138-149, Mar. 1966.

21. T.S. Chu and R.A. Semplak, " Gain of electromagnetic horns", Bell Syst. Tech. J., vol.44, pp.527-537, Mar. 1965.

22. E.V. Jull, "On the behaviour of electromagnetic horns", Proc. IEEE, vol.56, pp.106-108, Jan. 1968.

23. S.A. Schelkunoff and H.T. Friis, "Antennas: Theory and Practice", New York: Wiley, 1952.

24. E.V. Jull, "Finite-range gain of sectoral and pyramidal horns", Electron. Lett., vol.6, pp.680-681, Oct. 1970.

25. E.V. Jull, "Errors in the predicted gain of pyramidal horns", IEEE Trans. Antennas Propagat., vol.AP-21, pp.25-31, Jan. 1973.

26. M.A.K. Hamid, "Diffraction by a conical horn", IEEE Trans. Antennas Propagat., vol.AP-16, pp.520-528, Sep. 1968.

27. E.I. Muehldorf, "The phase center of horn antennas", IEEE Trans. Antennas Propagat., vol.AP-18, pp.753-760, Nov. 1970.

28. John L. Kerr, "Short axial length broad-band horns",
     IEEE Trans. Antennas Propagat., vol.AP-21,
     pp.710-715, Sep. 1973.

29. E.V. Jull, "Reflection from the aperture of a long
     E-plane sectoral horn", IEEE Trans. Antennas
     Propagat., vol.AP-20, pp.62-68, Jan. 1972.

30. E.V. Jull, "Gain of an E-plane sectoral horn--A failure
     of the Kirchhoff theory and a new proposal",
     IEEE Trans. Antennas Propagat., vol.AP-22,
     pp.221-226, Mar. 1974.

31. E.V. Jull, "Aperture fields and gain of open-ended
     parallel-plate waveguides", IEEE Trans. Antennas
     Propagat., vol.AP-21, pp.14-18, Jan. 1973.

32. C.A. Mentzer, L. Peters, Jr., and R.C. Rudduck, "Slope
     diffraction and its application to horns", IEEE
     Trans. Antennas Propagat., vol.AP-23, pp.153-159,
     Mar. 1975.

33. A.J. Simmons and A.F. Kay, "The scalar feed--A high
     performance feed for large paraboloid reflectors",
     IEE Conf. Publn., vol.21, pp.213-217, 1966.

34. R.E. Lawrie and L. Peters, Jr., "Modifications of horn
     antennas for low sidelobe levels", IEEE Trans.
     Antennas Propagat., vol.AP-14, pp.605-610,
     Sep. 1966.

35. P.J.B. Clarricoats and P.K. Saha, "Theoretical analysis of cylindrical hybrid modes in a corrugated horn", Electron. Lett., vol.5, pp.187-189, May 1969.

36. B. MacA. Thomas, "Bandwidth properties of corrugated conical horns", Electron. Lett., vol.5, pp.561-563, Oct. 1969.

37. M.S. Narasimhan and B.V. Rao, "Hybrid modes in corrugated conical horns", Electron. Lett., vol.6, pp.32-34, Jan. 1970.

38. M.S. Narasimhan and B.V. Rao, "Diffraction by wide-flare-angle corrugated conical horns", Electron. Lett., vol.6, pp.469-471, Jul. 1970.

39. M.E.J. Jeuken, "Experimental radiation pattern of the corrugated conical-horn antenna with small flare angle", Electron. Lett., vol.5, pp.484-485, 1969.

40. M.E.J. Jeuken and C.W. Lambrechtse, "Small corrugated conical-horn antenna with wide flare angle", Electron. Lett., vol.5, pp.489-490, 1969.

41. P.J.B. Clarricoats and P.K. Saha, 'Propagation and radiation behaviour of corrugated feeds--pt.1--Corrugated-waveguide feed", Proc. Inst. Elec. Eng., vol.118, pp.1167-1176, Sep. 1971.

42. P.J.B. Clarricoats and P.K. Saha, "Propagation and radiation behaviour of corrugated feeds--pt.2--Corrugated--conical horn feed", Proc. Inst. Elec. Eng., vol.118, pp.1177-1186, Sep. 1971.

43. P.J.B. Clarricoats, A.D. Olver, and P.K. Saha, "Near-field radiation characteristics of corrugated horns", Electron. Lett., vol.7, pp.446-448, Aug. 1971.

44. R. Baldwin and P.A. McInnes, "Surface wave excitation from a corrugated horn", Electron. Lett., vol.6, pp.259-260, Apr. 1970.

45. J.B. Anderson, "Radiation from surface wave antennas", Electron. Lett., vol.3, pp.251-252, 1967.

46. C.A. Mentzer and L. Peters, Jr., "Properties of cutoff corrugated surfaces for corrugated horn design", IEEE Trans. Antennas Propagat., vol.AP-22, pp.191-196, Mar. 1974.

47. C.A. Mentzer and L. Peters, Jr., "Pattern analysis of corrugated horn antennas", IEEE Trans. Antennas Propagat., vol.AP-24, pp.304-309, May 1976.

48. R. Baldwin and P.A. McInnes, "Corrugated rectangular horns for use as microwave feeds", Proc. IEE, vol.122, pp.465-469, May 1975.

49. R. Baldwin and P.A. McInnes, "A rectangular corrugated feed horn", IEEE Trans. Antennas Propagat., pp.814-817, Nov. 1975.

50. P. Bielli, E. Pagana and G. Rosenga, "A new method for computing corrugated horns phase centre", CSELT Rapporti tecniei, vol.IV, pp.153-158, Sep. 1976.

51. P. Bielli, S. De Padova and E. Pagana, "Analysis and synthesis of corrugated conical horns", CSELT Rapporti tecniei, vol.VI, pp.55-60, Mar. 1978.

52. C.S.Pao, "Shaping of primary patterns of horn feeds", Radiation Laboratory Report, No.655, 1945.

53. S. Hariharan and K. Gopalakrishnan Nair, "An experimental investigation of the change in radiation patterns in the Fresnels region of sectoral electromagnetic horn antennas due to shorting grills", J. Inst. Telecom. Engrs., vol.7, pp.189-196, 1961.

54. S. Hariharan and K. Gopalakrishnan Nair, "Impedance matching of sectoral electromagnetic horn antennas by shorting grills", J. Inst. Telecom. Engrs., vol.8, pp.246-251,1962.

55. K.G. Nair, G.P. Srivastava and S. Hariharan, "Sharpening of E-plane radiation patterns of E-plane sectoral horns by metallic grills", IEEE Trans. Antennas Propagat., vol.AP-17, pp.91-93, Jan. 1969.

56. K.G. Nair, G.P. Srivastava and S. Hariharan, "Effect of conducting grills on the E-plane radiation patterns of E-plane sectoral horns", Int. J. Electronics, vol.26, pp.561-572, 1969.

57. A.R.G. Owen and L.G. Reynolds, "The effect of flanges
     on the radiation patterns of small horns", J.
     Inst. Elec. Eng., vol.93, pt.IIIA, pp.50-51,
     Mar-May 1946.

58. P.C. Butson and G.T. Thompson, "The effect of flanges
     on the radiation patterns of waveguides and
     sectoral horns", J. Inst. Elec. Eng., vol.106,
     pt.B, pp.422-426, 1959.

59. K.G. Nair and G.P. Srivastava, "Beam shaping of H-plane
     sectoral horns by metal flanges", J. Inst. Telecom.
     Engrs., vol.13, pp.76-82, Feb. 1967.

60. K.G. Nair, V.K. Koshy and G.P. Srivastava, "A theoretical
     study of the asymmetric excitation of conducting
     flanges by a primary aperture antenna and the
     consequent radiation patterns", Int. J. Electronics,
     vol.24, pp.497-500, 1968.

61. K.G. Nair, G.P. Srivastava, S.B. Singh and V.K. Koshy,
     "A study of the effect of the relative position
     of metal flanges on the radiation pattern of
     H-plane sectoral horn", Int. J. Electronics,
     vol.25, pp.153-164, 1968.

62. V.K. Koshy, S.B. Singh, K.G. Nair and G.P. Srivastava,
     "Effect of asymmetry in amplitude of excitation
     of secondary sources by a primary aperture
     antenna", Int. J. of Electronics, vol.25,
     pp.289-291, 1968.

63. K.G. Nair, G.P. Srivastava and S.B. Singh, "Some
      effects of metal flanges on the radiation pattern
      of H-plane sectoral horns", J. Inst. Telecom.
      Engrs., vol.14, pp.352-358, 1968.

64. S.B. Singh, K.G. Nair and G.P. Srivastava, "Experi-
      mental confirmation of the effect of asymmetric
      flanges on the radiation pattern of aperture
      antennas", Int. J. Electronics, vol.26, pp.173-177,
      1969.

65. K.G. Nair, "A modified theory for the radiation
      pattern of an aperture antenna and two secondary
      sources excited by the primary", Int. J. Electronics,
      vol.28, pp.459-462, 1970.

66. V.K. Koshy, K.G. Nair and G.P. Srivastava, "Analysis
      of radiation from a flanged aperture antenna",
      IEEE Trans. Antennas Propagat., vol.AP-18,
      pp.407-411, May 1970.

67. V.K. Koshy, K.G. Nair and G.P. Srivastava, "Gain
      improvement of flanged sectoral horn antennas
      by flange angle variations", Ind. J. Pure. Appl.
      Phys., vol.9, pp.476-478, Jul. 1971.

68. K.G. Nair, V.K. Koshy and G.P. Srivastava, "E-plane
      sectoral horns yield to flange technique", Int.
      J. Electronics, vol.24, pp.93-98, 1968.

69. Ching C. Han and A.N. Wickert, "A new multimode rectangular horn antenna generating a circularly polarized elliptical beam", IEEE Trans. Antennas Propagat., vol.AP-22, pp.746-751, Nov. 1974.

70. R.W. Gruner, "A 4- and 6-GHz, prime focus, CP feed with circular pattern symmetry", Int. IEEE/AP-S symp. Program and Dig., pp.72-74, June 1974.

71. T. Ebisui, T. Katagi and M. Mizusawa, "A circularly polarised dual-mode horn antenna for communication satellite", Int. IEEE/AP-S Symp. Program and Dig., pp.313-316, June 1977.

72. T.Ebisui, T. Katagi and M. Mizusawa, "A circularly polarised flare-iris type dual-mode horn antenna", Trans. IECE, (Japan), vol.E62, pp.904-905, Dec.1979.

73. J.D. Kraus, "Antennas", McGraw-Hill Book Company, New York, 1950.

74. E.B. Moullin, "Theory and performance of corner reflector and aerials", J. IEE, pt.III, vol.92, pp.58, 1945.

75. J.R. Wait, "On the theory of an antenna with an infinite corner reflector", Can. J. Phys., vol.32, pp.365-371, 1954.

76. E.F. Harris, "An experimental investigation of the corner reflector antenna", Proc. IRE, vol.41, pp.645-651, 1953.

77. H.V. Cottony and A.C. Wilson, "Gains of finite-size
    corner reflector antennas", IRE Trans. Antennas
    Propagat., vol.AP-6, pp.366-369, 1958.

78. A.C. Wilson and H.V. Cottony, "Radiation patterns of
    finite-size corner reflector antennas", IRE Trans.
    Antennas Propagat., vol.AP-8, pp.144-157, 1960.

79. Y. Ohba, "On the radiation pattern of a corner reflector
    finite in width", IEEE Trans. Antennas Propagat.,
    vol.AP-11, pp.127-132, Mar. 1968.

80. D. Proctor, "Graphs simplify corner reflector antenna
    design", Microwaves, vol.14, pp.48-52, Jul. 1975.

81. Kazuo Aoki and Takehiko Tsukiji, "Radiation field of
    a finite size corner reflector antenna", Trans.
    IECE (Japan), vol.57-B, pp.549-556, 1974.

82. Y.H. Ja, "Numerical evaluation of phase centres of
    corner reflector antennas", Electron. Lett.,
    vol.15, pp.1-2, Jan. 1979.

83. O.M. Woodward, Jr., "A circularly polarised corner
    reflector antenna", IRE Trans. Antennas Propagat.,
    vol.AP-5, pp.290-297, Jul. 1957.

84. R.W. Klopfenstein, "Corner reflector antennas with
    arbitrary dipole orientation and apex angle",
    IRE Trans. Antennas Propagat., vol.AP-5, pp.297-305,
    Jul. 1957.

85. A.W. Love, "The diagonal horn antenna", Microwave J.,
       vol.5, pp.117-122, Mar. 1962.

86. Steven Galagan, "Understanding microwave absorbing
       materials and anechoic chambers - Part II",
       Microwaves, pp.44-49, Jan. 1970.

87. Steven Galagan, "Understanding microwave absorbing
       materials and anechoic chambers - Part III",
       Microwaves, pp.47-50, Apr. 1970.

88. Steven Galagan, "Understanding microwave absorbing
       materials and anechoic chambers - Part IV",
       Microwaves, pp.69-73, May 1970.

89. E.F. Buckley, "Outline of evaluation procedures for
       microwave anechoic chambers", Microwave J.,
       vol.6, pp.69-75, Aug. 1963.

90. S. Silver, "Microwave antenna theory and design",
       McGraw-Hill Book Company, New York, 1949.

91. E.B. Moullin, "Radio Aerials", Oxford University
       Press, London, 1949.

92. C.G. Montgomery, "Techniques of microwave measurements",
       McGraw-Hill Book Company, New York, 1949.

93. H.M. Barlow and A.L. Cullen, "Microwave measurements",
       Constable and Company, London, 1950.

94. A.E. Booth, "Microwave data tables", Iliffe and Sons
       Ltd., London, 1959.

95. E.A. Jasik, "Antenna engineering hand book", McGraw-Hill Book Company, New York, 1961.

96. "Test procedure for antennas", Institute of Electrical and Electronics Engineers, New York, 1965.

97. E.C. Jordan, "Electromagnetic waves and radiating systems", Prentice-Hall of India, New Delhi, 1967.

98. Harry E. Thomas, "Hand book of microwave techniques and equipment", Prentice-Hall Inc., Englewood Cliffs, New Jersey, 1972.

99. R.E. Collin and F.J. Zucker, "Antenna theory - Part I", McGraw-Hill Book Company, New York, 1969.

100. R.E. Collin and F.J. Zucker, "Antenna theory - Part II", McGraw-Hill Book Company, New York, 1969.

101. K.K. Srivastava, "Anechoic chambers (design, evaluation and measurements)", Proc. IEEE Workshop on Design, Measurements and Evaluation of Microwave Antenna Systems, New Delhi, Sep.28-30, 1978.

LIST OF PUBLICATIONS

1. "Beam shaping and impedance matching of sectoral electromagnetic horn antennas using corrugated flanges", Ind. J. Radio. Space. Phys., vol.8, pp.24-28, Feb. 1979.

2. "Metal flanges with more parameters for beam shaping", IEEE Trans. Antennas Propagat., vol.AP-27, pp.708-711, Sept. 1979.

3. "Microwave absorber using rubber and carbon", Ind. J. Pure Appl. Phys. vol.18, pp.216-218, Mar. 1980.

4. "Fabrication of an antenna turn-table with remote control systems for anechoic chamber investigations", Journal of the Institution of Engineers (communicated).

5. "A corrugated corner reflector system", IEEE Trans. Antennas Propagat., vol.AP-30 (Scheduled for publication in May 1982).

6. "An analysis of radiation patterns of corrugated corner reflector antenna systems", Ind. J. of Radio. Space. Phys. (communicated).

199

G 3199 -